THE MECHANISM OF HEME TRANSFER FROM THE STREPCOCCAL CELL SURFACE PROTEIN SHP TO HTSA OF THE HTSABC TRANSPORTER

by

Yanchao Ran

A dissertation submitted in partial fulfillment
of the requirements for the degree

of

Doctor of Philosophy

in

Immunology & Infectious Diseases

MONTANA STATE UNIVERSITY
Bozeman, Montana

December 2010

APPROVAL

of a dissertation submitted by

Yanchao Ran

This dissertation has been read by each member of the dissertation committee and has been found to be satisfactory regarding content, English usage, format, citation, bibliographic style, and consistency and is ready for submission to the Division of Graduate Education.

Dr. Benfang Lei

Approved for the Department of Immunology and Infectious Diseases

Dr. Mark T. Quinn

Approved for the Division of Graduate Education

Dr. Carl A. Fox

STATEMENT OF PERMISSION TO USE

In presenting this dissertation in partial fulfillment of the requirements for a doctoral degree at Montana State University, I agree that the Library shall make it available to borrowers under rules of the Library. I further agree that copying of this dissertation is allowable only for scholarly purposes, consistent with "fair use" as prescribed in the U.S. Copyright Law. Requests for extensive copying or reproduction of this dissertation should be referred to ProQuest Information and Learning, 300 North Zeeb Road, Ann Arbor, Michigan 48106, to whom I have granted "the exclusive right to reproduce and distribute my dissertation in and from microform along with the non-exclusive right to reproduce and distribute my abstract in any format in whole or in part."

Ran, Yanchao

December 2010

ACKNOWLEDGEMENTS

I would like to thank my advisor, Dr. Benfang Lei, for guidance with patience, consideration in general and criticism in science. The past and current members at Lei lab have also been helpful for my scientific growth. My graduate committee members, Dr. Mark Quinn, Dr. Allen Harmsen, Dr. Valerie Copie, and Dr. Li Huang, have provided important suggestions to proceed further for this project. I also would like to thank my parents, sisters, brother-in-laws, nieces, and my dog for always being supportive and encouraging me to go through good and bad times with confidence.

TABLE OF CONTENTS

TABLE OF CONTENTS - CONTINUED

TABLE OF CONTENTS - CONTINUED

TABLE OF CONTENTS - CONTINUED

LIST OF TABLES

Table Page

LIST OF FIGURES

Figure Page

LIST OF FIGURES - CONTINUED

Figure Page

ABSTRACT

Group A Streptococcus relies on heme as a source of iron. The proteins Shp and HtsA are part of the heme acquisition machinery of Group A *Streptococcus*. Shp rapidly transfers its heme to HtsA; however, the mechanism of the Shp/HtsA reaction is unknown. This project was conducted to elucidate the structural basis and molecular mechanism of this rapid heme transfer reaction. Site-directed mutagenesis was used to identify the axial ligands of the heme iron in Shp and HtsA, and kinetic and spectroscopic analyses and animal infection were used to assess the effects of the elimination of the axial ligands on coordination and spin state of the heme iron, kinetic mechanism of the heme transfer, autoxidation of the Shp heme iron, and GAS virulence. The axial ligands of the heme iron in Shp and HtsA were found to be Met66/Met153 and Met79/His229, respectively. The $Met153^{Shp}$ and $His229^{HtsA}$ residues are critical for the affinity of the proteins for heme, and the other axial side of the heme irons is more accessible to solvent. The Met66Ala and Met153Ala replacements of Shp alter the kinetic mechanism of Shp-to-HtsA heme transfer and unexpectedly slow down heme transfer, which allows detection of transfer intermediates. The $HtsA^{Met79Ala}$ and $HtsA^{His229Ala}$ mutant proteins cannot acquire heme from ferrous Shp but induce rapid autoxidation of ferrous Shp. The significance of these findings is three-fold. Firstly, the structural basis of the heme binding in Shp and HtsA and the spectral properties of their axial ligand mutants enable the interpretation of the kinetics and spectral changes of the heme transfer reactions. Secondly, HtsA axial mutant-induced autoxidation of ferrous Shp provides evidence for the activated heme transfer mechanism and the formation of a Shp-HtsA complex that weakens the heme binding in Shp. Thirdly, the findings allow us to propose a reaction model in which the side chains of the axial residues from HtsA are inserted into the axial positions of the heme in Shp to extract it from the surface protein and pull it into the transporter active site. The project significantly advances the understanding of how heme is rapidly transferred from one protein to another in heme acquisition.

BACKGROUND

Streptococci

Streptococci are a class of Gram-positive cocci that are spherical in shape and grow in chains. Many of streptococci are non-pathogenic and are part of the commensal flora of the mouth, skin, intestine, and upper respiratory tract of humans and other animals, and others cause diseases. The initial streptococcus genus belongs to Bacteria kingdom, Firmicutes phylum, Bacilli Class, Lactrobacillales Order, Streptococcaceae Family (1).

Shottmuller (2) made the earliest attempt at differentiating the streptococci using blood agar to differentiate strains that were beta-hemolytic from those that were not. Beta-hemolysis is complete rupture of red blood cells, giving distinct, wide, and clear areas around bacterial colonies on blood agar. Beta-hemolytic streptococci are further classified into groups A to V (except I and J) via the Lancefield serotyping, which is based on specific carbohydrate antigens in the bacterial cell wall (3). Sherman divided the streptococci into four divisions, the pyrogenic division, the viridians division, the lactic division, and the enterococci (4). The taxonomy of streptococci has experienced a number of changes during the last 30 years which is mostly due to the application of molecular biology techniques such as DNA-DNA re-association experiments and 16 S rRNA gene sequencing. Based on molecular and chemotaxonomic analyses, the lactic cocci and enterococci were excluded from the streptococcus genus in the 1980s (5, 6). Both beta- and non-beta-hemolytic streptococci contain several important human and animal pathogens (7). The group of beta-hemolytic streptococci contains *Streptococcus*

pyogenes, which is commonly known as group A *Streptococcus*, *Streptococcus agalactiae* (group B *Streptococcus*), and *Streptococcus equi* (group C *streptococcus*) that cause human pharyngitis, neonatal sepsis, and equine strangles, respectively. *Streptococcus pneumoniae* and *Streptococcus mutants*, which cause pneumonia and dental caries, respectively, belong to the non-beta-hemolytic group.

Group A *Streptococcus*

Typing

Group A *Streptococus* (GAS) is an important member and major pathogen of the streptococci genus. Like many major bacterial pathogens, GAS clinical isolates display high polymorphism in both genetic contents and gene sequences. The M protein, a major cell surface protein and virulence factor, is encoded by the *emm* gene and is highly variable in the N-terminal region. In the 1920s, Dr. Rebecca Lancefield found that antiserum raised to extractable M proteins often conferred strain-specific protection. This finding led to the M typing, which uses antiserum directed to M proteins of different isolates. More than 80 distinct M types were identified (8). T-protein typing and detection of streptococcal serum opacity factor further enhanced GAS characterization (9). However, the M-typing could not identify all GAS strains because of scarcity of M antisera. This problem was solved by the *emm* gene sequence typing (10). The *emm* type is defined by the 5′ end region of the *emm* gene, and genes assigned the same *emm* type have > 92% nt sequence identity. More than 200 *emm* types are currently listed online in the the Centers for Disease Control and Prevention (CDC) database (11). The *emm* pattern genotypes are fairly strong markers for preferred tissue site of infections and

diseases among GAS strains (12). Therefore, typing of GAS strains is important for understanding the role of unique microbial properties in pathogenesis.

Infections and Diseases

GAS is a major human pathogen that causes a variety of infections and diseases. This organism commonly causes pharyngitis, which is also called "strep throat", and localized skin infections, such as impetigo, erysipelas, and cellulitis. Strep throat is GAS infection of the pharynx and possibly the larynx, and the common symptoms include high fever, sore throat, swollen tonsils, and enlarged lymph nodes. This contagious infection spreads through close contact. Impetigo is a highly contagious bacterial skin infection that is most common among pre-school children and people who play close contact sports such as rugby. American football and wrestling are also susceptible, regardless of age. Erysipelas and cellulitis are characterized by multiplication and lateral spread of GAS in deep layers of the skin. Cellulitis is a diffuse inflammation of connective tissue with severe inflammation of dermal and subcutaneous layers of the skin. Cellulitis can be caused by normal skin flora or by exogenous bacteria, and often occurs where the skin has previously been broken: cracks in the skin, cuts, blisters, burns, insect bites, surgical wounds, or sites of intravenous catheter insertion. Skin on the face or lower legs is most commonly affected by cellulitis, though this infection can occur on any part of the body.

GAS also causes severe invasive infections in which GAS bacteria get into parts of the body where bacteria usually are not found, such as the blood, muscle, and the lungs. A major type of severe invasive GAS infections is necrotizing fasciitis, which is also called flesh-eating disease. This disease involves GAS infection of the deeper layers of

skin and subcutaneous tissues in which GAS easily spreads across the fascial plane within the subcutaneous tissue and destroys muscles, fat, and skin tissue and disseminate into blood and various organs. The systemic dissemination causes sepsis syndrome or streptococcal toxic shock syndrome (STSS), which shows rapid drop of blood pressure and sudden failure of the organs. About 20% of patients with necrotizing fasciitis and more than half with STSS die. About 10%-15% of patients with other forms of invasive GAS diseases die.

GAS infections can cause post-infection sequelae, such as rheumatic fever and glomerulonephritis. Rheumatic fever is characterized by inflammation of the joints and/or heart, and glomerulonephritis is inflammation of the renal glomerulus. The post-infection diseases are believed to be caused by anti-GAS antibodies that cross-react with host molecules.

Epidemics

In the late 18th century and early 19th century, infections by GAS claimed many lives, especially since the organism was the most important cause of puerperal fever, sepsis after childbirth, and scarlet fever, a severe complication of streptococcal infection. Because of the introduction of antibiotic therapy in 1940s, these diseases are not common and lethal any more. Similarly, erysipelas has become less common.

Severe invasive GAS infections have markedly increased in developed countries since the 1980s (13). Recent invasive GAS infections in England indicate that almost 40% of those affected had no predisposing illnesses or risk factors, and the proportion of children with infections has risen (14). In Finland, the nationwide surveillance during

1998-2007 showed an increase of invasive GAS diseases, and clinicians were alarmed by severe disease manifestations. The average annual incidence of invasive GAS infections was 2.5/100,000 population, with a peak in 2007 (3.9/100,000) (15). In Sweden, a recent cluster of 30 patients with severe GAS infections from December 2006 to May 2007 was reported, and 16 of the patients had soft tissue infections (16). A U.S. surveillance found 3.5 severe GAS invasive infection cases per 100,000 persons with a fatality rate of 13.7% (17).

Globally there are about 663,000 new severe invasive GAS infection cases and 163,000 deaths each year. In addition, there are also approximately 517,000 deaths each year due to acute rheumatic fever, rheumatic heart disease, post-streptococcal glomerulonephritis, and invasive GAS infections. The prevalence of these severe GAS diseases is at least 18.1 million cases, with 1.78 million new cases each year. The greatest burden is rheumatic heart disease, with a prevalence of about 15.6 million cases, with 282,000 new cases and 233,000 deaths each year. In addition, there are more than 111 million prevalent cases of GAS pyoderma and over 616 million cases of GAS pharyngitis per year (18).

These epidemic data highlight the worldwide outbreaks of severe GAS infections and indicate the importance of surveillance for prompt identification of more aggressive isolates in the community, thereby increasing awareness among healthcare professionals on these life-threatening infections. In the United States, CDC began surveillance for invasive GAS infections in 5 US sites in 1995 as part of the Active Bacterial Core surveillance (ABDs) program of the Emerging Infection Program Network (19). The Strep-EURO collaborative program has contributed to enhancement of the knowledge of

the spread of invasive disease caused by GAS within Europe and established the surveillance system for case report and characterization of clinical strains (20).

Pathogenesis and Virulence Factors

GAS produces abundance of extracellular proteins and other molecules to mediate its pathogenesis. The sequenced M1 GAS strain SF370 encodes 123 known and putative cell wall-linked or secreted proteins (21). These proteins play roles in adhesion, evasion of host defenses, and invasion of host tissues.

Adherence of GAS to pharyngeal and dermal epithelial cells is critical for GAS to colonize in the host. Without strong adherence mechanisms, GAS could not attach to host tissues and would be removed by salivary fluid-flow mechanisms and exfoliation of the epithelium. GAS produces multiple adhesins (22), including M protein (23), hyaluronic acid capsule (24), lipoteichoic acid LTA (25), fibronectin-binding protein F/Sfb (26), glyceraldehyde-3-phosphate dehydrogenase (27), a galactose-binding protein (28), a vitronectin binding protein (29), a collagen-binding protein (30), serum opacity factor (31), and FBP54 (32).

GAS evades host defenses by several mechanisms. First, GAS produces the cell wall-linked peptidases ScpA and SpyCEP to cleave the chemoattractants C5a peptide and IL-8, respectively, inhibiting neutrophil recruitment (33-35). Secondly, the hyaluronic acid capsule confers resistance to phagocytosis by neutrophils (24). Thirdly, M protein binds to fibrinogen, C4b-binding protein (C4BP), and the complement regulator factor H (36-38), blocking the activation of the alternate complement pathway and crucially contributing to resistance to phagocytosis. Fourthly, GAS produces the endoglycosidase

EndoS and proteinase Mac/IdeS to specifically hydrolyze the asparagine-linked glycan in the CH2 domain of IgG and cleave IgG in the hinge region, respectively, inhibiting opsonophagocytosis (39-41). Additionally, GAS produces the streptococcal inhibitor of complement (SIC) to block formation of the membrane attack complex of complement by binding to the C5b-7 complex (42) and to interfere with the antimicrobial activity of defensins (43). Several important virulence factors are introduced in more details below.

The M Protein. The M protein is a homodimer that has a coiled-coil structure and is attached to the cell wall. The molecule consists of 4 repeat regions designated A, B, C, and D repeats, and a proline/glycine rich region most likely located in the peptidoglycan layer of the cell wall. The N-terminal portion of the molecule (A repeat) is hypervariable and confers serotype specificity. The type specificity of the M protein is largely determined by the epitope located in 40 to 50 amino acid residues at the N-terminus (44). The N-terminal region of the M protein contains protective epitopes that are not likely cross-reactive with human tissues. M proteins are normally anchored to the cell wall but can be released from the bacterial surface by the action of host- or bacterium-produced proteinases (45).

The M protein is one of the most important GAS virulence factors and has several functions (22, 46, 47). Firstly, the M protein has antiphagocytic properties. This protein recruits the inhibitory regulators of the complement pathways, including protein H, factor H like-1, C4-binding protein C4BP, and CD46 complement regulatory protein, inhibiting complement activation on the streptococcal surface. Some M protein variants bind fibrinogen, blocking the classical pathway of the complement system and reducing the

deposition of the opsonin C3bi (36-38). Secondly, the M protein can elicit antibodies that react with human proteins, and it is thought that the molecular mimicry of the M protein plays a role in acute rheumatic fever (46). Thirdly, the M protein plays an important role in adhesion and colonization. Fourthly, M protein is critical for the internalization of GAS into host cells (48). Lastly, the M protein binds with coagulation factors such as fibrinogen in the plasma and affects hemostasis (46).

Hyaluronic Acid Capsule. The layers covering the streptococcus from inside to outside are the cytoplasmic membrane, cell wall, and capsule. The hyaluronic acid capsule is the outside layer, which is composed of a polymer of hyaluronic acid containing repeating units of glucuronic acid and N-acetylglucosamine. The hyaluronic acid is an important adherence factor in the pharynx, binding to CD44 on epithelial cells (49), and the binding induces cytoskeleton changes, which can lead to cellular invasion (50). The capsule is also required for resistance to phagocytosis (51). Enhanced capsule production is associated with severe invasive infections and the delayed sequelae of rheumatic fever (47, 52-54).

Streptococcal C5a Peptidase. The C5a peptidase, ScpA, is a surface-linked protein that specifically degrades the C5a peptide that is derived from activation of the complement system. By cleaving this chemotactic peptide, ScpA contributes to the inhibition of recruitment of neutrophils and other phagocytes to the site of infection (34, 46).

Other than the important virulence factors listed above, cell-associated virulence factors also include fibronectin binding protein, streptococcal protective antigen, heme-

binding proteins, HtrA protease, protein G-related alpha-like surface protein, lipoprotein of GAS, CD15-related antigen, plasmin(ogen)-binding proteins, and serum opacity factors. Secreted virulence factors are listed in following paragraphs.

Streptococcal Pyrogenic Toxin B. SpeB was initially thought to be a superantigen called pyrogenic toxin B but is actually a non-specific cysteine protease. This protein can alter the disease process and host defenses by degrading host proteins such as immunoglobulins (56-58) and GAS proteins such as M protein (55).

Streptokinase. Ska enzymatically activates plasminogen into plasmin, a proteolytic enzyme, which in turn digests fibrin and other proteins. Therefore, Ska can lyse clots, enhancing the spread of GAS infection (59, 60).

DNases. GAS produces four antigenically distinct DNases to protect the bacteria from being trapped in neutrophil extracellular traps (NETs) by digesting the NETs' web of DNA, helping GAS escape from killing by serine proteases of neutrophil in the trap (47). In addition, several DNases have been identified as mitogenic factors (42, 61, 62).

Superantigens. These proteins are able to nonspecifically activate proliferation of T lymphocytes, resulting in the release of interleukins and cytokines. This family includes SpeA, SpeB, SpeC, SpeD, SpeF, SpeG, SpeH, SpeJ, SpeK, SpeL, SpeM, SSA, SMEZ, and SMEZ-2 (47).

Streptococcal Inhibitor of Complement. This protein can interact with various host cell proteins and components of the immune system (43, 63). It can evade innate

defense system by inhibiting the action of the complement system (64), inactivating alpha-defensins, such as LL37 (43), lysozyme and secretory leukocyte proteinase inhibitor (63). This protein also decreases colonization of the mucosal surface as well as internalization and killing of GAS, thereby enhancing bacterial survival by avoidance of the intracellular environment of PMNs (65, 66).

Streptolysins. GAS secretes two hemolysins, streptolysin O (SLO) and steptolysin S (SLS), and encodes three other putative hemolysins (42). Streptolysin S (SLS) is a potent cytolysin and is primarily responsible for the characteristic zone of beta-hemolysis surrounding GAS colonies grown on blood-agar medium (67). SLO interacts with membrane cholesterol, forming pores following aggregation in the membrane of host cells, such as erythrocytes, macrophages, leukocytes, and platelets. Recently, research suggests SLO can deliver proteins from the bacterial cytoplasm directly into the cytosol of a host cell (68-70). However, other research found that cytolysin-mediated translocation does not require pore formation by streptolysin O (71).

Regulation of Virulence Factors. GAS must adapt to the various niches that they encounter in the human host. Therefore, regulatory elements must respond to environmental signals and control the expression of virulence genes in GAS. GAS encodes two main types of regulatory proteins, namely stand-alone regulators (RRs) and two-component gene regulatory systems (TCS). Three RRs (Mga, RofA-like protein and Rgg/RopB) and two TCSs (CsrRS/CovRS and FasBCAX) are the major regulators of the virulence genes (72). Recent research indicates that mutations in virulence regulators can profoundly alter expression of virulence genes and thus modulate the infection niches and

severity. A pharyngeal infection strain and an invasive strain differ in transcription of 10% of the total genes, but the only genetic difference between them was a 7-bp frame-shift deletion in the *covS* gene of the invasion in the genome (73). A mutant strain carrying an 11-base insertion in the *covS* gene was isolated from the blood of a patient that was apparently infected with a wild-type pharyngeal infection strain (74). These findings suggest that the host infection niches provide an environment for selection of GAS mutants to survive at a particular niche.

Vaccine Studies

Several targets in GAS have been chosen for vaccine development. Since M protein is a critical virulence factor of GAS, development of a GAS vaccine has been primarily focused on the M protein. Some studies focused on the type-specific epitopes present at the amino terminus of the protein, and others evaluated conserved epitopes present in the C-repeat region towards the carboxy terminus of the protein. Although antibodies directed against the M protein enhance opsonophagocytosis and confer protection (75, 76, 77), M protein-based vaccines have various problems. Variable epitope-based vaccine cannot provide protection against all serotypes, and conserved epitope-based vaccine lacks high efficacy. Therefore, other vaccine candidates, such as the carbohydrate antigen, C5a peptidase, SpeB, and Sfb1, also have been explored.

Several GAS vaccines are currently in development. First, M protein-based multivalent, type-specific vaccine covers 26 different *emm* types (78). These 26 types represent the most common types found in US. The vaccine also includes one conserved epitope of a protective antigen (Spa) that is expressed in several serotypes. This is the

only GAS vaccine currently in human trials. The advantage of this vaccine is that it uses a known, highly-immunogenic epitope of the M proteins and does not contain any known cross-reactive epitopes. The disadvantages, as outlined above, are that even a 26-valent vaccine may be insufficient to protect against the wide variety of GAS strains in highly endemic populations and the potential that any protection may be short-lived as new *emm* types emerge that are not included in the vaccine. Another M protein vaccine candidate is based on a conserved epitope in the C-repeat region. A minimal B cell epitope has been identified within peptide 145, which is located within the conserved C-repeat region of the M protein and does not contain any T cell epitopes. This experimental vaccine may not have the risk of inducing an autoimmune response, because rheumatic valvulitis is predominantly T cell-mediated (79). This vaccine formulation is currently ready for phase I clinical trials (80). The third vaccine candidate is the GAS carbohydrate antigen. Antibodies to the GAS carbohydrate provide passive protection in a mouse challenge model (81). The fourth vaccine candidate is based on the C5a peptidase. Recombinant GAS C5a peptidase induces production of C5a peptidase-specific serum IgA and IgM and mucosal IgA in mice (82). This GAS vaccine candidate is presently being developed by Wyeth Lederle Vaccines (253). Other vaccine candidates tested include SpeB (83), adhesin Sfb1 (84), lipoteichoic acid (LTA), FBP54, streptolysin S, and pyrogenic exotoxins A (SpeA) and C (SpeC).

Iron and Iron Complex

Essential Metal Nutrients for Living Organisms

Metals are very important in biochemistry. As super acids, metals can increase the electrophilicity or nucleophilicity of reacting species, increase the acidity of a reacting species, and promote heterolysis (85). They also function as redox centers, carry oxygen, and use their abilities to bind ligands to act as molecular "switches" in signal transduction (86). Many enzymes must associate with a particular metal cofactor to function (87).

The biological metal ions are grouped into two types based on reaction mechanisms. One is the redox-inert metal ions that are used in enzymes to stabilize negative charges and to activate substrates by virtue of their Lewis acid properties. Magnesium, zinc and calcium are examples for this type. The other type is the redox-active metal ions that can be used both as Lewis acids and as redox centers. The most common metal ion of the second type is iron. This group also includes manganese, cobalt, molybdenum, copper and nickel (85).

Iron is one of the most critical metals in living organisms. Iron functions as a cofactor in proteins and participates in many major biological processes, such as oxygen transport, photosynthesis, N_2 fixation, methanogenesis, H_2 production and consumption, respiration, the tricarboxylic acid cycle, gene regulation, amino acid and DNA biosynthesis, and peroxide reduction. With three exceptions, all living organisms have an absolute requirement for iron in the range 0.4-4 μM (88-91). One of the three exceptions are the *Lactobacilli*, which are the only organisms that absolutely do not need iron (92,

93). The other two exceptions are *Borrelia burgdorferi* and *Treponema pallidum*. Both are intracellular parasites with minimal genomes and rely upon the iron-dependent metabolic processes of their host for energy and biosynthesis. Therefore, *B. burgdorferi* and *T. pallidum* still depend upon iron, albeit indirectly (94, 95).

Chemistry of Iron

Iron exists from oxidation state −2 to +6. Under physiological conditions, it mainly exists in one of two readily interconvertible redox states: the reduced or ferrous form (Fe^{2+}) and the oxidized or ferric form (Fe^{3+}). It can also adopt different spin states (high or low) in both the ferric and ferrous forms, depending on the ligand environment. These properties make iron an extremely versatile prosthetic component for incorporation into proteins as a biocatalyst and electron carrier (95).

The availability of Fe^{3+} and Fe^{2+} under various conditions is different. In aerobic environments, iron exists primarily in the ferric form. But the solubility of Fe^{3+} is low at physical pH (10^{-18} M at pH 7 and 10^{-24} M at pH 7.4). The solubility of Fe^{3+} increases at lower pH (10^{-8} M at pH 3). Fe^{2+} is highly soluble in water, but tends to be oxidized to Fe^{3+} in air. Fe^{2+} is the major form of iron under anaerobic or reducing conditions (96).

Iron is usually incorporated into proteins as a mono- or bi-nuclear species, in a more complex form as part of iron-sulfur clusters, or as heme. There are several reasons for iron binding to protein. First, iron is not stable in air. Second, free Fe^{2+} is deleterious for most macromolecules because it activates the Fenton reaction ($Fe^{2+} + H_2O_2 \rightarrow Fe^{3+} + OH^- + OH\bullet$), leading to the partial reduction of oxygen into hydroxyl radicals. Protection against the potential toxicity of Fe^{2+} is achieved by iron sequestration into

carrier proteins (97). Third, the biological functionality is almost entirely dependent upon its incorporation into protein. Insertion of iron into proteins allows its local environment to be controlled such that iron can adopt the necessary redox potential, geometry and spin state required for it to fulfill its designated biological function. Due to the wide range of redox potential, iron is particularly suited to participating in a wide range of electron-transfer reactions (95).

Heme

Heme is a prosthetic group that consists of an iron atom coordinated in the center of a large heterocyclic organic ring called a porphyrin. Sometimes heme refers to the ferrous iron-porphyrin complex, whereas the oxidized form is known as hemin. Both forms are commonly called heme, and we will apply this convention throughout this dissertation. As a prosthetic group in many proteins and enzymes, heme plays many roles in many fundamental biological processes, including O_2 storage and transport (e.g., myoglobin and hemoglobin), respiration and electron transfer (e.g., cytochromes), activation of the O-O bond (e.g., P450 enzymes and peroxidase), signal transduction and gas sensing (e.g., CooA, nitric oxide synthase (NOS) and soluble guanylate cyclase), and control of gene expression and microRNA processing. Heme can also serve as a source of both iron and porphyrin for microbes.

In mammals, the organs mainly involved in heme synthesis are the liver and the bone marrow, whereas degradation of heme begins inside macrophages of the spleen. The enzymatic process that produces heme is properly called porphyrin synthesis, as all the

intermediates are tetrapyrroles, which are chemically classified as porphyrins. In the degradation process, heme is converted to biliverdin and iron is released.

Heme usually binds into hemoproteins. Heme is a lipophilic molecule with low molecular weight, so it can easily intercalate into membranes and thus impair lipid bilayers and organelles and destabilize the cytoskeleton. Furthermore, because heme catalyzes the formation of reactive oxygen species, accumulation of heme inside cells will result in cellular damage, oxidative stress and tissue injury. Therefore, free heme is harmful to cells. When heme-containing molecules are degraded, released heme will be rapidly bound by molecules such as hemopexin and serum albumin. In the presence of those scavenging proteins, the concentration of free heme within mammals is maintained at very low levels.

Iron Sources of Bacteria

The level of free iron in the environment or in the host is below that required for microbial growth. As discussed in the previous paragraphs, iron usually is protected by associating into carrier protein or iron-complex. Mammalian hosts also can decrease the available iron to an even lower level in response to bacterial infection (98). The iron in the serum is decreased by a hypoferric response (90, 99, 100) and in the cell by iron depletion (101). Two mechanisms are involved in iron depletion in the cell. One mechanism is interferon gama-stimulated reduction in the expression of transferrin receptors (255). The other mechanism is removal of non-heme iron via the action of the reactive nitrogen intermediates, nitric oxide, nitrate and nitrite produced on conversion of L-arginine to L-citrulline (102, 103). Since the concentration of free iron in the physical

environment is very low, free iron is not the major source of iron for bacterial pathogens under normal physical condition but is the major iron source only under extreme conditions. Instead, iron-complexes and iron proteins are the major iron sources under physical conditions. The iron sources for bacterial pathogens are described below.

Fe^{2+}. Under anaerobic and reducing conditions, Fe^{2+} is the major form of iron. It is sufficiently soluble that it can be taken up by anaerobic bacteria without the help of iron chelators. Fe^{2+} diffuses freely through the outer membrane porins of Gram-negative bacteria. It is transported through the cytoplasmic membrane by a ferrous ion-specific ABC transporter (104).

Fe^{3+}**.** Fe^{3+} is more soluble at lower pH. Therefore, acid-tolerant bacteria might find enough Fe^{3+} to cover their iron needs (96). Under most environmental conditions, concentrations of Fe^{3+} are too low to meet the cell's iron requirements (10^5-10^6 irons per bacterial cell per generation). Some bacteria lower the external pH to render ferric iron more soluble. Others reduce ferric iron to the relatively soluble ferrous form or employ ferric iron chelators as solubilizing agents (95).

Ferric Transferrin and Lactoferrin Complexes. Transferrin is the iron carrier in the blood and lactoferrin is the iron carrier in mucosal secretions. Both proteins exhibit an extremely high affinity for Fe^{3+} and have much lower affinities for Fe^{2+}. Many bacterial species, such as *Neisseria meningitidis* and *Neisseria gonorrhoeae*, have iron-uptake systems to directly acquire iron from ferric transferrin and ferric lactoferrin complexes (105). In Gram-negative bacteria, iron from transferrin/lactoferrin is extracted by an outer

membrane protein at the cell surface (97). Some Gram-positive bacteria also acquire iron from ferric transferrin. Staphylococci express transferrin-binding protein A, which is a cell wall-anchored protein (106). Not all bacteria can use transferrin iron. GAS cannot use transferrin iron, nor can *Bacillus anthracis*.

Ferritins. Ferritins are spherical, shell-like iron-storage proteins. Ferritin consists of 24 subunits assembled into a hollow sphere, with a diameter of ~120 Å, filled with several thousand of Fe^{2+} ions (107). These cytoplasmic proteins store iron, making it available in case of iron shortage, and protect the cells from the toxic effects of iron accumulation. Following cell lysis, ferritins are also found in the plasma. Ferritin as an iron source for bacteria is not common, although research indicates that exogenous ferritin is reduced by *Listeria monocytogenes* (108) and the addition of ferritin to *Pasteurella multocida* changes gene expression (109). In addition, recent research indicates that *Burkholderia cenocepacia* can utilize ferritin as an iron source (110).

Heme. Heme is scarcely found free in mammals. However, in laboratory conditions, heme can be used as an iron source by many bacterial species.

Hemoglobin. Hemoglobin is a tetramer with two alpha and two beta chains. Each subunit binds a heme molecule. Heme iron is penta-coordinated to four nitrogen atoms in the porphyrin ring and to the imidazole of one histidine residue. The sixth coordination site is free in methemoglobin (the oxidized form of hemoglobin) and can be occupied by oxygen or carbon dioxide in hemoglobin (the reduced form of hemoglobin) (111). Many bacterial pathogens have uptake systems to acquire heme from

methemoglobin, and *N. meningitidis* takes up methemoglobin faster than oxyhemoglobin (113). The uptake systems usually contain a receptor that binds hemoglobin and extracts heme from it (112). Hemoglobin binding to whole cells has been detected by various techniques, whereas globin binding has never been observed. This does not mean that the peptide part does not contribute to binding to receptors because heme ligation to globin has profound effects on globin conformation.

Haptoglobin-Hemoglobin. Haptoglobin is a tetrameric glycoprotein. In serum, haptoglobin binds released hemoglobin with high affinity and inhibits its oxidative activity. The haptoglobin-hemoglobin complex can be used as the iron source for some bacterial organisms (114, 115).

Hemopexin. Hemopexin can bind with heme that is released into the plasma. Hemopexin is a 60-kDa glypoprotein with two similarly folded domains that tether the ligand by a bis-histidyl ligation (116). Several bacteria have been reported to bind and/or to use heme-hemopexin. For example, *Haemophilus influenzae* has a surface hemopexin binding protein and can acquire heme from hemopexin for use as a source of both essential porphyrin and iron (117).

Albumin. Albumin is a serum heme carrier and can be used as iron source for bacteria. However, no albumin-specific receptors have been described. As the affinity of albumin for heme might be in the same range as that of bacterial surface receptors for heme, it is likely that heme bound to albumin is recognized by heme/hemoglobin receptors and passively transferred from albumin to the receptors (97).

Other Hemoproteins. There are many other hemoproteins in which heme is not covalently linked to the proteins. They include leghemoglobin, catalase, and type b cytochrome, and most of them are satisfactory heme sources for bacteria in laboratory media. However, bacteria do not have specific receptors for any of these proteins. Thus, it is likely that heme is the molecule recognized. Heme may be stripped off at the cell surface by an as yet uncharacterized mechanism or could be released after hemoprotein degradation by surface proteases or extracellular proteases (118). Indeed, many bacterial extracellular proteases are induced in iron-restricted media.

Intracellular Fate of Heme in Bacteria

Once internalized, protoporphyin of heme is degraded into biliverdin and CO_2 to release iron. This degradation reaction is catalyzed by heme monoxygenase (119). To date, two types of heme oxygenase systems have been described in Gram-positive pathogens, HmuO from *Corynebacterium diphtheria* (120) and IsdG and IsdI from *S. aureus* (121).

Iron and Heme Transport in Gram-Negative Bacteria

Facing the extremely low free iron levels, both in the environment and in vivo, bacteria have evolved a number of different strategies to obtain sufficient amounts of this essential nutrient. The iron/heme acquisition systems in bacteria can be divided into two categories based on how iron and its complexes are caught in the first step of the acquisition process. The first category involves direct acquisition of iron and heme from iron sources by specific receptors on the bacterial surface. Uptake systems of the second

category rely on small iron chelators called siderophores and heme-binding proteins called hemophores that are released by bacteria into the extracellular medium to acquire iron or heme from various sources. In Gram-negative bacteria, following being caught by specific receptors or iron chelators, iron/heme will be transported through the outer membrane and then the cytoplasmic membrane. Each of those steps and the two categories of the first step are discussed in detail next.

Siderophores

Siderophores are produced by many microorganisms that chelate ferric ion with extremely high affinity, allowing the solubilization and extraction of iron from most mineral or non-heme iron complexes. Siderophores are small compounds (less than 1000 molecular weight) that are highly electronegative and bind Fe^{3+}, preferentially forming hexacoordinated complexes. Siderophores can be produced by Gram-positive and Gram-negative bacteria and can be recognized at the cell surface by specific membrane-anchored proteins in Gram-positive bacteria and by specific outer membrane receptors in Gram-negative bacteria. Unlike iron-binding proteins that strip iron on the cell surface of Gram-negative bacteria, siderophores are internalized through the outer membrane as a whole. More than 500 different siderophores have been described. Most have a peptide backbone with several non-protein amino acid analogs including both modified amino acids and D-amino acids. The iron ligation groups have been classified into three main types: hydroxamate, catechol rings, and hydroxyl acid. Some siderophores contain more than one of these three iron-chelating groups (97).

Hemophores

Hemophores are secreted by bacteria and are specialized extracellular proteins that capture free heme or extract heme from diverse sources. After capturing heme, hemophores bring it to a specific outer membrane receptor in Gram-negative bacteria and a surface protein in Gram-positive bacteria. One of the examples for hemophores is HxuA produced by *H. influenza*, which is an organism that lacks the heme biosynthesis pathway and requires exogenous heme for aerobic growth. HxuA is a 100-kDa secreted protein which binds heme-loaded hemopexin (122). The heme-hemopexin-HxuA complex is presented to HxuC, a specific outer membrane receptor (123). Another example for hemophores is HasA, which has been identified in several bacteria including *Serratia marcescens, Pseudomonas aeruginosa, P. fluorescens, Yersinia pestis,* and *Y. enterocolitica.* HasA acquires heme from hemoglobin and delivers it to HasR, the receptor for HasA-heme complex. *Porphyromonas gingivalis* also has a novel hemophore-like protein HusA (125). Hemophore is rare in Gram-positive bacteria. The only known hemophore in gram-positive bacteria is IsdX1, which is produced by *Bacillus anthracis* (124).

Outer Membrane Receptors

Siderophores, heme, and iron/heme binding proteins are too big to diffuse through porins in the outer membrane and are also generally present at low concentrations in the extracellular medium. Thus, Gram-negative bacteria produce outer membrane receptors that specifically catch those iron and iron complexes.

These receptors share common characteristics. They have five conserved residues at the N terminus. This motif is involved in interaction with a protein called TonB and is thus named the "TonB box" (126, 127). The receptors have a "plug and beta-barrel" organization derived from the first ~160 residues at the N-terminus that is positioned in the pore towards the periplasmic end of the barrel (128-133). The plug or hatch is folded inside the beta-barrel. The plug gates the channel, limiting access to the periplasm. Binding of substrates triggers small conformational changes of the plug; larger movements are seen on the periplasmic side where the TonB box is found. Closure of the outside loops prevents release into the medium (97).

The specificity for iron forms of outer membrane receptors is different. For example, The HemR protein of *Y. enterocolitica* recognizes heme (134). The HasR receptor can use three substrates: free heme, hemoglobin, and the holo-HasA hemophore (135). Several bacteria express bipartite receptors for either hemo- or ferri-protein. The transferrin receptor from *Neisseria* strains and the hemoglobin/haptoglobin or hemopexin receptors from *Hemophilus* strains belong to this class (97).

Transport of Iron, Iron-siderophore,
and Heme Across the Outer Membrane

The outer membrane receptors have specific mechanisms to ensure stripping of iron and heme from iron protein complexes and hemoproteins on the extracellular surface of the outer membrane and replacement of iron- and heme-free ligands with iron- and heme-containing substrates as well. The iron-free proteins are released extracellularly. Only the prosthetic group is transported across the outer membrane.

Transport of iron, ferri-siderophores or heme through outer membrane requires energy. This energy is provided by the electrochemical charge gradient of the cytoplasmic membrane and is delivered by the energy-transducing TonB-ExbB-ExbD protein complex (95). The TonB protein is anchored in the cytoplasmic membrane by an uncleaved leader sequence and spans the periplasmic space to interact directly with the outer membrane receptors. A conserved hydrophobic seven-amino acid segment, the "TonB box" at the N-terminus of TonB-dependent outer membrane receptors, physically interacts with the TonB protein. Other regions of outer membrane receptors are also involved in TonB interaction. ExbB and ExbD are integral cytoplasmic membrane proteins. It is believed that ExbB and ExbD use the membrane electro-chemical charge gradient to produce an "energized" form of TonB that mediates a conformational change in the liganded outer membrane receptor. This in turn leads to translocation of the ligand to the periplasmic space and de-energization of TonB (136, 137). In the most recent model, discharged TonB is then recycled to the cytoplasmic membrane to be re-energized by the energy coupling proteins, ExbB/D (138, 139).

Iron Siderophore and Heme
Transport across the Cytoplasmic Membrane

Transport of heme or ferri-siderophore across the cytoplasmic membrane is mediated by ATP-binding cassette (ABC) transporters. ABC transporters consist of a periplasmic substrate-binding protein, a membrane protein called permease, and an intracellular ATPase. The substrate-binding protein acts as a shuttle, collecting iron siderophore or heme released from the outer membrane receptor and delivering it to a cognate permease in the inner membrane. The best characterized substrate binding

protein is the ferric siderophore-binding protein, FhuD from *E. coli*. FhuD transports ferroc ferrichrome and other hydroxamate siderophore iron complexes. The crystal structure shows that the ferrichrome homolog gallichrome is held in a shallow pocket lined with aromatic groups; Arg and Tyr side chains interact directly with the hydroxamate moieties of the siderophore (256). The ABC permease complexes consist of four modules: two identical or homologous integral membrane permease modules and two ABC modules located on the inner surface of the inner membrane.

Feo is a ferrous iron transport system. A major component of this system is the FeoB protein. The iron transport function of Feo appears to be of particular importance during low oxygen conditions when ferrous iron remains stable and predominates over ferric iron. Some bacteria, such as *E. coli* and *H. pylori*, have extracellular ferric reductase to convert ferric iron to ferrous iron and transport iron using the ferrous iron transporter (140, 141).

Another type of bacteria iron transporter on the cytoplasmic membrane is the metal-transporting binding-protein-dependent ABC transporter system that has specificity for iron but does not require outer membrane receptors or siderophores. Such systems include the SfuABC, SitABCD, YfeABCD, FebABC and FutABC transporters of *S. marcescens*, *Salmonella typhimurium*, *Yersinia pestis*, *N. gonorrhoeae*, and *Synechocystis* PCC 6803 (95).

Iron and Heme Acquisition Systems in Gram-positive Bacteria

Unlike Gram-negative bacteria, Gram-positive bacteria do not have the outer membrane but have a thick cell wall composed of murein sacculus, attached

polysaccharides, teichoic acids, and cell wall proteins. Many surface proteins, including hemoglobin receptors, in Gram-positive bacteria are linked to the cell wall by sortase, a transpeptidase that recognizes a conserved LPXTG motif at the C-terminus of surface protein substrates and covalently links the protein to the peptidoglycan cross-bridges (142). The cell wall is typically 15–30 nm thick and is a substantial barrier for ligands bound at the surface to move to the membrane. Thus, surface proteins may be used by the cell if passive diffusion through the cell wall is not sufficient. The surface proteins relay heme to specific ATP-binding cassette (ABC) transporters. ABC transporters in Gram-positive bacteria are similar to the ABC transporters in Gram-negative bacteria and consist of three components, a lipoprotein substrate receptor found on the external surface of the membrane, one or two transmembrane permease proteins and an ATPase. The ATPase interacts with the permease and couples active transport to ATP hydrolysis.

Iron and Heme Acquisition Systems in GAS

Iron Sources for GAS. A number of heme-containing proteins can support in vitro growth of this organism, including hemoglobin, the haptoglobin−hemoglobin complex, myoglobin, heme−albumin, and catalase (143). However, GAS cannot use transferrin or lactoferrin iron. The preferred iron source for GAS is heme.

Iron Acquisition Systems. GAS genome encodes three ABC transporters, namely, FtsABCD, MtsABC, and HtsABC. FtsB, the lipoprotein of FtsABCD, binds Fe^{3+} ferrichrome, and inactivation of *ftsB* or *ftsC*, but not *htsA* or *mtsA*, diminished Fe^{3+} ferrichrome uptake, indicating that FtsABCD is the transporter that takes up Fe^{3+}

ferrichrome (144). FtsABCD is also called the Siu system that was reported to acquire iron from hemoglobin, heme, blood and serum (145). However, FtsB, the lipoprotein component, does not bind heme.

MtsA, the lipoprotein of MtsABC, binds iron, zinc and manganese in vitro and is involved in uptake of manganese and ferric iron (146). The order of the binding affinity of MtsA for metal ions is $Fe^{2+} > Fe^{3+} > Cu^{2+} > Mn^{2+} > Zn^{2+}$, and bicarbonate increases the affinity of MtsA for Fe^{2+} (147). These findings suggest that Fe^{2+} is the primary substrate for MtsA under physiologically relevant conditions. The crystal structure of MtsA (148) is similar to those of the manganese receptors PsaA and MntC, consistent with the similar coordination requirements of Fe^{2+} and Mn^{2+}. Thus, MtsABC may take up both Fe^{2+} and Mn^{2+}.

HtsA, the lipoprotein of HtsABC, binds heme (149). HtsABC, which is also called sia (streptococcal iron acquisition) (150), is co-transcribed with 6 other genes, including the surface proteins Shr and Shp (151, 152). These characterizations indicate that the Shr/Shp/HtsABC locus encodes a heme uptake system.

Iron and Heme Acquisition Systems of *Staphylococcus aureus*

The Isd Heme Uptake System. *S. aureus* produces transporter systems to acquire heme, ferrous iron, iron siderophore complexes, and transferrin iron. The most characterized system is the iron-regulated surface determinants (Isd) system, which is involved in heme acquisition. The Isd system contains nine proteins, including the cell wall-linked proteins IsdA, IsdB, IsdC and IsdH (also referred to as HarA), the ABC

transporters IsdDEF, and cytoplasmic heme-degrading enzymes IsdG and IsdI (153-154, 121, 252).

Siderophore Uptake Systems. There are four iron-regulated ABC transporters in *S. aureus*, and three of them have been demonstrated to be involved in uptake of Fe^{3+} siderophore complexes (155). HtsABC is involved in uptake for staphyloferrin A. SirABC can transport staphyloferrin B and staphylobactin (156). FhuCBG-D1-D2 is required for uptake of Fe^{3+} hydroxamate complexes. The substrate for the fourth iron-regulated ABC transporter (SstABCD) has not been identified (157).

Heme Uptake System in *Bacillus anthracis*

B. anthracis has an Isd heme uptake system that consists of IsdC, IsdX1, IsdX2, IsdE1, IsdE2, IsdF and IsdG. These genes fall into three putative transcriptional units, each flanked by a Fur-box consensus sequence. This system is different from the *S. aureus* Isd system in that the *B. anthracis* Isd system uses secreted proteins IsdX1 and IsdX2 to scavenge heme. IsdX1 and IsdX2 are two NEAT domain-containing proteins to remove heme from hemoglobin and deliver heme to IsdC. IsdC is anchored to the cell wall by the sortase SrtB (153, 154, 158-161).

Another *B. anthracis* heme scavenger called S-layer protein K (BslK) harbors a NEAT domain, binds heme, and directionally transfers it to IsdC. The S-layer is a crystalline array of protein that surrounds the bacterial cell and may serve a multitude of functions, including maintenance of cell architecture and protection from host immune components. This finding suggests that the Isd system can receive heme from multiple

inputs and may reflect an adaptation of *B. anthracis* to change iron reservoirs during infection (162).

Iron and Heme Uptake Systems in *Listeria monocytogenes*

L. monocytogenes encodes potential Fur-regulated iron transporters *fhu*, *feo*, *srtB*, and *hupDGC*. Deletions of the *fur-fhu* and *hupDGC* loci diminished iron uptake from ferric hydroxamates and heme/hemoglobin, respectively. Deletion of *hupC* eliminated the uptake of heme and hemoglobin, and decreased the virulence of *L. monocytogenes* by 50-fold in mice. Deletion of *fhuD* or *fhuC* also strongly reduced [^{59}Fe]-ferrichrome uptake.

Heme Uptake System in *Corynebacterium diphtheriae*

C. diphtheriae proteins involved in uptake and utilization of heme as an iron source include the ABC transporter HmuTUV genes, surface proteins HtaB and HtaC, and heme oxygenase HmuO (163). HmuT, hmuU and hmuV, shared striking homology with genes in ABC (ATP-binding cassette) transport system. HtaA and HtaB are able to bind heme, suggesting that these proteins may function as heme/hemoglobin receptors.

Iron and Heme Uptake in *Streptococcus pneumoniae*

Pneumococci have been reported to utilize ferric and ferrous iron salts, hemoglobin, and heme as iron sources (164, 165, 254). Several transporters have been studied (166). First, the choline-binding surface protein PspA binds human lactoferrin, suggesting a role in iron acquisition (167, 168). Second, heme-binding proteins were located in both soluble extract and envelope fractions of pneumococcal cells (169). Two genetic loci, *pit*1 and *pit*2, encoding homologues of ABC iron transporters are responsible

for the hemoglobin utilization of *S. pneumoniae* (164). A solute heme binding protein PiuA in *S. pneumonia* has been reported. PiuA is a lipoprotein, binds heme and hemoglobin, and resides on the cytoplasmic membrane (170). Although pneumococci do not secrete any detectable siderophores, a ferric hydroxamate transport system has been detected, which can transport ferric ferrichrome and ferric ferrioxamine B as iron sources (171). This transport system is a predicted ABC transporter composed of lipoprotein FhuD, permease FhuB and FhuG, and ATPase FhuC.

Structural Basis and Mechanisms of Heme Acquisition in Bacteria

Heme-Binding Proteins

Proteins involved in heme acquisition in bacterial pathogens usually bind heme with extremely high affinity (association constants for heme binding are $>10^{10}$ M^{-1}). Heme iron in hemoproteins is either in a pentacoordinate or hexacoordinate form with four ligands from protoporphyrin IX and one or two axial ligands from the side chains of His, Lys, Tyr, Met, and/or Cys residues of proteins. Combinations of the strong ligands, His, Lys, Met, and Cys, in the hexacoordinate binding usually result in the low spin iron state. The low spin Fe(II) state is characterized by a strong optical absorption Soret peak and two Q_{ov} or $\alpha\beta$ bands. Pentacoordinate heme iron is in the high spin state and lacks the dominant α band at the Fe^{2+} state (172). The wavelength of the Soret peak is determined by the number of coordination and axial ligands. Furthermore, the hexacoordinate and pentacoordinate heme irons have dramatic differences in intensity of the Soret band in their magnetic circular dichroism spectra properties (173, 174). Both the axial coordination and the interaction between the heme pocket in proteins and the

protoporphyrin of heme are critical to affinity of proteins for heme. Different ligation combinations can also have subtle or dramatic shifts in absorption spectra of bound heme.

Shr, Shp, and HtsA of the GAS system and IsdB, IsdA, IsdC, and IsdE of the *S. aureus* system bind heme (175-178). The heme iron in the three GAS proteins is hexacoordinate, and Met66/Met153 and Met79/His229 residues were confirmed or identified as the axial ligands of the Shp and HtsA heme irons, respectively, whereas IsdA, IsdC, and IsdE use Tyr, Tyr, and Met/His as their axial ligand(s), respectively (179-181).

Heme Transfer between Proteins

Heme transfer among heme-binding proteins of heme acquisition machineries in bacteria at a biochemical level has only been studied in a few systems. One is the hemophore HasA/HasR system of Gram-negative *S. marcescens* (182, 183), and heme transfer from hemoglobin to HasA and from HasA to HasR has been demonstrated. Structural and thermodynamic studies of heme transfer in this system suggest that formation of a HasA-HasR complex may be the driving force for heme transfer (182, 184). The *Shigella dysenteriae* outer-membrane receptor was reported to take up heme from hemoglobin. Although the mechanism of this heme transfer is not clear, it has been shown that the axial ligands in ShuA are essential for substrate recognition, heme coordination, and transfer (185). A recent structural study of ShuA suggests an induced fit mechanism of heme binding in ShuA, which is comparable to the binding of the heme-HasA complex by HasR in *S. marcescens* (244).

Our laboratory has demonstrated heme transfers from one protein to another in the GAS, *Streptococcus equi*, and *S. aureus* heme acquisition systems, including the transfer from Shr to Shp (186), from SeShp to SeHtsA (187), from IsdA to IsdC (188), from methemoglobin to IsdB, from IsdB to IsdA and IsdC, and from IsdC to IsdE (189).

Pathway of Heme Acquisition in GAS and *S. aureus*

Shr efficiently transfers its heme to Shp, but not to HtsA (190), and Shp directly donates its heme to HtsA (191, 192). Our results support a pathway of heme uptake by GAS in which Shr extracts heme from methemoglobin (metHb) and Shp relays heme from Shr to HtsA.

The current model of heme transfer through the cell wall by the *S. aureus* Isd system is based on the kinetics of heme transfer among the Isd proteins and their cellular localizations. The surface heme-binding proteins that move heme through cell wall are positioned at varying depths in the cell wall. IsdB and IsdH are exposed to the environment, while IsdA is partially exposed and IsdC is buried within the cell wall (153). The localization of these proteins led to the proposed mechanism of transfer from IsdB/IsdH to IsdA to IsdC to IsdE (193). The kinetics of heme transfer among the Isd proteins in vitro support this model of the heme acquisition pathway (190, 194, 195). Heme is transferred from metHb to IsdB or IsdH. Heme is transferred rapidly from IsdB to apoIsdA and apoIsdC. Heme bound to IsdA can then move to IsdC, and only IsdC efficiently transfers heme to IsdE. Alternatively, Muryoi et al. demonstrated that heme transfer to IsdE may occur directly from IsdB-N2 or IsdH-N3 (194). Since protein localization on the cell wall likely affects transfer rates, it is more likely that IsdA and

IsdC relay heme from IsdB to IsdE. Each proposed heme transfer step is rapid and occurs between recombinant proteins and between recombinant NEAT domains alone. Since heme transfer rates between NEAT domain-containing Isd proteins are at least 10,000 times greater than the rate of heme dissociation, transfer is likely mediated by activated complex formation (190, 194, 195). Isd protein–protein complexes have not yet been physically observed or characterized on a molecular level.

Mechanism of Heme Transfer

Ferric Shp transfers heme to apoHtsA at a rate constant of $43 \pm 3\ s^{-1}$, which is ~ 4,000 times greater than the rate of simple heme dissociation from ferric Shp into solvent. In the reaction of ferrous Shp with apoHtsA, heme is transferred to apoHtsA with a rate constant of $28 \pm 6\ s^{-1}$, and the resulting ferrous HtsA product then autoxidizes to ferric HtsA (196). This detailed kinetic analysis of Shp-apoHtsA heme transfer found that the heme transfer reactions follow a concerted two-step kinetic mechanism in which Shp first forms a complex with apoHtsA and then transfers its heme to apoHtsA with a single kinetic phase (196). The formation of the transient Shp-apoHtsA releases free energy that is used to speed up heme transfer (196). These kinetic and thermodynamic results suggest that Shp-to-HtsA heme transfer involves an activated Shp-apoHtsA complex. Another kinetically characterized heme transfer reaction, heme transfer from IsdA to IsdC also suggests an activated donor-aceptor complex prior to heme transfer (188) (197) (198). However, there is no direct evidence for that Shp/apoHtsA or IsdA/apoIsdC interaction alters heme binding in Shp or IsdA before heme transfer.

Heme transfer from the cytoplasmic protein PheS to heme oxygenase pa-HO of *Pseudomonas aeruginosa* was also recently reported (199). These two proteins have much lower affinity for heme than the heme acquisition proteins of GAS and *S. aureus* (188). K_d values for binding of ferric heme to PheS and pa-HO are ~10^{-7} M versus ~10^{-10} -10^{-13} M for ferric heme-binding to Shp, HtsA, IsdA, and IsdC, and the rate constant for heme transfer from PheS to pa-HO is about 1/100 of that for heme transfer from Shp to HtsA.

Apparently, the heme transfer processes outside the cell have evolved novel mechanisms to rapidly transfer heme, even though heme donors have extremely high affinity for heme. However, the chemical mechanism of heme transfer remains unknown.

Objective

The objective of this project is to elucidate the molecular mechanism of heme transfer from Shp to HtsA as a model to understand how heme is directly transferred from one protein to another in heme acquisition. The kinetic mechanism of the Shp-apoHtsA reaction implies that the reaction follows either a sequential axial displacement mechanism where the first axial displacement is rate-limiting or a simultaneous axial displacement mechanism in which the two axial bonds of the heme iron in the holoHtsA product are formed at about the same time. We hypothesize a “plug-in” mechanism for the Shp-apoHtsA heme transfer reaction. In this hypothetic model, the empty heme pocket in apoHtsA plugs in along the two sides of the bound heme in Shp, and the side chains of the axial ligands in apoHtsA approach the two axial bonds of the Shp heme iron

and displace the Shp axial residues to pry the cofactor out of Shp. We tested this model by examining the effects of Ala replacements of the axial ligand residues of the Shp and HtsA heme iron on heme transfer and autoxidation of ferrous Shp. The first part of the research identified the axial ligands of the HtsA heme iron and characterized the axial mutants of Shp and HtsA in the coordination, spin state, and accessibility of the heme iron and stability and heme affinity of the mutants by using the UV-visible, electron paramagnetic resonance, Magnetic CD, and Resonance Raman spectroscopies and pH titration. The information obtained is crucial for monitoring of heme transfer and interpreting transfer data.

The second part investigated the effect of the elimination of the axial ligands of the Shp heme iron on Shp-HtsA heme transfer, providing evidence supporting the "plug-in" model. The third part examined the effect of the elimination of the axial ligands of the HtsA heme iron on Shp-to-HtsA heme transfer and autoxidation of ferrous Shp, yielding information on the critical role of the axial ligands of the HtsA heme in heme transfer and conclusive evidence for the formation of an activated Shp-apoHtsA complex.

SPECTROSCOPIC IDENTIFICATION OF HEME AXIAL LIGANDS OF HTSA THAT ARE INVOLVED IN HEME ACQUISITION BY GROUP A STREPTOCOCCUS

Abstract

Mutagenesis and spectroscopic analyses were performed to identify the heme axial ligands in HtsA and to characterize axial mutants of HtsA. Replacements of the M79 and H229 residues, not the other methionine and histidine residues, with alanine convert UV−Vis spectra of HtsA with a low-spin, hexacoordinate heme iron into spectra of high-spin heme complexes. Ferrous M79A and H229A HtsA mutants possess magnetic circular dichroism (MCD) spectra that are similar with those of proteins with pentacoordinate heme iron. Ferric M79A HtsA displays UV−Vis, MCD, and resonance Raman (RR) spectra that are typical of a hexacoordinate heme iron with histidine and water ligands. In contrast, ferric H229A HtsA has UV−Vis, MCD, and RR spectra that represent a pentacoordinate heme iron complex with a methionine axial ligand. Imidazole readily forms a low-spin hexacoordinate adduct with M79A HtsA with a K_d of 40.9 μM but not with H229A HtsA, and cyanide binds to M79A and H229A with K_d of 0.5 and 19.1 μM, respectively. The ferrous mutants rapidly bind CO and form simple CO complexes. These results establish the H229 and M79 residues as the axial ligands of the HtsA heme iron, indicate that the M79 side is more accessible to the solvent than the H229 side of the bound heme in HtsA, and provide unique spectral features for a protein with pentacoordinate, methionine-ligated heme iron. These findings will facilitate elucidation of the molecular mechanism and structural basis for rapid and direct heme transfer from Shp to HtsA.

Introduction

The proteins involved in heme acquisition in bacteria usually bind heme. Heme iron in hemoproteins is either in a pentacoordinate or hexacoordinate form, with four ligands from protoporphyrin IX and one or two axial ligands from the side chains of histidine, lysine, tyrosine, methionine, and/or cysteine residues of proteins. Combinations of the strong ligands, histidine, lysine, methionine, and cysteine, in the hexacoordinate binding result in the low-spin Fe(III) and Fe(II) states with strong absorption Soret peak and two Q_{ov} or αβ bands, whereas pentacoordinate heme iron is in the high-spin state and lacks the dominant α band at the reduced state (200). The heme iron in Shp and HtsA is hexacoordinate and in the low-spin state (201), and the Shr heme iron is also hexacoordinate (202). According to the crystal structure and protein engineering experiments, the heme iron axial ligands of the Shp heme iron are methionine 66 and methionine 153 (231, 192). In contrast, the IsdA, IsdC, and IsdE proteins of the *S. aureus* system utilize tyrosine, tyrosine, and methionine/histidine residues as their axial ligand(s), respectively (16, 204, 205). Spectroscopic analyses indicate that the HtsA heme iron has a low-spin hexacoordination with methionine and histidine axial ligands (206). However, the identities of these axial ligands have not been experimentally established.

The Shp-to-HtsA heme transfer reaction follows a concerted two-step kinetic mechanism in which Shp first forms a complex with heme-free HtsA (apoHtsA) and transfers its heme to apoHtsA in a single kinetic phase with a rate constant of 43 s^{-1}, which is ~40,000 times greater than the rate of simple heme dissociation from oxidized Shp (201). This kinetic mechanism implies that the reaction follows either a sequential

axial displacement mechanism where the first axial displacement is rate-limiting or a simultaneous axial displacement mechanism in which the two axial bonds of the heme iron in the holoHtsA product are formed at about the same time. Heme axial mutants of HtsA and their properties in coordination, spin state, various spectra, and accessibility on the axial sides will be valuable to vigorously establish the axial displacement mechanism of the Shp/HtsA reaction. Thus, each of the histidine and methionine residues of HtsA was replaced with alanine by site-directed mutagenesis, and resulting HtsA mutants were characterized by UV−Vis, MCD, EPR, and RR spectroscopies, and accessibility to exogenous ligands. The results demonstrate that the heme iron of the H229A mutant protein is pentacoordinate and inaccessible to imidazole, and the M79A mutant protein has a hexacoordination with water and His ligands, indicating that the M79 and H229 residues are the axial ligands of heme in HtsA and that the M79 side of the heme pocket is more accessible than the H229 side.

Materials and Methods

Materials

The QuickChange site-directed mutagenesis kit was purchased from Stratagene (La Jolla, CA). Resins for protein purification were from GE Healthcare Biosciences (Piscataway, NJ). Bovine hemin chloride was from Sigma. Imidazole, sodium fluoride, and potassium cyanide were purchased from ACROS Organics.

Gene Cloning and Site-Directed Mutagenesis

A histidine residue in the 6×His tag of 6×His-tagged M79A HtsA at high concentrations could ligate to the heme iron in this mutant. To avoid the 6×His tag in recombinant HtsA, the *htsA* gene in pLP1795 (207) was PCR cloned into pET-21d at the NcoI and EcoRI sites using primers 5′-ACCATGGGTAGTGCTGAAACTGGTGTGAATCAGCACCCTAAAAC-3′ and 5′-CGAATTCTTAGTTTTCACTTGATAAGATTG-3′, yielding pLP1795-2. The nucleotides underlined were included in the primer to introduce a 7 amino acid residue tag (MGSAETG) that is fused to the second residue, asparagine 21, of mature HtsA. This peptide fragment was included to achieve overexpression of HtsA because, for unknown reason, there was no overexpression of mature HtsA without any tag. Each histidine or methionine residue of HtsA was replaced with alanine using the QuickChange XL site-directed mutagenesis kit, plasmid pLP1795-2, and paired primers with an alanine codon replacing the corresponding histidine or methionine codon according to manufacturer's protocol. The cloned *htsA* and mutant genes were entirely sequenced to rule out spurious mutations and to confirm desired mutations.

Protein Purification

Recombinant HtsA and its mutant proteins were expressed in *Escherichia coli* BL21(DE3) containing corresponding plasmids by IPTG induction. The cell pellet from a 6 L culture was resuspended in 50 mL of Tris-HCl, sonicated on ice for 15 min, and centrifuged. The supernatant obtained was loaded onto a DEAE column (2.5 × 10 cm), and the column was washed with 200 mL of Tris-HCl, pH 8.0, and eluted with a 150 mL

linear gradient of 0−0.25 M NaCl. Fractions containing HtsA were pooled, and the sample was adjusted to 1.3 M $(NH_4)_2SO_4$ and loaded onto a phenyl-Sepharose column (1.5 × 5 cm). The column was washed with 100 mL of 1.3 M $(NH_4)_2SO_4$ and eluted with a 100-mL linear gradient of 1.3−0 M $(NH_4)_2SO_4$. Fractions containing >95% HtsA, as assessed by SDS−PAGE, were pooled and dialyzed against 20 mM Tris-HCl.

Preparation of Holo-HtsA Proteins

Purified HtsA proteins were a mixture of holo and apo forms. Homogeneous holoHtsA proteins were obtained by reconstitution with heme, as previously described (207). Protein concentrations were determined using the modified Lowry protein assay kit from Pierce with bovine serum albumin as a standard. Heme contents of holoHtsA proteins were measured with the pyridine hemochrome assay using ε_{418} = 191.5 mM^{-1} cm^{-1} (208).

MCD Measurements

MCD spectra of oxidized and reduced holoHtsA proteins in 50 mM phosphate buffer at indicated pH were recorded using JASCO J-710 spectropolarimeter equipped with an Alpha Scientific 3002-1 electromagnet under the following conditions: Bandwidth, 1 nm; accumulation, 3 scans; scan rate, 100 nm/min; resolution, 0.5 nm; magnetic field, 12.9 kG (1.29 T); and temperature, 25 °C. The spectra of the reduced proteins were taken in the presence of excess dithionite. Buffer blank-corrected CD spectra obtained without magnetic field were subtracted from corresponding buffer-corrected MCD spectra using the Jasco software. These processed MCD data were then used to calculate the final MCD data in units of $\Delta\varepsilon_M$ $(M\ cm\ T)^{-1}$ based on protein

concentration, light path, magnetic field, and molar ellipticity Θ_M (deg cm^2 $dmol^{-1}$ T^{-1}) = 3300 $\Delta\varepsilon_M$.

Resonance Raman (RR) Spectroscopy

RR spectra of HtsA proteins in 20 mM Tris-HCl buffer were recorded with a krypton ion laser (I-302-Coherent) equipped with a Spex Triplemate Raman spectrophotometer and a liquid nitrogen-cooled CCD detector using the following conditions: Laser excitation wavelength, 413.1 nm; number of scans, 3−25; integration time per scan, 25 s; and power, 10−20 mW. Raman frequencies were calibrated using aspirin.

Electron Paramagnetic Resonance (EPR) Measurement

EPR spectra of HtsA proteins were measured with a Bruker EMX spectrometer using the following conditions: Frequency, 9.6 GHz; power, 3 mW; modulation amplitude, 10 G; modulation frequency, 100 kHz; and temperature, 10 K. Estimation of the low-spin signals was based on comparison of the area of the g = 3 absorption-like signal with the analogous low-spin signal of metmyogolbin at pH 9.5 (Mb(Fe(III)OH)).

Binding of Imidazole and Cyanide to HtsA Proteins

One milliliter of 7 μM wild-type, M79A, or H229A HtsA protein was mixed with imidazole or potassium cyanide at 5−500 μM and incubated at 20°C for at least 10 min, and UV−Vis and MCD spectra were recorded. The dissociation constants (K_d) of the bindings were calculated by analyzing absorbance change (ΔA) using the method of Wu and Hammes (209) (Eq. 2.1)

$$K_d = ([\text{HtsA}]_o - [\text{P}])([\text{ligand}]_o - n[\text{P}])/[\text{P}] \quad (1)$$

where $[\text{HtsA}]_o$ and $[\text{ligand}]_o$ are the total molar concentrations of wild-type or mutant HtsA and imidazole or cyanide, respectively, and *n* and [P] are the number of imidazole or CN^{-1} binding sites per HtsA molecule and the concentration of the HtsA/ligand complex, respectively. [P] at different $[\text{ligand}]_o$ was calculated using the equation $P = (\Delta A/\Delta A_{max})[\text{HtsA}]_o$, where ΔA_{max} was ΔA when HtsA was saturated with the ligand and determined from the intercept on the *Y* axis in the double reciprocal plotting of ΔA and $[\text{ligand}]_o$.

Binding and Rebinding of Carbon Monoxide (CO) to HtsA Proteins

To examine CO binding, wild-type (3.3 μM), H229A (3.8 μM), and M79A (2.2 μM) HtsA proteins were reduced by dithionite and equilibrated with 1 atm of 100% CO (1 mM CO), and the spectra of the samples were recorded. Rapid CO association kinetics were measured by photolysis of the preformed complexes of reduced HtsA H229A and M79A with CO each at 2 μM using a 0.5 μs excitation pulse (577 nm, phase-R 2100 dye laser) in the presence of 1 mM CO. Time courses of CO rebinding were monitored at 420 nm.

Results

Alterations of HtsA Absorption Spectra Caused by H229A and M79A Replacements

To find out which histidine residue is a heme axial ligand in HtsA, each of the five histidine residues at positions 24, 229, 251, 289, and 293 was replaced with alanine by site-directed mutagenesis. The optical absorption spectra of the H24A, H251A,

H289A, and H293A mutant proteins at both ferric and ferrous states are very similar to those of wild-type HtsA (data not shown). However, reduced H229A has reduced intensity of the Soret peak and no longer displays the dominant α band at 560 nm (Figure 2.1A), indicating that the heme iron in H229A is not in a hexacoordinate complex with two strong axial ligands. The Soret absorption peak of oxidized H229A shifts to 402 nm from 412 nm in wild-type HtsA (Figure 2.1B). In addition, the 532- and 560-nm peaks in wild-type HtsA are replaced with peaks at 482 and 600 nm in H229A (Table 2.1). These observations suggest that His229 is one of the two axial ligands of the heme iron in HtsA.

To determine which methionine residue is the other axial ligand, the six internal methionine residues at positions 79, 126, 173, 216, 238, and 270 were individually replaced with alanine by site-directed mutagenesis. Among the six mutant proteins, only M79A shows dramatically different absorption spectra from the wild-type protein. Like reduced H229A, ferrous M79A has a reduced intensity of the Soret peak and lacks the resolved α and β bands (Fig. 2.1A), suggesting that reduced M79A also has a pentacoordinate heme iron. Ferric M79A has a spectrum with peaks at 402, 498, 536, and 630 nm with a greater extinction coefficient of the Soret peak than that of the wild-type protein (Fig. 2.1B), and the profile in the region of 460 to 700 nm is similar to that of aquometHb (210), suggesting that oxidized M79A has a hexacoordinate heme iron with histidine and water axial ligands. These results strongly suggest that methionine 79 is the other axial ligand of the heme iron in HtsA.

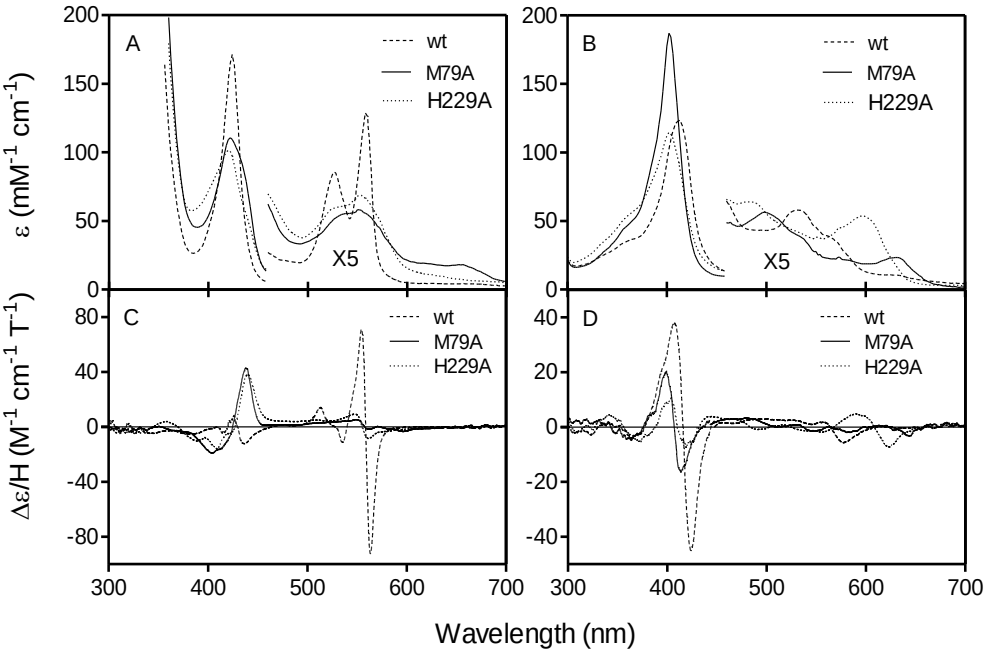

Figure 2.1. UV−Vis Absorption and MCD Spectra of Ferrous (A and C) and Ferric (B and D) Wild-Type (wt), M79A, and H229A HtsA. The spectra of the reduced proteins were recorded in the presence of excess dithionite.

MCD Spectra of the HtsA Proteins

As Sook et al. described (206), the MCD spectrum of ferrous HtsA is similar to ferrous cytochrome c, which contains a low-spin, hexacoordinate heme iron with the Met and His axial coordination (211, 212). Replacements of H229 and M79 with alanine dramatically reduce and increase the intensities of the Q and Soret bands, respectively, and eliminate the trough of the derivative feature of the Soret band (Figure 2.1C). The MCD spectrum of ferrous M79A is similar to that of ferrous horseradish peroxidase (213), which is known to contain pentacoordinate heme iron with a histidine ligand (214). The intensities of the ferrous H229A MCD spectrum are similar to those of the M79A MCD spectrum, suggesting that ferrous heme iron in H229A is also pentacoordinate.

However, the MCD profiles of ferrous M79A and H229A are obviously different, apparently reflecting the fact that the remaining axial ligand residue in the two mutant proteins is different. These results support that H229 and M79 are the axial ligands of the HtsA heme iron.

Table 2.1: Heme Coordination and Spectral Features of Wild-type and Mutant HtsA Proteins

Protein[a]	Known/ proposed axial ligand(s)	Absorption Peaks			Major MCD Features			
		Soret (nm)	ε mM^{-1} cm^{-1}	Visible (nm)	Soret (nm)	Δε/H (M cm T)$^{-1}$	Visible (nm)	Δε/H (M cm T)$^{-1}$
wt HtsA	Met/His	412	123	532 562[b]	407 416 423	38 0 -45	557 564 578	1.9 0 -5.6
M79A HtsA	His/H_2O	403	187	498 536[b] 630	399 407 414	20 0 -16.5	548 580 643	-1.5 -2 -3.3
H229A HtsA	Met	402	114	482 524 600	404 410 419	11 0 -7.5	517 555 589 608 624	0.8 -2 4.9 0 -7.2

[a]All spectra were measured at pH 8.0 unless specified
[b]Estimated from shoulders

Ferric wild-type HtsA has a MCD spectrum typical of a low-spin, hexacoordinate heme iron with histidine and methionine axial ligands (Figure 2.1D), confirming the previous finding (206). As expected, the MCD spectrum of ferric M79A is high spin (Figure 2.1D), and the profile of the M79A spectrum in the charge transfer region is

similar to that of aqueous metMb (215), suggesting again that ferric M79A has a water- and histidine-ligated hexacoordinate heme iron.

The H229A replacement caused more profound change in the MCD spectrum than the M79A mutation (Figure 2.1D). Notably, the intensities of the peak and trough of the Soret band of ferric H229A are small and similar to those of ferric horseradish peroxidase, Aplysia myoglobin, cyanogen bromide-modified myoglobin, and H64L and H64V myoglobin whose heme irons have a pentacoordination with a histidine axial ligand (214, 216), suggesting that ferric H229A has a pentacoordination. However, the MCD spectrum profile of ferric H229A is obviously different from those of these proteins with histidine-ligated, pentacoordinate heme iron, particularly possessing a band with a derivative feature around 608 nm. The different MCD profile of H229A HtsA from the proteins with histidine-ligated, pentacoordinate heme iron is most likely because H229A HtsA has a methionine ligand.

Resonance Raman Spectra

The high frequency region of the RR spectra of the HtsA proteins in Figure 2.2 possesses bands characteristic of the oxidation (ν_4) and spin and coordination (ν_2, ν_3) states of the heme iron atom (217). M79A protein had the ν_4, ν_3, and ν_2 peaks at 1369, 1478, and 1562 cm^{-1}, respectively, which are close to the ν_4 (1370 cm^{-1}), ν_3 (1480 cm^{-1}), and ν_2 (1559 cm^{-1}) peaks of $(Me_2SO)_2Fe^{III}PP^+$, a high-spin hexacoordinate model compound (218), and the ν_3 (1481 cm^{-1}) and ν_2 (1561 cm^{-1}) peaks of the aquometHb protein in which the heme iron has a high-spin hexacoordination with water and histidine ligands (219). The ν_4, ν_3, and ν_2 peaks of the H229A mutant were at 1370, 1490, and

1571 cm^{-1}, respectively, which are close to the 1374 cm^{-1} (v_4), 1491 cm^{-1} (v_3), and 1572 cm^{-1} (v_2), respectively, of the His(F8)Tyr Mb mutant, which has five-coordinate, high-spin iron (218). Since previous studies have established that protein-induced shifts of the heme frequencies above 1300 cm^{-1} are much smaller than those induced by changes in spin and ligation state (220, 221), our results indicate that the heme irons in H229A and M79A are high-spin, pentacoordinate and high-spin, hexacoordinate, respectively.

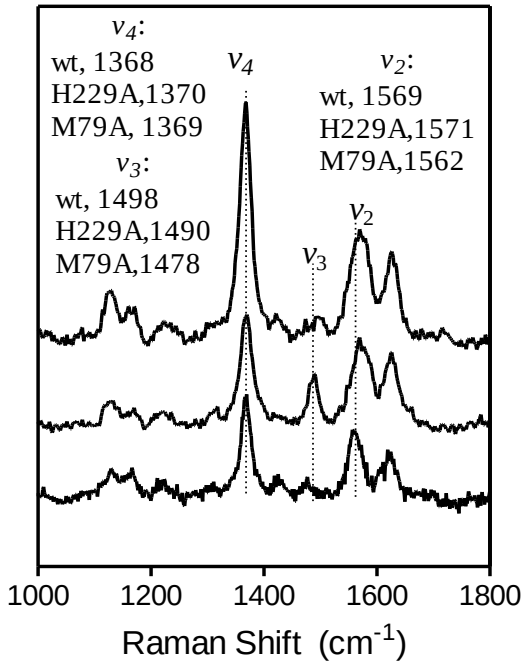

Figure 2.2. Raman Spectra of wt, M79A, and H229A HtsA Proteins. The spectra were recorded with each protein at 200 μM in 20 mM Tris-HCl, pH 8.0, using excitation at 413.1 nm.

EPR Results

As expected, >90% of ferric wild-type HtsA heme iron has a rhombic low-spin signal with g_z = 2.94 and g_y = 2.28 (Figure 2.3), which are identical with or close to g_z = 2.94 and g_y = 2.29 of 6×His-tagged HtsA (201), and no low-spin signal was detected in

ferric H229A HtsA (Figure 2.3A). Surprisingly, ~70% of the ferric M79A HtsA heme iron had a rhombic low-spin signal with g_z = 3.24 (Figure 2.3B). This unexpected result was not consistent with the high-spin features of the UV−Vis absorption, MCD, and RR spectra at room temperature, suggesting that low temperature might have caused a coordination change.

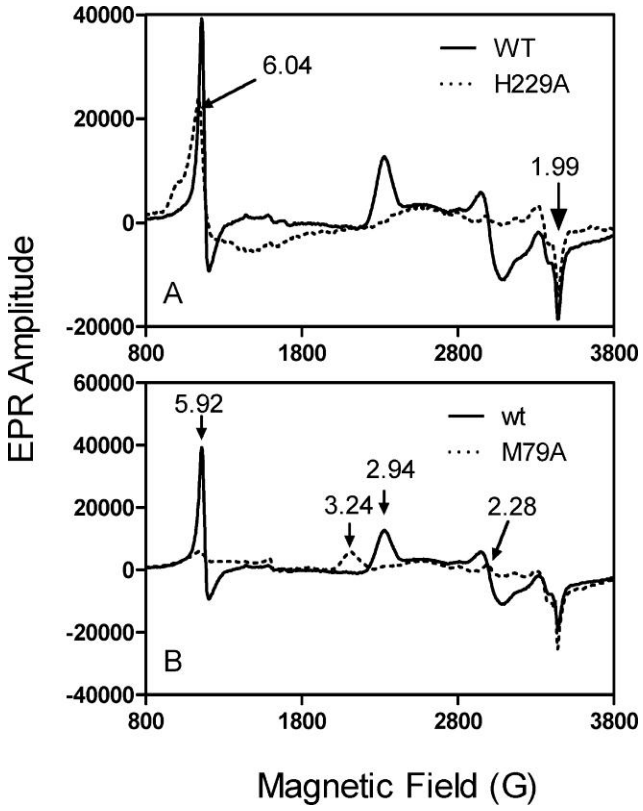

Figure 2.3. EPR Spectra of wt, M79A, and H229A HtsA Proteins. The spectra were recorded at 100 μM of each protein in 20 mM Tris-HCl, pH 8.0.

Accessibility of the Heme Iron in HtsA Axial Mutants to Imidazole

To examine the accessibility for exogenous iron ligands of the H229 and M79 sides of the bound heme in HtsA, the binding of imidazole, which has the same structure with the side chain of histidine, to H229A and M79A was examined by UV−Vis and

MCD spectroscopy. Addition of imidazole causes a dose-dependent shift of the M79A absorption spectrum to one that is typical of a hexacoordinate low-spin heme iron (Figure 2.4A), and the analysis of the spectral change data using Eq. 1 found that the mutant protein binds one imidazole per protein molecule with a K_d of 40.9 μM (Table 2.2). These results indicate that imidazole ligates to the M79A heme iron. The MCD spectrum of M79A in the presence of 0.5 mM imidazole is consistent with the imidazole binding (Figure 2.4B). In contrast, imidazole at 0.5 mM did not alter the absorption and MCD spectra of H229A HtsA (Figure 2.4C & 2.4D), indicating that imidazole cannot bind to H229A under these conditions. These results suggest that imidazole can access the alanine 79 position of M79A HtsA but not the alanine 229 position of H229A HtsA.

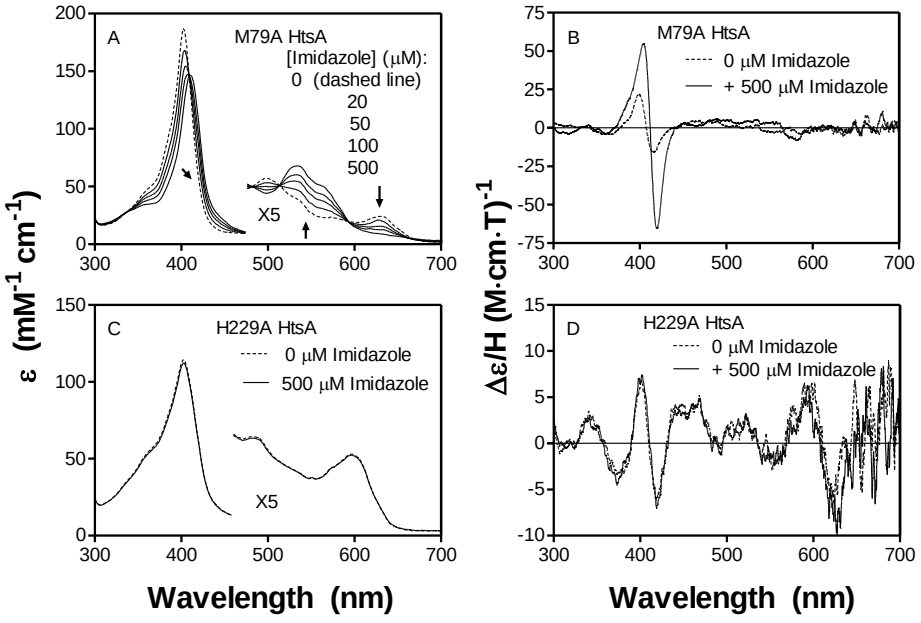

Figure 2.4. Effects of Imidazole on UV−Vis and MCD Spectra of M79A and H229A HtsA. The UV−Vis and MCD spectra of each HtsA protein in 20 mM Tris-HCl (for UV−Vis) or 50 mM potassium phosphate (for MCD), pH 8.0, at the indicated imidazole concentrations are shown. The arrows in panel A indicate the directions of the spectral shifts as imidazole concentration increased.

Binding of Cyanide to HtsA

To determine whether the alanine 229 position of the H229A HtsA mutant is completely inaccessible to external ligands, the binding of cyanide, a small and strong external ligand, to the HtsA heme iron was examined. Cyanide binds to the heme iron in both M79A and H229A, causing shifts in the absorption and MCD spectra that are consistent with the formation of hexacoordinate heme iron complexes (Fig. 2.5). M79A and H229A were found to bind one cyanide with K_d of 0.5 and 19.1 μM, respectively. Thus, the alanine 229 site of the H229A mutant is not completely inaccessible. However, the cyanide binding to the H229A heme iron is weaker than the binding to the M79A heme iron by about 40-fold, indicating that the H229 side of the HtsA heme is more sterically packed than the M79 side. It has been shown that wild-type HtsA binds cyanide (206). The absorption and MCD spectra of wild-type and M79A HtsA in the presence of 0.5 mM potassium cyanide were almost identical but were different from those of the H229A−cyanide mixture (Figure 2.5C & 2.5D), suggesting that cyanide replaces the M79 ligand in the cyanide binding to wild-type HtsA.

Table 2.2: Dissociation Constants for Imidazole and Cyanide Binding to the HtsA and Shp Proteins

Protein	K_d for imidazole binding (μM)	K_d for cyanide binding(μM)
wt HtsA	No binding	55
M79A HtsA	44.1	0.5
H229A HtsA	No binding	19.1

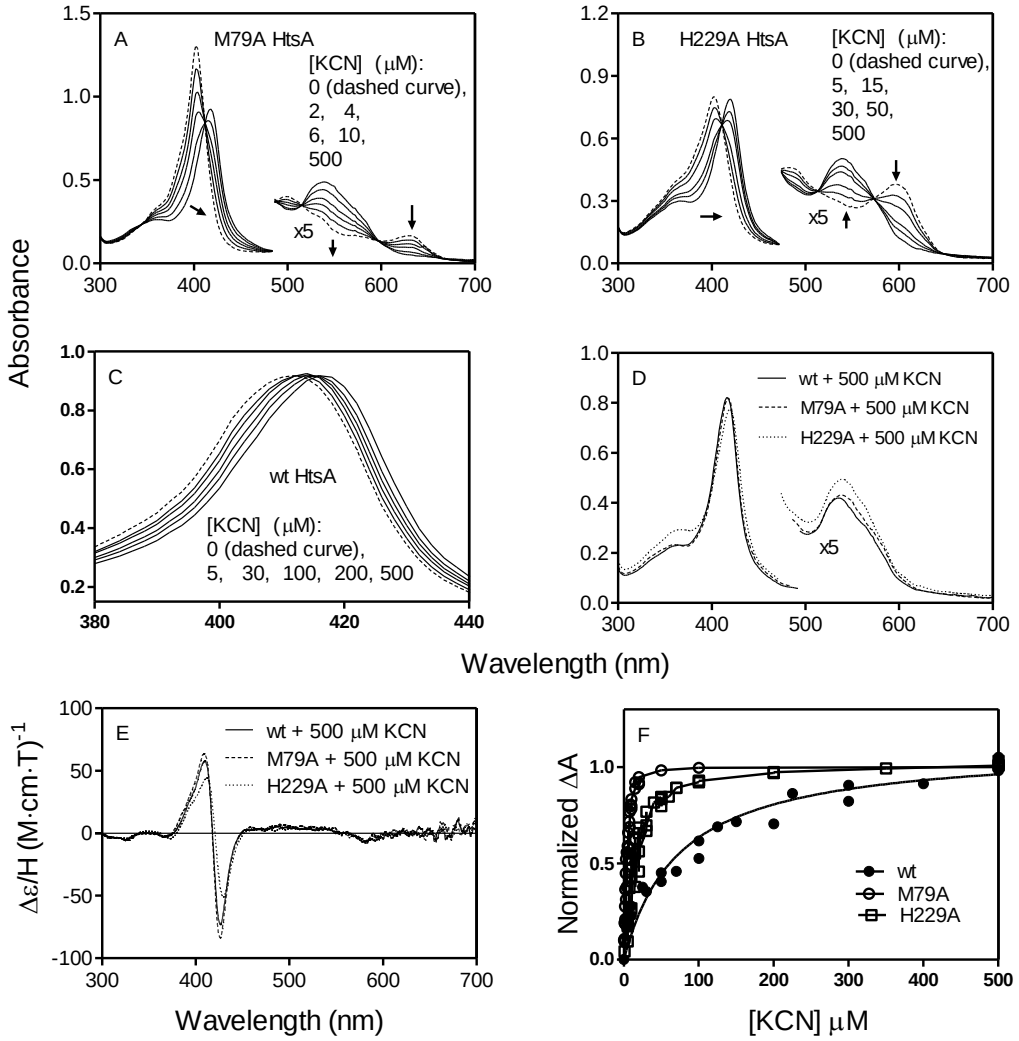

Figure 2.5. Binding of Cyanide to wt, M79A, and H229A HtsA. A−C, cyanide concentration-dependent shifts of the UV−Vis spectra of 7 μM M79A (A), H229A (B), and wt (C) HtsA in 20 mM Tris-HCl, pH 8.0. D & E, overlays of the UV−vis (D) or MCD (E) spectra of wt, M79A, and H229A HtsA in the presence of 500 μM KCN. (F) Cyanide titration of absorbance change during cyanide binding. The absorbance changes were normalized by setting the maximum absorbance changes at 1.

Binding and Rebinding of CO to HtsA

To analyze ferrous ligand binding, we examined the binding and rebinding of CO to ferrous wild-type and mutant HtsA proteins. The ferrous wild-type HtsA bound CO but

not completely after incubation with 1 mM CO for 25 min, and the ferrous H229A and M79A mutants formed a simple CO complex (Figure 2.6). The apparent first-order rate constants of CO association after photolysis at 1 mM CO were 2.1×10^4 s^{-1} and 1.1×10^4 s^{-1} for the M79A and H229A mutants, respectively, suggesting that the mutants can bind CO rapidly. Absorbance change during photolysis of the wild-type HtsA−CO complex was very small, and formation of the wild-type HtsA−CO complex took more than 10 min (data not shown). These results support the conclusion that the H229 and M79 residues are the axial ligands of the HtsA heme iron.

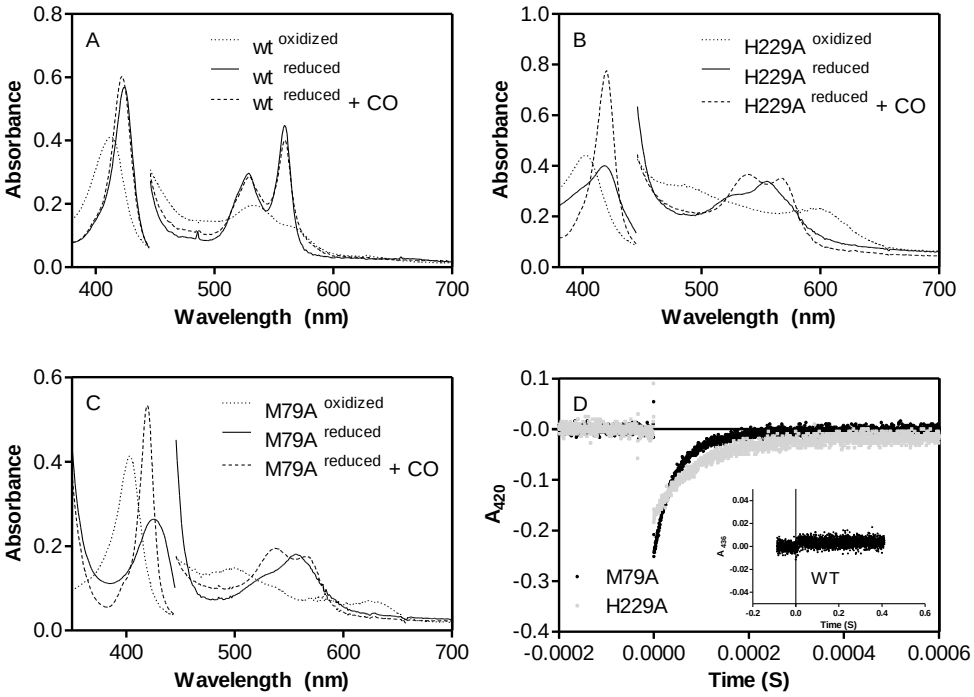

Figure 2.6. Binding of CO to HtsA Proteins. A−C, spectra of ferric and ferrous wt (3.3 μM) (A), H229A (3.8 μM) (B), and M79A (2.2 μM) (C) HtsA proteins and their mixtures with 1 mM CO in 100 mM potassium phosphate, pH 7.0. D, rapid CO association kinetics after photolysis. A_{420} was measured using 2 μM M79A (black) or H229A (gray) protein and 1 mM CO in potassium phosphate, pH 7.0.

Discussion

Site-directed mutagenesis and spectroscopic analyses have been used to identify the axial ligand residues of the HtsA heme iron and to characterize the axial mutants of HtsA. The H229 and M79 residues were found to be the heme axial ligands in HtsA. The ferrous heme irons of H229A and M79A HtsA mutant proteins are pentacoordinate and in high-spin state and so is the heme iron of ferric H229A HtsA, whereas the ferric M79A heme iron appears to have hexacoordination with water and histidine axial ligands. The H229 side of the HtsA heme is more sterically limited than the M79 side of the HtsA heme. These findings will be important in rationally designing experiments to elucidate the molecular mechanism and structural basis for the rapid, direct heme transfer from Shp to HtsA. In addition, this study provides spectroscopic features of a protein with methionine-ligated, pentacoordinate heme iron.

A previous spectroscopic analysis has unveiled that the hexacoordinate HtsA heme iron is ligated to histidine and methionine residues (206). The identities of these axial ligands have now been experimentally identified as the M79 and H229 residues in this study. This conclusion is first supported by the effects of alanine replacements of the HtsA histidine and methionine residues on UV−vis spectra of HtsA. The absorption spectrum of ferric H229A HtsA is similar to the spectra of ferric H102M and R98C/H102M cytochrome b_{562} mutants, which has a methionine axial ligand (218). This similarity supports that the H229A replacement results in a mutant protein with a methionine ligand. Conversely, the absorption spectrum of M79A is similar to that of aquometHb whose heme iron has a hexacoordination with water and histidine axial

ligands (219), implying that the M79A replacement results in a mutant protein with a histidine axial ligand. Furthermore, both H229A and M79A at the ferrous state lose the features of hexacoordinate, low-spin heme iron with two strong ligands of wild-type HtsA, lacking the dominant α band in the absorption spectra, a feature possessed by deoxyHb whose ferrous heme iron is pentacoordinate. In addition, ferrous H229A and M79A, but not wild-type HtsA, rapidly form complexes with CO, which have absorption spectra similar with that of the Hb:CO complex.

MCD spectroscopy is particularly useful for providing information on coordination ligands and numbers of unknown hemoproteins by comparing their MCD spectra with those of hemoproteins with known heme binding properties (173, 174). The MCD spectrum of ferrous M79A HtsA resembles the MCD spectrum of ferrous horseradish peroxidase (213), which is known to contain pentacoordinate heme iron with a histidine ligand (214), supporting that the ferrous M79A heme iron has a pentacoordination with a His axial ligand. The MCD spectrum of ferric M79A HtsA is similar to the MCD spectra of native metmyoglobin and a benzohydroxamic acid adduct of ferric horseradish peroxidase, which are high spin and have hexacoordination with water and histidine ligands (215), further supporting that the sixth coordination site of the heme iron in oxidized M79A HtsA is occupied by a water molecule. These MCD features of M79A HtsA further support the conclusion that the methionine 79 and histidine 229 are the axial ligands in HtsA. The RR spectrum of M79A supports this conclusion.

There had been no firmly established examples for hemoproteins with Met-ligated pentacoordination of heme iron. The heme iron of a H102M mutant of cytochrome b_{562} ligates to a methionine residue, and its other axial ligand cannot be identified (218);

however, whether the heme iron in this protein is pentacoordinate has not been established. The RR analysis of H229A HtsA indicates that the heme iron in oxidized H229A HtsA is pentacoordinate. This conclusion on the coordination of the H229A heme iron is supported by the observations that H229A HtsA has a blue shift and smaller extinction coefficient for the Soret absorption peak compared with those of the wild-type protein and small intensities of the MCD peaks in the Soret band, like those of known proteins with pentacoordinate heme iron, such as horseradish peroxidase, Aplysia myoglobin, cyanogen bromide-modified myoglobin, and H64L and H64V myoglobin (215, 216). The axial ligand of the pentacoordinate heme iron in H229A HtsA is apparently methionine since the UV−Vis spectrum of H229A HtsA is similar with that of the cytochrome b_{562} H102M mutant (218) but not with those of the pentacoordinate heme iron with a His axial ligand. In summary, ferric H229A HtsA has a pentacoordinate, methionine-ligated heme iron with novel MCD and UV−Vis spectral features (Table 2.1), including particularly an absorption peak at ~600 nm.

Exogenous imidazole can readily ligate to the heme iron of M79A HtsA but not to H229A HtsA, indicating that the coordination site is sterically less accessible on the histidine 229 side of the bound heme in HtsA than the other side. This assertion is further supported by the observations that cyanide replaces M79 but not H229 in the wild-type HtsA protein, that the binding of cyanide to H229A HtsA is weaker than the cyanide binding to M79A HtsA, and that the CO binding to ferrous H229A HtsA is slower than the CO binding to ferrous M79A. Furthermore, H229 is more important than M79 for the affinity of HtsA for heme. These observations strongly suggest that the M79 side of the heme pocket in HtsA is more exposed to the solvent than the H229 site.

The M79 and H229 axial residues of HtsA are corresponding to the M78 and H229 axial ligands of *S. aureus* IsdE (205, 222). IsdE is also the lipoprotein component of the ABC transporter and shares 39% amino acid sequence identity with HtsA. HtsA directly and rapidly acquires heme from the surface protein Shp (201, 223), and IsdE directly but slowly extracts heme from the surface protein IsdC (224, 225). The H229 side of the IsdE heme pocket is also more buried than the M78 side (204). However, there are some differences between these two proteins. Prepared IsdE is a mixture of ferric and ferrous forms (222), whereas purified HtsA is in the ferric form. H229A IsdE is in a low-spin hexacoordinate complex, which was proposed to be a NO complex, and cannot interact with cyanide (222). H229A HtsA is in a high-spin state and can form a low-spin complex with cyanide. These differences might be due to the different preparation methods but more likely imply difference in heme binding in these proteins.

Note: Tyler Nygaard generated H229A HtsA mutant; Dr. Marian Fabian performed the EPR and CO binding measurements; and Ms. Doreen Brown measured the RR spectra.

BIS-METHIONINE LIGATION TO HEME IRON IN THE STREPTOCOCCAL CELL SURFACE PROTEIN SHP FACILITATES RAPID HEME TRANSFER TO HTSA OF THE HTSABC TRANSPORTER

Abstract

The surface protein Shp of *Streptococcus pyogenes* rapidly transfers its heme to HtsA, the lipoprotein component of the HtsABC transporter, in a concerted two-step process with one kinetic phase. The structural basis and molecular mechanism of this heme transfer have been explored by mutagenesis and truncation of Shp. The heme-binding domain of Shp is in the amino-terminal region and is functionally active by itself, although inclusion of the carboxy-terminal domain speeds up the process by approximate 10-fold. Single alanine replacements of the axial methionine 66 and 153 ligands (Shp^{M66A} and Shp^{M153A}) cause formation of pentacoordinate heme-Met complexes. The association equilibrium constants for heme binding to wild-type, M66A, and M153A Shp are 5,300, 22,000, and 38 μM^{-1}, respectively, showing that the Met^{153}-Fe bond is critical for high affinity binding and that Met^{66} destabilizes heme binding to facilitate its rapid transfer. Shp^{M66A} and Shp^{M153A} rapidly bind to heme-free HtsA (apoHtsA), forming detectable transfer intermediates. These intermediates appear to be Shp-heme-HtsA complexes with one axial ligand from each protein and decay to the products with rate constants of 0.4-3 s^{-1}. Thus, the M66A and M153A replacements alter the kinetic mechanism and unexpectedly slow down heme transfer by stabilizing the intermediates. These results, in combination with the structure of the Shp heme-binding domain, allow us to propose a "plug-in" mechanism in which the side chains of the axial residues from apoHtsA are inserted into the axial positions of heme in Shp to extract it from the surface protein and

pull it into the transporter active site. When pH decreases, Shp^{M66A} undergoes a conversion from pentacoordinate heme iron complex into a hexacoordinate heme-H_2O-iron-Met iron complex with an apparent K_a of 7.65. Shp^{M153A} does not form a similar hexacoordinate complex but the M66-iron axial bond is broken at pH 5. These pH titration results suggest that the heme pocket in Shp can open up at the M66 side of the bound heme and this opening is controlled by a titratable base group.

Introduction

Heme exchange from one protein to another has been demonstrated biochemically in only a few bacterial systems, including transfers from hemoglobin to *Serratia marcescens* hemophore HasA (226); from the cell surface protein Shp to HtsA, the lipoprotein component of the HtsABC transporter, in *Streptococcus pyogenes* and *Streptococcus equi* (227, 2); from HasA to its outer membrane receptor HasR (226); and from hemoglobin to *Shigella dysenteriae* outer membrane receptor ShuA (185). A detailed kinetic mechanism has only been proposed for the *S. pyogenes* Shp/HtsA reaction (2). This process occurs in a single kinetic phase with transfer rate constants that are >100,000 times greater than that for simple heme dissociation from Shp. The structural basis for this rapid and concerted heme transfer is unknown.

In some hemoproteins, iron is hexacoordinate, with four ligands from protoporphyrin IX and two axial ligands from the side chains of His, Lys, Tyr, Met, and/or Cys. Combinations of the strong ligands, His, Lys, Met, and Cys, usually result in the low spin ferrous and ferric states with an intense Soret absorption peak and two

resolved Q_{ov} or αβ bands in the visible wavelength region for ferrous hemoproteins (228, 6). The axial ligands of heme iron in HasA (229), HasR (3), ShuA (185), and *Porphyromonas gingivalis* heme receptor HmuR (230) are critical for heme transfer and acquisition. However, it is unclear whether these axial ligands contribute to just binding affinity or have additional catalytic roles in heme transfer. Thus, detailed examination of the roles of the axial ligands in heme binding and transfer should provide insight into the molecular mechanisms of these processes.

The Philips group in collaboration with our laboratory has determined the crystal structure of the heme-binding domain of Shp (231), which reveals two methionine thiol ether sulfur atoms (Met^{66} and Met^{153}) as the axial ligands of the heme iron. In order to gain insight into the structural mechanism of rapid heme transfer from Shp to HtsA, we examined these processes for Shp mutants containing only the NH_2-terminal heme-binding domain or full-length Shp in which the Met axial ligands were replaced with alanine (Ala) or histidine (His). Both the heme-binding domain and COOH-terminal region contribute to rapid heme transfer. Met^{153}, but not Met^{66}, appears to be critical for the high affinity of Shp for heme, whereas both Met^{66} and Met^{153} are critical for rapid heme transfer. The replacement of either Met^{66} or Met^{153} with Ala result in detection of an intermediate in heme transfer to heme-free HtsA (apoHtsA), indicating multiple first order reaction steps. Taken together, these data suggest a mechanism in which the two axial Met ligands in wild-type Shp are simultaneously displaced by groups from apoHtsA after the two proteins have formed a transient binary complex.

Methods

Protein Preparation

The preparation of the heme-binding domain of Shp containing amino acids 30–180 (designated Shp^{180}) has been described (176). Ala and His replacement mutants of Met^{66} and Met^{153} of Shp (designated Shp^{M66A}, Shp^{M153A}, Shp^{M66H}, and Shp^{M153H}) were generated by site-directed mutagenesis using the Stratagene QuikChange site-directed mutagenesis kit. The mutant proteins were expressed in *Escherichia coli* (DE3) containing the appropriate plasmid. The majority of the mutant proteins were expressed in inclusion bodies. Except for Shp^{M153H}, the heme-binding forms (holo-forms) of these mutant proteins were prepared starting from inclusion precipitates. All solutions were buffered with 20 mM Tris-HCl, pH 8.0 (Tris-HCl), unless otherwise specified. The cell pellet from a 6-liter culture was resuspended in 50 ml of Tris-HCl, sonicated on ice for 15 min, and centrifuged to obtain the pellet. The inclusion bodies were dissolved in 50 ml of 8 M urea. Each denatured protein was refolded by diluting with 40-fold Tris-HCl in the presence of excess hemin. The sample was loaded onto a DEAE column (2.5 × 10 cm), and the column was washed with 100 ml of Tris-HCl and eluted with a 100-ml linear gradient of 0–0.25 m NaCl. Each protein was dialyzed against 3 liters of 10 mM acetate buffer, pH 5.5, and loaded onto an SP-Sepharose column (1.5 × 6 cm). The column was eluted with a 100-ml linear gradient of 0–0.25 mM NaCl in the acetate buffer. The fractions containing >95% mutant protein were pooled, dialyzed against 3 liters Tris-HCl, and concentrated using Centricon Plus 20 filtration devices. $HoloShp^{M153H}$ was prepared

by incubating purified apoShp^{M153H} with excess hemin, loading the mixture onto a Sephadex G-25 column (1 × 20 cm), and eluting with Tris-HCl.

ApoShp and mutant proteins were prepared from inclusion bodies as described above except that hemin was absent in the refolding step. ApoHtsA was prepared, as described previously (4).

EPR Measurement

EPR spectra of wild-type and mutant Shp were measured with a Bruker EMX spectrometer using the following conditions: Frequency, 9.6 GHz; power, 3 milliwatts; modulation amplitude, 10 G; modulation frequency, 100 kHz; and temperature, 10 K. The high spin signal at g = 6 was quantified by double integration between 800 and 1700 G and comparison with the signal of a high spin sperm whale metmyoglobin at pH 7. Quantification of the low spin signals was based on comparison of the area of the $g = 3$ absorption-like signal with the analogous low spin signal of metmyoglobin at pH 9.5.

Magnetic Circular Dichroism (MCD) Measurements

MCD spectra of Shp proteins in 50 mM phosphate buffer at indicated pH were recorded using JASCO J-710 spectropolarimeter equipped with an Alpha Scientific 3002-1 electromagnet under the following conditions: Bandwidth, 1 nm; accumulation, 3 scans; scan rate, 100 nm/min; resolution, 0.5 nm; magnetic field, 12.9 kG (1.29 tesla); and temperature at 25ºC. The spectra of the reduced proteins were taken in the presence of excess dithionite. Buffer blank-corrected CD spectra obtained without magnetic field were subtracted from corresponding buffer-corrected MCD spectra using the Jasco software. These processed MCD data were then used to calculate the final MCD data in

units of $\Delta\varepsilon_M$ (M.cm.tesla)$^{-1}$ based on protein concentration, light path, magnetic field, and molar ellipticity Θ_M (deg.cm^2 .dmol^{-1}. tesla^{-1}) = 3300 $\Delta\varepsilon$M.

pH Titration

Buffers with pH range from 5 to 9 were prepared by mixing 50 mM KH_2PO_4 and 50 mM K_2HPO_4 with various ratios. Citric acid/citrate and K_2HPO_4/Na_3PO_4 buffers (50 mM) were used for pH $\leq$ 5 and > 9, respectively. In titration of UV-Vis absorption spectra, concentrated proteins were diluted with buffer by 100 fold and incubated at 22°C for at least 10 min before pH and spectra were measured. The pH values of the diluted samples were measured using an IQ125 ISFET pH meter (IQ Scientific, USA). In titration of MCD spectra, protein samples were dialyzed against desired buffer overnight before MCD measurements.

Rates of Heme Dissociation from Shp Mutants

The rates of heme dissociation from Shp^{M66A}, Shp^{M153A}, and Shp^{M153H} were measured using H64Y/V68F apomyoglobin as a heme scavenger as described previously (232). Each Shp mutant protein (3 µM) was incubated with 58 µM apomyoglobin in 1 ml of 20 mM Tris-HCl, and the changes in absorbance at 410 nm (A_{410}) for Shp^{M153A} and at both 405 and 410 nm for Shp^{M66A} were monitored. The ΔA_{410} and $\Delta(A_{410} - A_{405})$ time courses were fit to a single exponential equation to obtain the rate constants for heme dissociation from Shp^{M153A} and Shp^{M66A}.

Kinetic Analyses

A stopped-flow spectrophotometer equipped with a photodiode array detector (SX20; Applied Photophysics) was used to measure the rates of heme transfer from Shp mutants to apoHtsA and the binding of heme to apoShp mutants. In these measurements, 2.4 μM holoShp or 2 μM hemin in one syringe were mixed with apoprotein at ≥5× [holoShp] or [hemin] in another syringe. Spectra were recorded with time in each reaction. Changes in absorbance at appropriate wavelengths were fitted to a single or double exponential expression, yielding pseudo-first-order rate constants for each reaction step for further analysis as described under "Results."

Results

The Heme-Binding Domain of Shp

Shp and its homologue in *S. equi* share 75 and 25% identify in amino acid sequence in the regions over amino acids 28–173 and 174–291, respectively (2), suggesting that the heme-binding domain of Shp is located in the amino-terminal region. To test this idea, Shp^{180}, consisting of amino acids 30–180, was prepared. The spectra of oxidized and reduced Shp^{180} are almost identical to those reported for full-length Shp (4). Like Shp, reduced Shp^{180} is stable in air. These data indicate that the heme-binding domain of Shp is located in the region of amino acids 30–180. This conclusion is confirmed by the crystal X-ray structure of Shp^{180} (231).

Heme Transfer from Ferrous and Ferric Shp^{180} to ApoHtsA

When ferrous Shp^{180} reacts with excess apoHtsA, the absorbance at 424 nm (A_{424}) rapidly increases on millisecond time scales due to heme transfer from Shp to apoHtsA and slowly decreases on second time scales due to autoxidation of the heme bound to HtsA, as is also seen for heme transfer from full-length Shp to apoHtsA (4). The time course for heme transfer from ferric Shp^{180} to apoHtsA measured at 414 nm also resembles that for transfer from full-length Shp. The basis for these optical changes is the difference in the maximum wavelengths of the Soret band of reduced/oxidized Shp^{180} and HtsA, which are 428/419 and 424/412 nm, respectively. Both heme transfer reactions are pseudo-first-order processes at excess [apoHtsA], and the observed rate constants depend hyperbolically on [apoHtsA] as in the full-length Shp-apoHtsA reactions (4). Thus, the mechanism established for the full-length Shp-apoHtsA reactions (4) applies to the reactions of apoHtsA with Shp^{180}. In both cases, the observed time courses can be analyzed by Scheme 3.1, which involves rapid formation of a Shp^{180}-apoHtsA complex (K_d = 90 and 107 μM for the oxidized and reduced Shp^{180}-apoHtsA complexes, respectively) (Table 3.1) and a first order decay involving intra-complex heme transfer.

$$Shp^{180} + apoHtsA \underset{k_2}{\overset{k_1}{\rightleftharpoons}} Shp^{180}\text{-}apoHtsA \xrightarrow{k_{transfer}} apoShp^{180} + HtsA$$

Scheme 3.1

Truncation to residues 30–180 does slow the rate of intra-complex hemin transfer from 43 to 2.9 s^{-1} and that for heme transfer from 26 to 4.4 s^{-1} compared with full-length

Shp. Thus, although the heme-binding domain retains the ability to directly and efficiently transfer heme to apoHtsA, the COOH-terminal domain does play a significant role by enhancing 6–15-fold the intra-complex transfer rate.

Table 3.1. Kinetic Parameters for Hemin/Heme Transfer from Shp Proteins to apoHtsA

	Kinetic parameter					
Heme or hemin Donor	k_2/k_1 or K_d (μM)	$k_{transfer}$ (s^{-1})	k_{t1} (s^{-1})	k_{t2} (s^{-1})	[c] $k_{transfer}/K_d$ or k_{t1}/K_d ($\mu M^{-1}s^{-1}$)	Reference
[a]Ox. Shp	48 ± 7	43 ± 3			0.8	(191)
[a]Re. Shp	120 ± 18	28 ± 6			0.3	(191)
[a]Ox. Shp^{30-180}	90 ± 5	2.9 ± 0.9			0.03	This work
[a]Re. Shp^{30-180}	107 ± 12	4.4 ± 0.4			0.04	This work
[a]Ox. Shp^{M153H}	6.6 ± 0.5	3.5 ± 0.4			0.5	This work
[b]Ox. Shp^{M66A}	11.4 ± 0.3		8.7 ± 0.3	0.38 ± 0.08	0.76	This work
[b]Ox. Shp^{M153A}	170 ± 8		120 ± 30	2.5 ± 0.2	0.7	This work

[a]The values were determined according to Scheme I as described in reference (191). Note that no hemin transfer could be detected in the Shp^{M66H}–apoHtsA reaction, indicating either complete inhibition of formation of the Shp-HtsA complex or that affinity of $apoShp^{M66H}$ is ≥ 10 to 100 fold larger than that of wild-type apoHtsA. Ox. and Re. stand for Oxidized and Reduced, respectively.
[b]The values were determined according to Scheme 3.2. The values of K_d and k_{t1} were calculated from fits of the dependence of the observed rates of the formation of the transfer intermediate to Equation 3.2, and the values of k_{t2} were obtained directly from the double-exponential fits of the primary stopped-flow data.
[c]Apparent bimolecular rate constants at low [apoHtsA] for heme transfer from Shp and Shp^{180} and for the intermediate formation in the Shp^{M66A}- and Shp^{M153A}-apoHtsA reactions.

Ala and His Replacement Mutants of Shp Met^{66} and Met^{153}

To assess the contributions of the Shp axial ligands to heme binding and transfer, Met^{66} and Met^{153} were replaced by non-coordinating Ala. The Soret absorption peak shifts from 420 nm in wild-type oxidized Shp to 406 and 402 nm, respectively, in Shp^{M66A} and Shp^{M153A} (Fig. 3.1). In addition, there was a marked alternation in the visible absorbance spectrum (470–700 nm) with a new peak at around 600 nm indicative of a high spin Fe(III)-protoporphyrin IX complex. The UV-Vis spectra of Shp^{M66A} and Shp^{M153A} are similar to those of H64V and H64L human metmyoglobin mutants (7) and to the spectra of H229A HtsA described in Chapter II. The crystal structures of the analogous sperm whale metmyoglobin show pentacoordinate heme complexes with no coordinated water (233). H229A HtsA has a pentacoordinate heme iron with a Met axial ligand as determined by Raman resonance spectroscopy in Chapter II. Because the Shp proteins are not stable during resonance Raman measurement, we cannot determine the coordination of the Shp mutants by resonance Raman spectroscopy. However, the spectral features of the Shp mutants suggest that loss of one of the Met axial ligands leads to formation of a pentacoordinate heme-Met complex. This interpretation is supported by the spectra of the reduced Shp Ala mutants. The well resolved and intense α and β bands of reduced wild-type Shp, which are typical of hexacoordinate heme complexes with two strong axial ligands, are replaced with a single broad band for the Ala mutants (Fig. 3.1), which is similar to that of pentacoordinate deoxyhemoglobin. This result indicates that the reduced Shp mutants also form pentacoordinate heme complexes.

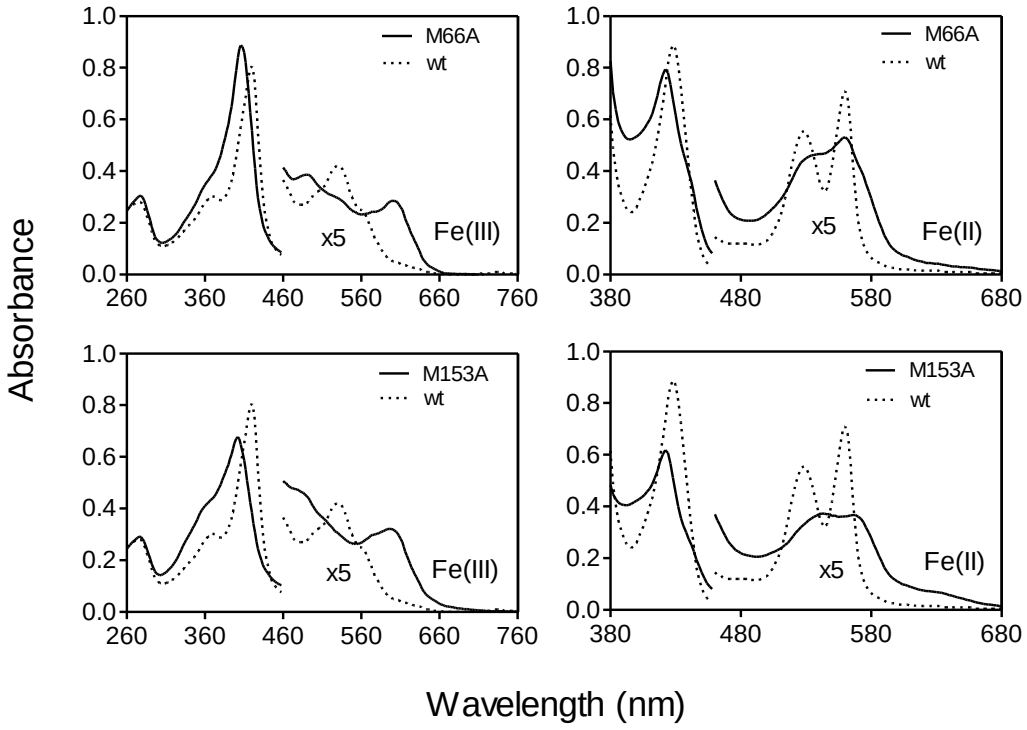

Figure 3.1: Optical Absorption Spectra of Oxidized and Reduced Wild-Type Shp, Shp^{M66A}, and Shp^{M153A}. Each protein was at 7.7 μM.

MCD Spectra of Shp Axial Mutants

To further examine the coordination of the heme iron in the Shp mutants, MCD spectra of the proteins were measured. MCD spectroscopy is particularly useful for providing information on the identity and number of coordination ligands of hemoproteins by comparing their MCD spectra with those of hemoproteins with known heme binding properties (173, 174). The MCD spectra of wild-type and axial mutant Shp proteins were measured at pH 8.0. Ferrous wild-type Shp displays a typical low spin hexacoordinate heme in the Q band region; however, its Soret band has higher ellipticities and a red shift compared with hemoproteins with Met-His or Met-Met

ligation (Fig. 3.2A). The MCD spectrum of ferrous M153A Shp is very similar to that of ferrous H229A HtsA (Fig. 2.1C). M66A and M153A share similar MCD profiles in the region of 350-450 nm, but M66A has a small derivative signal in the Q band that is similar to that of the wild-type Shp, suggesting that a small portion of ferrous M66A might be in a hexacoordinate complex.

Ferric wild-type Shp shows a typical hexacoordinate low-spin MCD spectrum (Fig. 3.2B). The MCD spectrum of ferric M153A is again very similar to that of ferric H229A HtsA (Fig. 2.1D), supporting that both HtsA H229A and Shp M153A have a Met axial ligand. Although the MCD profile of M66A Shp is very similar with those of H229A HtsA and M153A Shp, the ellipticities of M66A Shp at the Soret band is about three times as those of His229Ala HtsA and Met153Ala Shp. According to the results of pH titration described later, the higher ellipticities of M66A Shp at pH 8.0 appears to be partly due to that a small portion of M66A Shp has a hexacoordinate heme iron with a water molecule at the vacated coordination site.

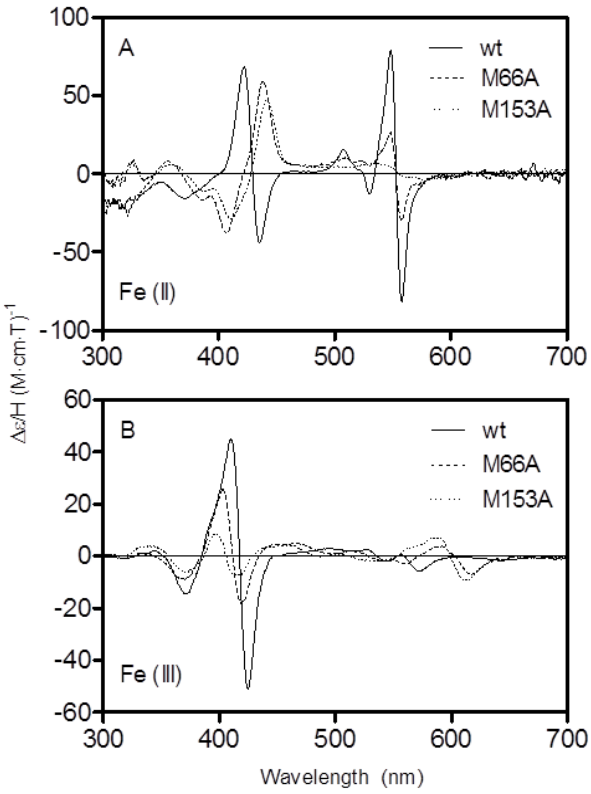

Figure 3.2: MCD Spectra of Ferrous and Ferric Wild-Type (wt), M66A, and M153A Shp. The reduced spectra were recorded in the presence of excess dithionite.

EPR Spectra of the Shp Mutants

Our interpretation of the coordinate state of Shp^{M66A} and Shp^{M153A} is further supported by the EPR spectra shown in Fig. 3.3. Shp^{M66A} and Shp^{M153A} both show EPR spectra with 100% high spin signals in the g = 6 region. In both cases multiple derivative signals occur, which are similar to those reported by Ikeda-Saito *et al*. (7) for pentacoordinate H64V and H64L metmyoglobin. The latter authors suggested an increase in rhombic symmetry in the apolar metmyoglobin mutants due to increased anionic character of the proximal imidazole and/or mixing of S = 3/2 and 5/2 spin states due to the pentacoordinate character of the hemin iron atom. The latter explanation probably

applies to the spectra of the Shp mutants, and in addition, some partial coordination with solvent water could occur and account for the very sharp feature at g = 5.81 (Fig. 3.3). In contrast, wild-type Shp exhibits an EPR spectrum with dominant low spin signals (>86%) due to strong coordination by the sulfur atoms of Met^{66} and Met^{153}.

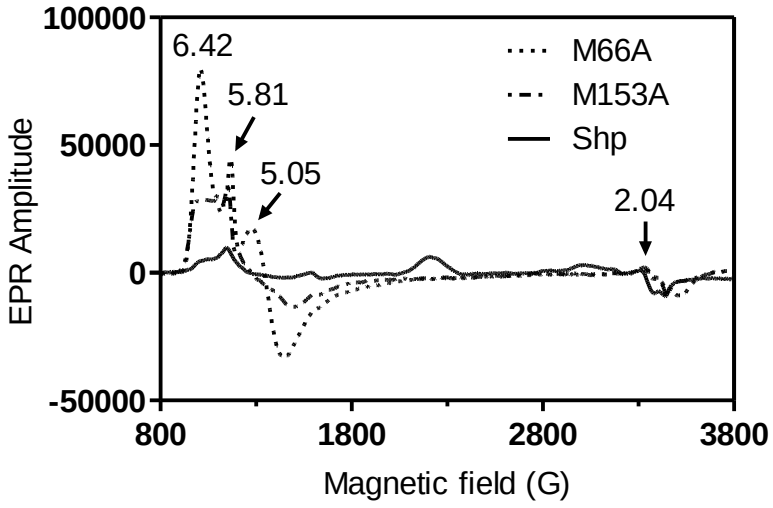

Figure 3.3: EPR Spectra of Oxidized Shp, Shp^{M66A}, and Shp^{M153A} Proteins. Each protein was at 100 μM. The numbers are the g values of the indicated EPR peaks.

His Replacement Mutants of Shp Met^{66} and Met^{153}

Shp^{M153H} appears to exhibit normal wild type-like hemichrome and hemochrome spectra (Fig. 3.4A and 3.4B), indicating axial His and Met coordination in both oxidation states. This conclusion is supported by the EPR spectrum of oxidized Shp^{M153H}, which shows 60% low spin character (Fig. 3.4B). Although reduced Shp^{M66H} displays a wild type-like spectrum indicative of His and Met coordination (Fig. 3.4B), oxidized Shp^{M66H} shows an optical spectrum (Fig. 3.4A) similar to that of high spin aquometmyoglobin (232, 7), suggesting hexacoordinate Met-Fe-OH_2 coordination. This coordination is

supported by the EPR spectrum of oxidized Shp^{M66H}, which shows a single g = 5.66 signal indicative of a purely high spin aquohemin form (Fig. 3.5). Thus, replacement of Met^{66} by His results in a coordination of the heme iron to a solvent water molecule, instead His^{66}, in the oxidized mutant, further supporting the idea that Met^{66} is only weakly coordinated to the heme iron atom.

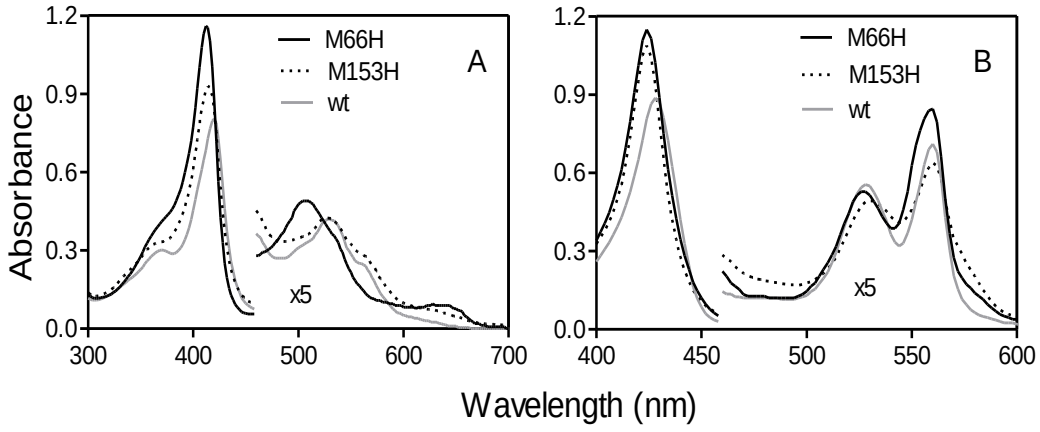

Figure 3.4: Optical Absorption Spectra of Shp^{M66H} and Shp^{M153H}. Absorption spectra of 7.7 μM Shp^{M66H}, Shp^{M153H}, and wild-type (wt) Shp in the oxidized (A) and reduced (B) states are shown.

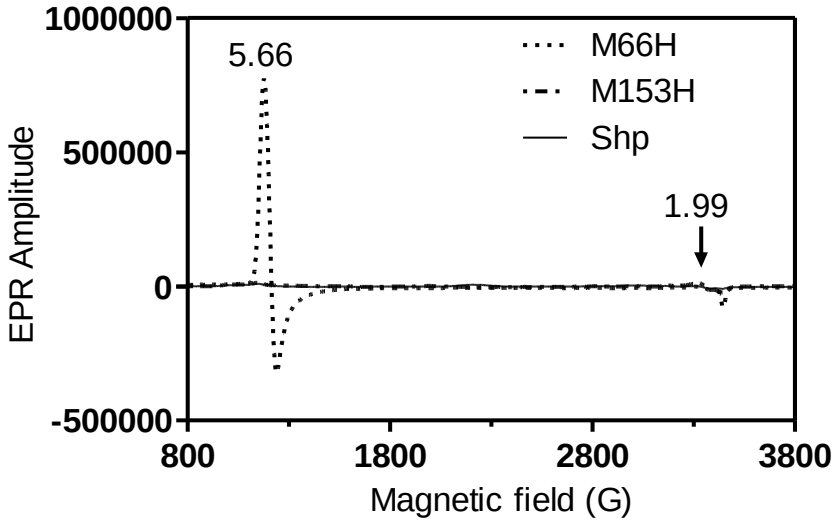

Figure 3.5: EPR Spectra of oxidized Shp^{M66H} and Shp^{M153H}. Each protein was at 100 μM. The numbers are the g values of the indicated EPR peaks.

Heme Binding to and Dissociation
from the Met^{66} and Met^{153} Mutants

To examine the individual contributions of the Met ligands to the overall affinity of Shp for heme, association and dissociation rate constants for heme binding to Shp^{M66A}, Shp^{M153A}, Shp^{M66H}, and Shp^{M153H} were measured and compared with the corresponding parameters for wild-type Shp (Table 3.2). Association equilibrium constants for heme binding to all five proteins were calculated from these parameters as described previously (4). When heme was mixed with each apoShp mutant, the spectrum of the reaction shifted from that of free hemin to those of the holoShp mutants within 1 s (Fig. 3.6A and 3.6B). The time course for each reaction could be described by a single exponential function, and the observed pseudo-first-order rate constants were hyperbolically dependent on [apoprotein] (Fig. 3.6C). The apparent bimolecular rate constant for heme association was estimated from the slope at low apoprotein concentration, which

mathematically is the limiting rate constant divided by the apparent K_d for the initial heme-apoprotein complex (4). Heme dissociation from the mutant Shp proteins was measured using H64Y/V68F apomyoglobin, and again, the observed time courses could be described by a single exponential expression with the rate of heme dissociation from Shp^{M153A} being much larger than that for Shp^{M66A} (Fig. 3.6D).The apparent equilibrium association constants, K_{heme}, for Shp^{M66A} and Shp^{M153A} were 22,000 and 38 μM^{-1}, respectively, which are 3-fold higher and 138-fold lower than K_{hemin} for wild-type Shp. Surprisingly, both Ala mutants had much greater heme association rate constants than wild-type Shp, and Shp^{M153A} had a 700-fold higher dissociation rate constant than either wild-type Shp or Shp^{M66A}. Although Shp^{M153H} had a heme dissociation rate constant similar to that for wild-type Shp, we could detect no heme dissociation from Shp^{M66H} at excess H64Y/V68F apomyoglobin, indicating that K_{hemin} for Shp^{M66H} is at least 10 times greater than that for the heme scavenger (*i.e.* $\geq$200,000 μM^{-1}) and that the dissociation rate constant is $\leq 0.00001\ s^{-1}$ (232).

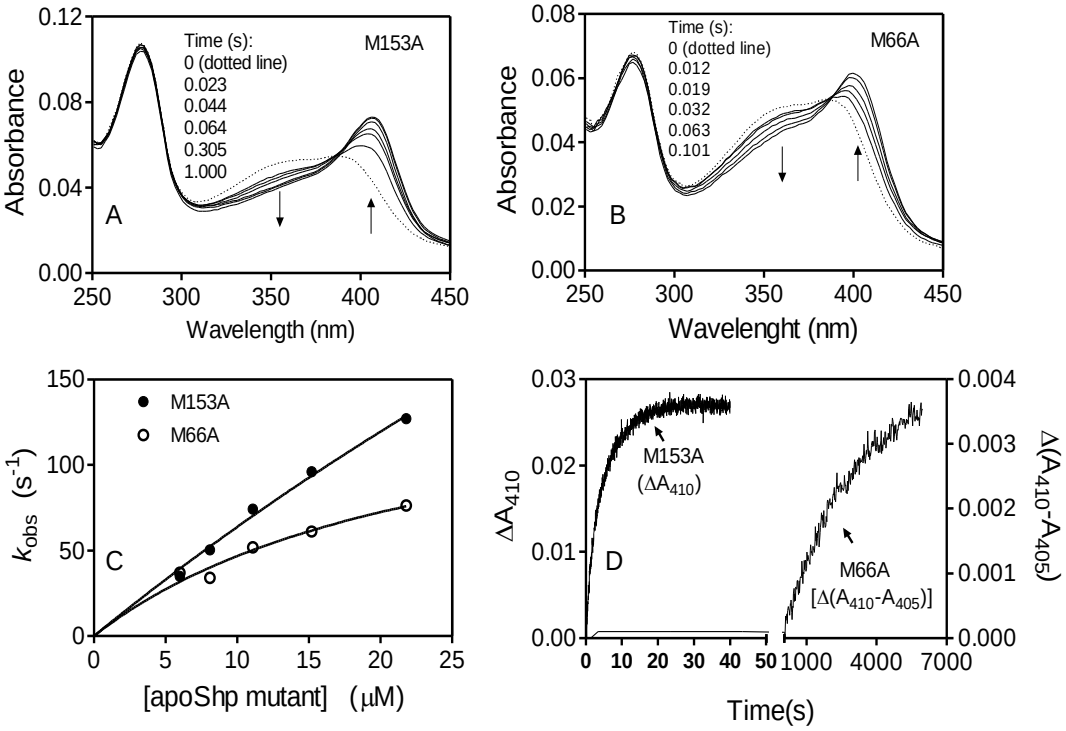

Figure 3.6: Heme Association to and Dissociation from Shp^{M66A} and Shp^{M153A}. A and B, spectral shifts in the reactions of 1.0 μM hemin with 6.0 μM apoShp^{M66A} and apoShp^{M153A}. The arrows in these panels indicate the direction of the spectral shifts with time. C, the observed pseudo-first-order rate constants for heme binding to apoShp^{M66A} and apoShp^{M153A} as a function of [apoprotein]. The curves are theoretical lines obtained by fitting the results to a hyperbolic one-site binding model. D, time courses for heme dissociation from 3 μM Shp^{M66A} and Shp^{M153A} using 58 μM H64Y/V68F apomyoglobin as a heme scavenger.

Table 3.2: Rate and Equilibrium Constants for Heme Binding to and Dissociation from Shp Proteins

	Protein				
Kinetic parameter	Shp	Shp^{M66A}	Shp^{M153A}	Shp^{M66H}	Shp^{M153H}
k_2/k_1 or K_d (hemin binding)[a] (μM)	22 ± 2	22 ± 2	62 ± 7	19 ± 5	58 ± 7
$k_{coordination}$ [a] (s^{-1})	35 ± 4	145 ± 47	490 ± 24	36 ± 8	48 ± 6
$k'_{hemin} \approx k_{coordination}/K_d$, apparent bimolecular rate constant at low [Protein] ($\mu M^{-1}s^{-1}$)	1.6	6.6	7.9	1.9	0.82
k_{-hemin} [b] (s^{-1})	0.0003	0.0003	0.21	≤ 0.00001[c]	0.005
$K_{hemin} \approx k'_{hemin}/k_{-hemin}$ (μM^{-1})	5,300	22,000	38	≥200,000[c]	11,600

[a]The heme binding reaction at 25°C in 20 mM Tris-HCl at pH 8.0 appears to occur by a two-step process involving an initial heme binding step followed by first order iron coordination. In this case, values for k_2/k_1 and $k_{coordination}$ were obtained from fits of the dependence of the observed rates of transfer on [apoprotein] to a hyperbolic one site-binding model. [b]The heme dissociation rate constants from oxidized Shp were determined by the H64Y/V68F apomyoglobin assay (232). [c]These parameters were estimated as k_{-hemin} less than that for H64Y/V68F metmyoglobin and K_{hemin} greater than 10 times the affinity of H64Y/V68F apomyoglobin for heme because no loss of heme was observed, even when the concentration of the heme scavenger was > 30 times that of Shp^{M66H}.

Kinetics of Heme Transfer from Shp Mutants to ApoHtsA

The loss and replacement of the Shp axial bonds were expected to have profound effects on the mechanism of its heme transfer to HtsA. Elucidation of these effects should provide insights into the molecular mechanism of the heme transfer. Thus, we performed the spectral and kinetic analyses of the Shp mutant-apoHtsA reactions. When Shp^{M153A} or Shp^{M66A} was mixed with excess apoHtsA, the A_{600} peak of the Shp mutants decreased rapidly with a concurrent red shift of the Soret peak. These initial changes were followed

by a slower additional red shift of the Soret band and an increase in the A_{530} peak, resulting in the spectrum of the holoHtsA product (Fig. 3.7A and 3.7B).

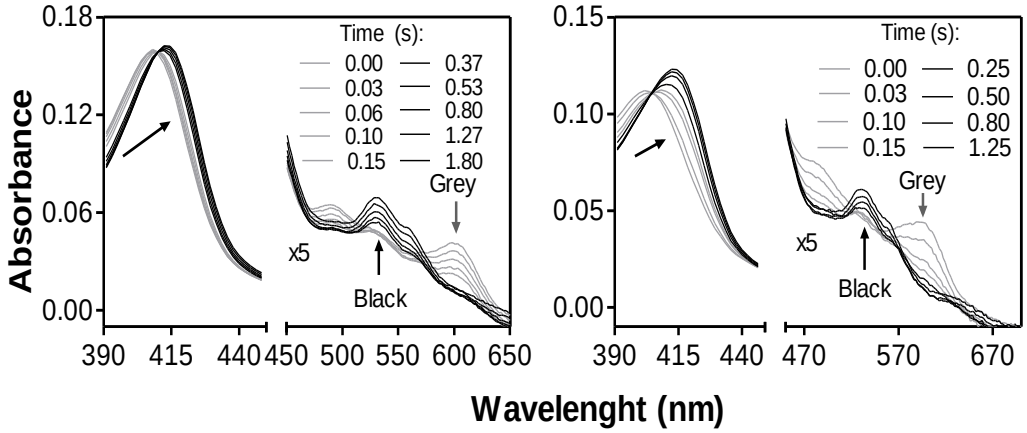

Figure 3.7: Spectral Shifts Demonstrating the Existence of an Intermediate in Heme Transfer from Shp^{M66A} or Shp^{M153A} to apoHtsA. Absorption spectra of 1.3 μM Shp^{M66A} (A) or Shp^{M153A} (B) are presented as a function of time for their reactions with 12 μM apoHtsA. The arrows indicate the directions of the spectral shifts.

The difference between the absorbance at 418 and 406 nm ($\Delta A_{406–418} = A_{406} - A_{418}$) in these two reactions fits to a two-exponential equation, with easily resolved phases (Fig. 3.8A). This result is in contrast to the wild-type Shp-apoHtsA reaction for which the $\Delta A_{425–406}$ time course fits well to a single exponential expression (inset in Fig. 3.8A). Thus, replacement of either Met^{66} or Met^{153} with Ala causes the internal heme transfer in the Shp-apoHtsA complex to become a two-step process.

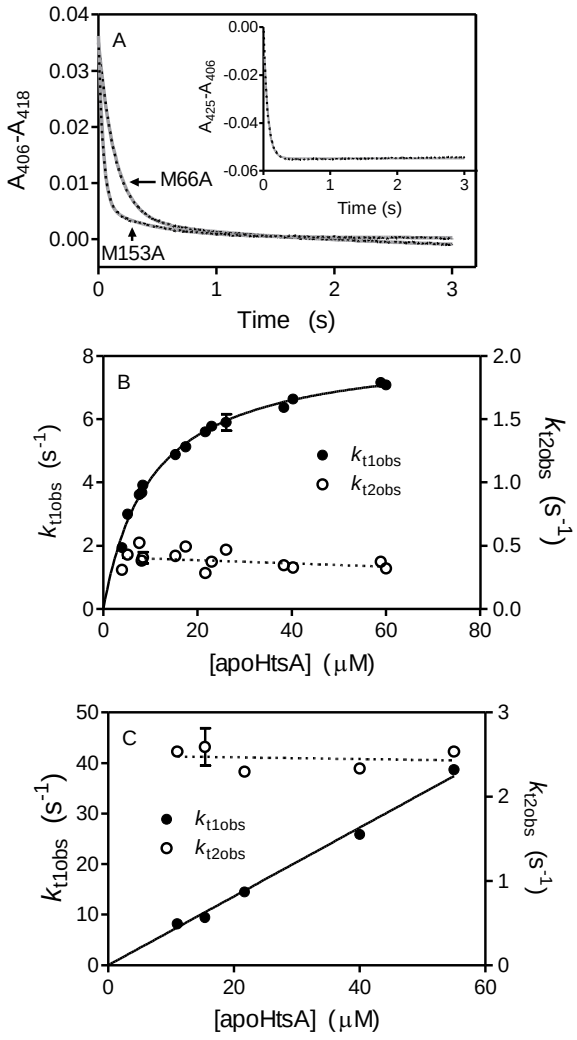

Figure 3.8: Kinetic Analysis of Heme Transfer from Shp^{M66A} and Shp^{M153A} to ApoHtsA. A, absorption time courses at the indicated wavelengths for the reactions of 1.3 μM ShpM66A, Shp^{M153A}, or wild-type Shp (inset) with 40 μM apoHtsA. The dotted curves represent the observed data, and the solid curves are theoretical lines obtained by fitting the data for the mutant and wild-type reactions to two-exponential and single exponential equations, respectively. B, the observed rate constants k_{t1obs} and k_{t2obs} plotted as a function of [apoHtsA] in the Shp^{M66A}-apoHtsA reaction. The rate constants at different [apoHtsA] were obtained from double-exponential fitting as in A. C, the observed rate constants k_{t1obs} and k_{t2obs} as functions of [apoHtsA] in the Shp^{M153A}-apoHtsA reaction.

Fitting the $\Delta A_{406-418}$ time courses for the Shp mutant-apoHtsA reactions to a two-exponential equation results in two observed rate constants, k_{t1obs} and k_{t2obs} that are the

rate constants of the fast and slow spectral changes, respectively. The values of k_{t1obs} depend on [apoHtsA] hyperbolically and almost linearly for the Shp^{M66A}/apoHtsA and Shp^{M153A}/apoHtsA reactions, respectively. In contrast, k_{t2obs} does not change with [apoHtsA] (Fig. 3.8B and 3.8C) and represents a simple first order process. These results can be interpreted in terms of the minimal model shown in Scheme 3.2. In this model, Shp^{M66A} or Shp^{M153A} (Shp^{A}) first forms a complex with apoHtsA, and heme transfer begins with the formation of an intermediate, which we propose to be hexacoordinate ShpA-heme-HtsA with one ligand from each protein. This true ternary complex then converts into $apoShp^{A}$ and holoHtsA in a simple first order process.

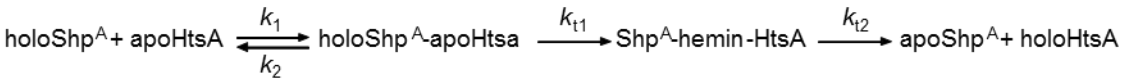

SCHEME 3.2

k_1 and k_2 are the rate constants for bimolecular formation and unimolecular dissociation of the initial Shp mutant-apoHtsA complex, respectively, and k_{t1} and k_{t2} are the first order rate constants for the formation of the intermediate and the products, respectively. When the initial [apoHtsA] is ≥5 [Shp^{A}], the time course for $\Delta A_{406-418}$ can be represented by Equation 3.1,

$$\Delta A_{406-418} = Ae^{-k_{t1obs}t} + Be^{-k_{t2obs}t} \quad \text{(Eq. 3.1)}$$

where t represents time, and k_{t1obs} is given by Equation 3.2.

$$k_{t1obs} = \frac{k_{t1}[apoHtsA]}{(k_2 + k_{t1})/k_1 + [apoHtsA]} \approx \frac{k_{t1}[apoHtsA]}{K_d + [apoHtsA]} \quad \text{(Eq. 3.2)}$$

K_d equals k_2/k_1, the dissociation constant of the ShpA-apoHtsA complex. According to this model, k_{t2obs} is directly equal to the rate constant k_{t2} for the final transfer step to form holoHtsA. K_d, k_{t1}, and k_{t2} were calculated from the data in Fig. 3.8 and are 11.4 ± 0.3 μM, 8.7 s^{-1}, and 0.38 ± 0.08 s^{-1}, respectively, for the Shp^{M66A}-apoHtsA reaction and 170 ± 8 μM, 120 s^{-1}, and 2.5 ± 0.2 s^{-1}, respectively, for the Shp^{M153A}-apoHtsA reaction (Table 3.1). Interestingly, the values of K_d, k_{t1}, and k_{t2} in the Shp^{M66A} reaction are all smaller than those in the Shp^{M153A} reaction. These results show that replacement of Met^{66} with Ala causes Shp to bind to HtsA more tightly but, at the same time, makes it more difficult for Shp to transfer its hemin to apoHtsA.

Shp^{M153H}, but not Shp^{M66H}, transfers its hemin to apoHtsA. The transfer process is a single exponential process, indicating that the M153H replacement does not alter the kinetic mechanism from that seen for wild-type Shp. However, the mutation decreases the dissociation equilibrium constant (K_d) for formation of the Shp-apoHtsA complex by 7-fold and decreased the intracomplex transfer rate constant by 12-fold. These results show that bis-Met coordination in Shp is more efficient than His-Met coordination for heme transfer from Shp to apoHtsA.

Effects of pH on Heme Binding to the Shp Axial Mutants

The UV-Vis spectra of ferric M66A Shp at pH >8.6 have peaks at 404, 489, and 600 nm. As pH decreases from pH 8.6 to ≤ 6, the Soret absorption peak increases in intensity and has a red shift as well, and the charge transfer bands in the visible region undergo dramatic changes as well, resulting in an absorption spectrum with peaks at 408, 502, 534, and 624 nm at pH 6 to 4.5 (Fig. 3.9A). These spectral changes fit an equation

describing the absorbance change with the titration of a single ionizable group with a pK_a of 7.6 ± 0.1 (Insert in Fig. 3.9A). The spectra of M66A Shp at pH > 8.6 are similar to that of the pentacoordinate H229A HtsA heme complex, and the spectra of M66A Shp at around pH 6.0 are similar to that of hexacoordinate, high spin M79A heme complex. Similarly, the MCD spectra of M66A Shp at high and low pH are similar to that of pentacoordinate H229A HtsA complex and hexacoordinate heme complex, respectively (Fig. 3.9B). These results indicate that the decrease in pH induces the conversion of the coordination of the M66A Shp heme iron from pentacoordination to hexacoordination. This conversion is associated with the protonation of a group.

There were some changes in the absorption spectrum of M153A when pH decreased from 8 to 6; however, the overall spectral pattern did not change (Fig. 3.10A). Consistent with this observation, the MCD spectrum of M153A Shp at pH 6.0 was still very similar to that of the protein at pH 8.0, indicating that the majority of the heme iron does not change the coordination when pH decreases from 8.0 to 6.0 (insert in Fig. 3.10A). However, as pH continues to drop from 6.0 to 5.0, the Soret peak drops and eventually disappears (Fig. 3.10B), indicating that the Met66-Fe axial bond in M153A Shp breaks down at low pH. To determine whether the heme is still associated with the M153A protein at pH 5.0, the protein at pH 5.0 was passed through a G-25 column, and 88% of heme was still associated with the protein. Thus, the heme is still associated with M153A Shp but the heme iron does not have axial bonds. These results suggest that the heme pocket can open on the M66 side of the bound heme.

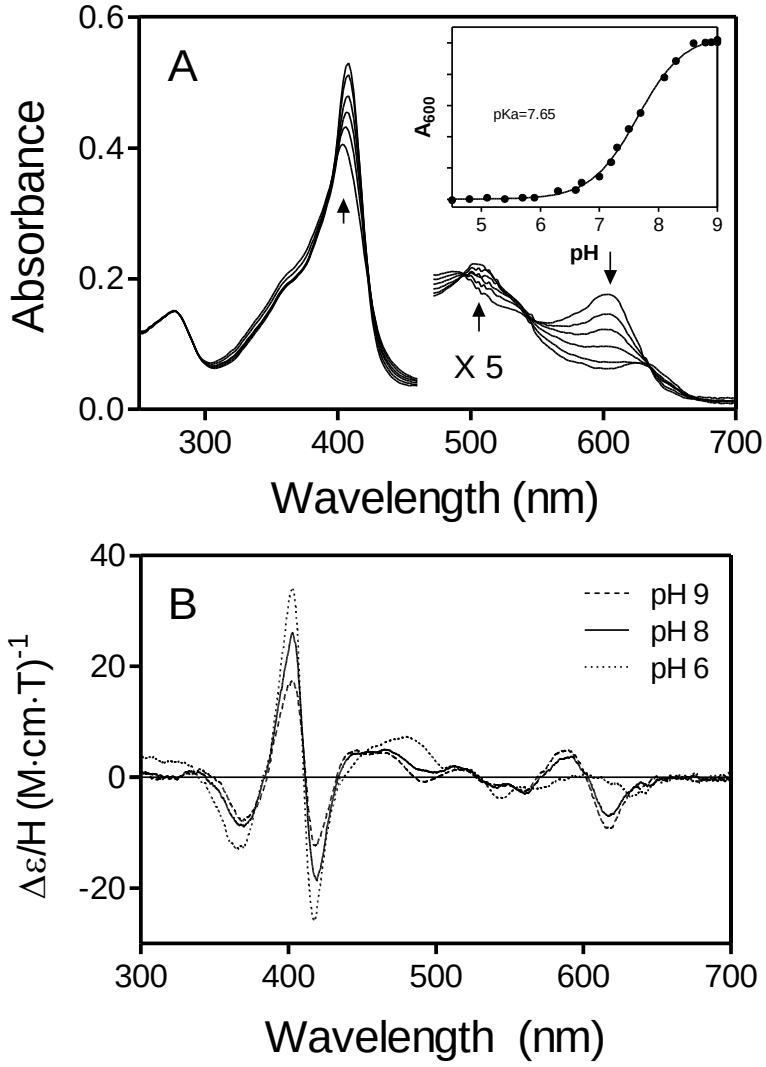

Figure 3.9: Effect of pH on Optical and MCD Spectra of Shp^{M66A}. A, spectra and absorption at 600 nm (insertion) of Shp^{M66A} in the pH range of 9-4.5. B, MCD spectra of Shp^{M66A} at pH 6, 8, and 9.

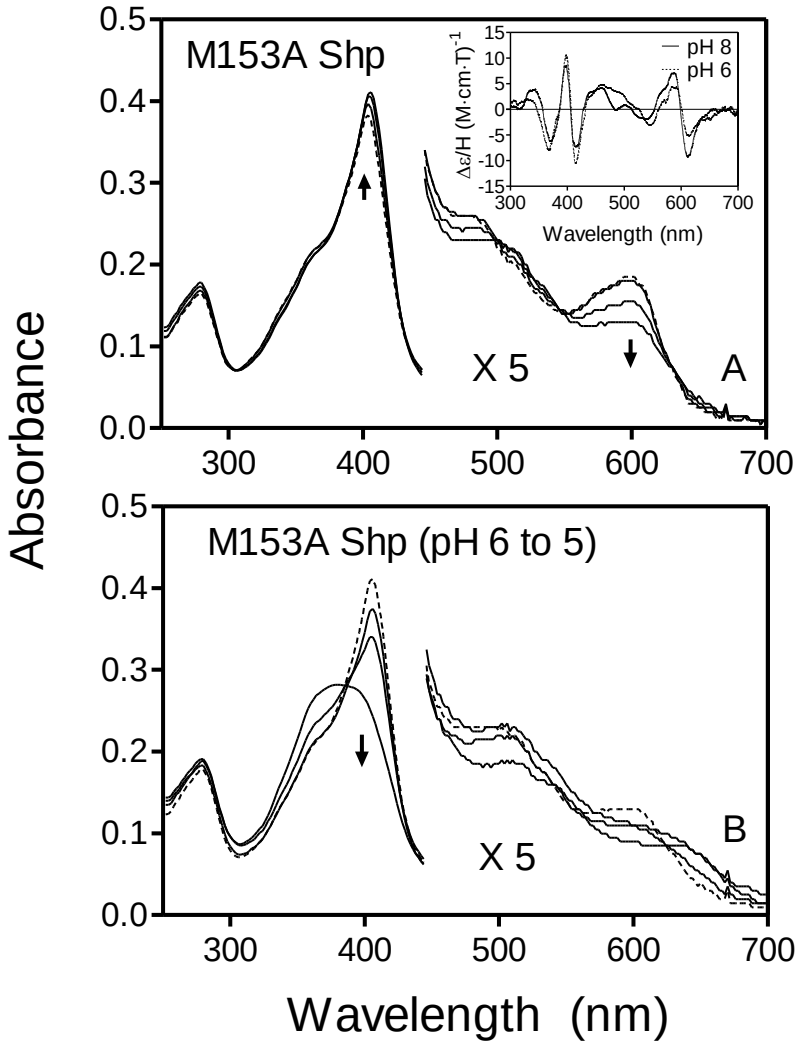

Figure 3.10: Optical and MCD Spectra of Shp^{M153A} in the pH range of 5-8. A, the optical and MCD (insertion) spectra in the pH range of 6-8. B, the optical spectra in the pH range of 5-6.

Discussion

We have been studying the Shp/HtsA system as a model to understand heme transfer from one protein to another. We previously examined the kinetic mechanism for the Shp-to-HtsA heme transfer with the wild-type proteins (4). In this study, the extensive

spectral and kinetic characterizations of the axial mutants of Shp, in combination with the high resolution structure for Shp^{180}, have further advanced our understanding of the heme transfer mechanism and helped elucidate molecular details of the reaction. The heme binding domain of Shp contains residues 30–180 and is functionally active. The axial Met^{153} residue of Shp is critical for its relatively high affinity for heme, whereas the other axial residue, Met^{66}, destabilizes the heme binding. Nonetheless, both Met^{66} and Met^{153} are critical for rapid heme transfer. More significantly, kinetic characterization of the Shp mutant-apoHtsA reactions has allowed us to detect intermediates during heme transfer and propose a novel mechanism of simultaneous attack on both sides of bound heme in Shp by ligand side chains from apoHtsA. In addition, the pH titration results suggest that the heme pocket in Shp can open up in a pH dependent way.

Truncated Shp^{180} has the same EPR and UV-visible spectral properties as full-length Shp. Its structure exhibits an immunoglobulin-like β-sandwich fold and is similar to the structures reported for the *S. aureus* heme uptake proteins IsdC and IsdA (180, 181). Shp^{180} has a well defined heme-binding site with two Met axial ligands (Fig. 3.12) and has retained the ability to transfer both hemin and heme to apoHtsA by the activated ternary complex mechanism that is observed for the full-length Shp-apoHtsA reaction.

However, the affinity of Shp^{180} for apoHtsA is 2-fold less than that of full-length Shp, and the rate of internal transfer in the Shp^{180}-apoHtsA complex is ∼10-fold slower. Thus, although the heme-binding domain is functionally active, the COOH-terminal region does play a role in enhancing the speed of the heme transfer reaction. An

understanding of structural cause of this enhancement will require determination of the structure of the full-length protein, which so far we have been unable to crystallize.

Shp^{M66A} and Shp^{M153A} share similar spectral features with apolar distal histidine mutants (H64V, H64L) of human and sperm whale metmyoglobin (7), including a broadened and blue-shifted Soret peak in the 395–405 nm region and a high spin, charge transfer band in the 600–650 nm region.

The MCD spectrum of ferric M153A is again very similar to that of ferric H229A HtsA (Fig. 3.2B). Although the MCD profile of M66A Shp is very similar with those of H229A HtsA and M153A Shp, the ellipticities of M66A Shp at the Soret band is about three times as those of H229A HtsA and Shp^{M153A}. According to the effects of pH on the MCD and UV-Vis spectra of these proteins described below, the higher ellipticities of M66A Shp at pH 8.0 appears to be partly due to that a small portion of Shp^{M66A} has a hexacoordinate heme iron with a water molecule at the vacated coordination site.

The multiple derivative peaks in the g = 6 region of the EPR spectra of the ferric forms of these Shp mutants are also very similar to those observed for H64V and H64L metmyoglobin (7), which have been shown by crystallography to be water-free, pentacoordinate heme complexes (233). Thus, oxidized Shp^{M66A} and Shp^{M153A} are almost certainly in pentacoordinate heme-Met form with only a small portion of water-heme-Met coordination.

The Met^{153}-Fe coordination bond confers the high affinity of Shp for heme. Replacement of Met^{153} with Ala increases the rate of heme dissociation by 700-fold and decreases the overall affinity of Shp for hemin by 2 orders of magnitude. The Met^{153} side of the bound heme in the crystal structure of Shp^{180} is less exposed to solvent than the

Met^{66} side, which is only partially covered by a three-turn α helix (Fig. 3.12, B and C). This interpretation is further supported by the observation that imidazole can coordinate to the heme iron of Shp^{M66A} but not Shp^{M153A} (data not shown).

Bis-Met coordination in Shp appears to be the result of selective evolutionary pressure to increase the speed of heme transfer. The affinity of Shp^{M66A} for heme is 3-fold higher than that of wild-type Shp. As pH drops from 6.0 to 5.0, the Met66-Fe bond in Shp^{M153A} breaks down at low pH. Replacement of Met^{66} with His prevents heme from being transferred to apoHtsA. The EPR spectrum of Shp^{M66H} is virtually identical to that of aquometmyoglobin, and its affinity for heme is very high, on the order of that of native sperm whale myoglobins (232). Utilizing Met^{66} as an axial ligand appears to destabilize the bound cofactor and facilitate its transfer. Although oxidized Shp^{M153H} exhibits a spectrum characteristic of a low spin hemichrome, the value of $k_{transfer}$ for heme transfer from Shp^{M153H} to apoHtsA is only one-twelfth of that in the wild-type Shp/HtsA reaction. Thus, bis-Met coordination in Shp facilitates rapid heme transfer. Bis-Met coordination has only been found previously in bacterioferritin (5), and its physiological role in this protein is unknown.

Heme transfer from wild-type Shp to apoHtsA is a concerted process, and only a single kinetic phase is observed (4). In contrast, heme transfer from Shp^{M66A} and Shp^{M153A} to apoHtsA shows two distinct kinetic phases and an intermediate that appears to be a true ternary Shp-heme-HtsA complex with one axial ligand provided by each protein. Although a change in mechanism of heme transfer due to loss of an axial ligand was not unexpected, the slowing of the overall exchange process was a surprise.

The distinct spectral intermediates in the reactions of apoHtsA with Shp^{M66A} and Shp^{M153A} are the loss of the 600-nm band, suggesting ligation to form a hexacoordinate heme complex (235). The simplest interpretation of the intermediate is binding of an axial ligand side chain from apoHtsA to the sixth coordination position of heme still bound to Shp to form a true ternary complex. A second feature in both mutant reactions is that loss of the A_{600} peak is the first fast phase. These results are significant, because they indicate that both sides of the bound heme in Shp can be attacked by the axial residues in apoHtsA after forming the initial holoShp-apoHtsA complex. The decay of the intermediate is observed by a further red shift and intensification of the Soret, α, and β bands, resulting in the spectrum of the hexacoordinate holoHtsA product. Thus, we propose that the two axial bonds in the HtsA product are sequentially formed in the transfer reactions of these mutants. The intermediates are Met^{153}-$Fe(III)^{heme}$-X and Met^{66}-$Fe(III)^{heme}$-Y ternary complexes, where X and Y are the axial ligands donated by HtsA (Fig. 3.11A and 3.11B). X and Y in HtsA are Met^{79} and His^{229}.

The features of the mutant Shp reactions have led us to propose a "plug-in" mechanism for the concerted one-step, internal heme transfer process carried out by wild-type holoShp. There are two possible interpretations of the one-step transfer reaction: 1) the displacement of the two Shp Met ligands is truly simultaneous, or 2) the displacement of the first Shp Met ligand is rate-limiting. In both interpretations, the two new coordination bonds are formed at effectively the same time (Fig. 3.11C) and would give equivalent kinetic results.

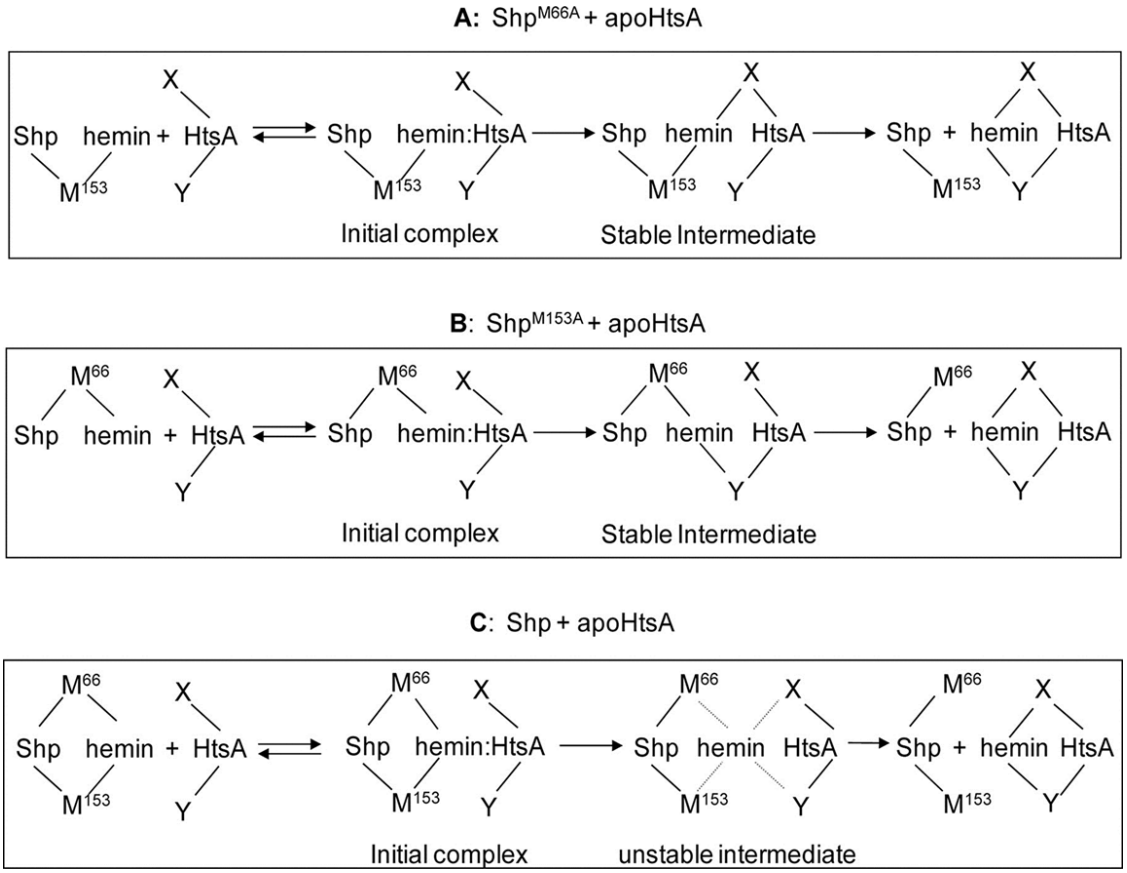

Figure 3.11: Proposed Schemes for the Reactions of the Wild-Type and Mutant Shp Proteins with ApoHtsA. Met^{66} and Met^{153} (M^{66} and M^{153}) are the axial ligands in Shp; X and Y are the axial ligands, Met^{79} and His^{229}, in HtsA; and the short lines to hemin represent the axial bonds. The two axial bonds of the HtsA product are formed at about same time in the wild-type Shp reaction but are sequentially formed in the M66A and M153A mutant reactions with a Shp-hemin-HtsA ternary complex intermediate with one ligand from each protein.

The two axial ligands of apoHtsA must be close to the two axial positions of hemin in the holoShp-apoHtsA binary complex. This idea implies that the empty heme pocket in apoHtsA either pre-exists or is induced quickly after the binary complex is formed. This view also requires that the HtsA axial side chains easily slide into the exposed Shp heme binding site to “pull or pry” the cofactor out of Shp. Thus, our initial interpretation can be called a plug-in mechanism for transferring the hemin actively from

one protein to another. The bound hemin in Shp^{180} has significant exposure to solvent on both Met^{153} and Met^{66} sides (Fig. 3.12). Thus, simultaneous ligand displacement by adjacent apoHtsA ligands in a Shp-HtsA complex is structurally feasible by sliding movements of the amino acid side chains across both sides of the hemin plane.

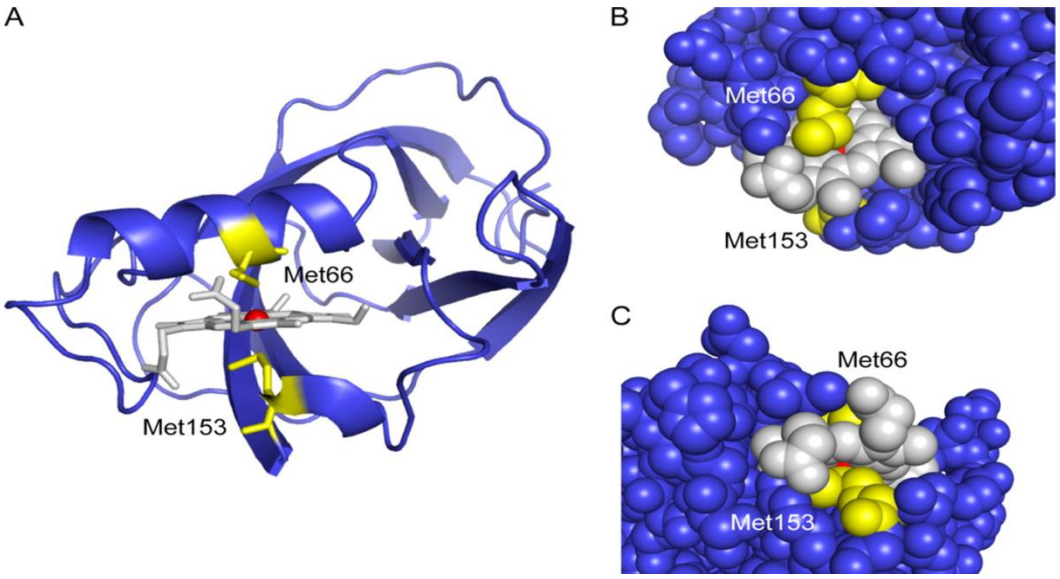

FIGURE 3.12: The Hemin Binding Site and its Solvent Exposure in the Crystal Structure of Shp^{180}. A, a ribbon representation of Shp^{180} structure showing hemin binding. The backbone, hemin group, iron, and Met axial ligands are blue lines and ribbons, gray sticks, a red ball, and yellow sticks, respectively. B and C, space-filling blow-ups of the hemin binding site, showing the solvent exposure of the porphyrin ring on the Met^{66} and Met^{153} sides. The colors of the different components are the same as those in A. The representations were derived from the crystal structure of Shp^{180} (Protein Data Bank code 2Q7A).

Both Shp^{M153A} and Shp^{M66A} appear to have no ligand at the mutated axial positions, and majority of Shp^{M66A} also has pentacoordinate heme complex pH 8.0. This open pentacoordinate geometry appears to facilitate insertion of the first apoHtsA ligand to generate a discrete and kinetically stable intermediate. The intermediates for Shp^{M153A} and Shp^{M66A} decay to holoHtsA at rates of 2 and 0.4 s^{-1}, respectively, which are ~20–

100-fold slower than $k_{transfer}$ for full-length Shp. The underlying cause for the appearance of the intermediate and the slowing of the second ligand displacement reaction is unclear. One possible reason is that the first displaced Met in the wild-type Shp reaction sterically clashes with the apoHtsA axial ligand, destabilizing the ternary complex intermediate but at the same time facilitating transfer by "pushing" the heme into the binding pocket of apoHtsA (Fig. 3.11C). The association rate constants of hemin binding to apoShp^{M66A} and apoShp^{M153A} are 4 and 14 times greater, respectively, than that for hemin binding to wild-type apoShp. This result suggests that the heme pocket in wild-type Shp is more sterically restricted and perhaps designed to help eject noncoordinated heme from its active site once the HtsA ligands have been inserted and to destabilize ternary complexes that slow the net rate of transfer. The Met-to-Ala replacements appear to relieve this steric pressure. Indeed, the M153A replacement apparently enhances the interaction between heme and the M153 side and weakens the Met66-iron bond, making for the Met66-iron bond to break more easily during pH titration. In addition, the lack of a sixth ligand or weaker coordination with water should strengthen the remaining Fe(III)–Met bond, making its displacement more difficult and probably requiring the binding of the first HtsA ligand to the unoccupied coordination site. This latter phenomenon appears to occur for the Shp^{M66A}/apoHtsA reaction.

The heme pocket in Shp appears to be able to open up on the Met66 side. This is consistent with the structure of Shp. The Met153 side of heme is more buried than the Met66 side and the bound heme interacts with beta sheets on the M153 side but with only an alpha helix on the Met66 side. A H bond may play a role in keeping the alpha helix at the closing position, and cleavage of the H bond by protonation during pH titration may

facilitate the moving of the alpha helix to open the heme pocket. This opening mechanism may play a role in direct heme transfer from Shp to HtsA. It is possible that Shp-HtsA interaction can open up the heme pocket partially by breaking this proposed H bond.

The findings in this work suggest a unique plug-in mechanism for hemin transfer from Shp to HtsA. The key features are insertion of the axial ligands of apoHtsA on both sides of the partially exposed hemin in Shp and subsequent, simultaneous displacement of the two axial bonds to pull the hemin from Shp to HtsA. Although the mechanism needs to be verified, these ideas may serve as an initial framework for examining a variety of other clinically relevant heme transfer processes in pathogenic bacteria, including the HasA/HasR, hemoglobin/ShuA and *S. aureus* Isd systems in which hemin transfer has been biochemically demonstrated.

Note: The EPR measurement was performed by Dr. Marian Fabian at Rice University.

PROBING THE MECHANISM OF HEME TRANSFER FROM THE SURFACE PROTEIN SHP TO THE LIPOPROTEIN HTSA OF GROUP A STREPTOCOCCUS USING HTSA HEME AXIAL MUTANTS

Abstract

The surface protein Shp of Group A *Streptococcus* rapidly transfers its heme to HtsA, the lipoprotein component of the HtsABC transporter, in a concerted two-step process with one kinetic phase. In chapter III, alanine replacement of the Met66 and Met153 axial ligands of the heme iron in Shp, the heme donor, cause similar alternation of the kinetic mechanism of the Shp/apoHtsA reaction, suggesting that the Met66 and Met153 residues are directly displaced by the axial ligand residues of apoHtsA. The structural basis and the molecular mechanism of this heme transfer reaction have been further explored by studying the effect of alanine replacement of the Met79 and His229 axial ligands of the HtsA heme iron on Shp-to-HtsA heme transfer. The H229A replacement decreases the affinity of HtsA for heme and consequently dramatically decreased the efficiency of heme transfer from ferric Shp to HtsA. In contrast, the M79A replacement has limited detrimental effect on the affinity of HtsA for heme, and the M79A HtsA, like wild-type HtsA, can efficiently acquire heme from ferric Shp. Interestingly, the M79A mutation changed the kinetic mechanism of the Shp-to-HtsA heme transfer reaction from a single kinetic phase to double kinetic phases. $HtsA^{H229A}$ and $HtsA^{M79A}$ cannot take up heme from ferrous Shp, indicating that both His229 and Met79 of HtsA are required for heme transfer from ferrous Shp to HtsA. Significantly, $HtsA^{H229A}$ and $HtsA^{M79A}$ induce rapid autoxidation of ferrous Shp, indicating HtsA and Shp interact to each other and cause alteration in the heme-protein interaction in Shp.

These results further support the direct axial ligand displacement mechanism and indicate the existence of an activated holoShp-apoHtsA intermediate during Shp-to-HtsA transfer. To evaluate the heme transfer mechanism *in vivo*, $M66H^{Shp}$, $M153A^{Shp}$ and $H229A^{HtsA}$ GAS mutant strains were generated. $M66H^{Shp}$ is more virulent than the wt strain, whereas $M153A^{Shp}$ and $H229A^{HtsA}$ were as virulent as the revertant strain. The implication of these results was discussed.

Introduction

Heme is an important iron source for Group A *Streptococcus* (GAS) and is critical for GAS growth under iron-limited conditions (236). The heme acquisition system in GAS includes the cell surface proteins Shr and Shp and the HtsABC transporter (175, 176, 186, 192, 196, 237-239). Shr can acquire heme from human methemoglobin and is a source of heme for Shp (186, 238). Heme can be directly transferred from Shp to HtsA (192, 196, 239), which is the substrate-binding component of the HtsABC transporter, but Shr did not efficiently donate its heme to apoHtsA. These findings support a heme acquisition pathway by the Shr/Shp/HtsABC system in which Shr directly extracts heme from metHb and Shp relays it from Shr to HtsA.

Ferric Shp rapidly transfers heme to apoHtsA through a ferric Shp-apoHtsA complex at a rate constant of $43 \pm 3\ s^{-1}$, which is ~ 4,000 times greater than the rate of simple heme dissociation from ferric Shp into solvent. In the reaction of ferrous Shp with apoHtsA, heme is transferred to apoHtsA with a rate constant of $28 \pm 6\ s^{-1}$, and the resulting ferrous HtsA product then autoxidizes to ferric HtsA (196).

Shp-to-HtsA heme transfer reaction follows a concerted two-step kinetic mechanism in which Shp first forms a complex with apoHtsA and then transfers its heme to apoHtsA with a single kinetic phase (196). This kinetic mechanism implies that the reaction follows either a sequential axial displacement mechanism where the first axial displacement is rate-limiting or a simultaneous axial displacement mechanism in which the two axial bonds of the heme iron in the holoHtsA product are formed at about the same time. Alanine replacement of the Met66 and Met153 axial ligands of the Shp heme iron both alters the kinetic mechanism and slow down heme transfer by stabilizing the intermediates, supporting a direct axial ligand displacement mechanism. In Chapter III, we proposed a "plug-in" reaction model in which the side chains of the heme axial ligands in apoHtsA are inserted into the axial positions of the bound heme in Shp to extract heme and pull it into the heme pocket of HtsA.

In heme transfer from Shp to apoHtsA and from IsdA to apoIsdC, heme donor and acceptor form a complex, releasing free energy (188, 196). The free energy released is used to weaken heme binding in heme donor and thus facilitate transfer to heme acceptor. Protein interaction also is critical for heme transfer from *Serratia marcescens* hemophore HasA to HasA receptor HasR (182). These studies indicate activated heme transfer from one protein to another in these heme acquisition systems. However, there is no direct evidence for the alteration of the heme binding in the donor during the donor-acceptor interaction yet.

To further examine the direct axial ligand displacement mechanism and search for evidence other than kinetic and thermodynamic ones of the activated heme transfer mechanism, the effects of axial ligand replacements in HtsA on Shp-to-HtsA heme

transfer have been studied. Chapter II described that the identification of the His229 and Met79 residues as the axial ligands of the HtsA heme iron and spectroscopic characterization of HtsA heme axial ligand mutants. Alanine replacement of His229 changes coordination of the heme iron from hexacoordination to pentacoordination, whereas alanine replacement of Met79 results in a hexacoordinate heme iron with water and histidine ligands. Accessibility to exogenous ligands for heme demonstrate that the Met79 side of the heme pocket is more accessible than the His229 side (240). In this chapter, H229A replacement decreases the affinity of HtsA for heme and consequently decreases the ability of HtsA to acquire heme from ferric Shp. On the contrary, HtsAM79A has high affinity of heme and acquires heme from ferric Shp efficiently. M79A mutation altered the kinetic mechanism of Shp-to-HtsA heme transfer from a single kinetic phase to double kinetic phases. Ferrous Shp cannot transfer heme to neither $HtsA^{H229A}$ nor $HtsA^{M79A}$ but it is oxidized rapidly in the presence of either $HtsA^{H229A}$ or $HtsA^{M79A}$. The results support the "plug-in" mechanism and provide an evidence for the Shp-apoHtsA interaction-mediated weakening of the axial bonds in Shp.

Materials and Methods

Materials

Resins for protein purification were from GE Healthcare Biosciences. Tris (hydroxymethyl)aminomethane, ammonium sulfate, sodium chloride and Luria-Bertani broth were purchased from EMD Chemicals. Bovine hemin chloride was from Sigma. Potassium ferricyanide and sodium dithionite were obtained from Fisher Scientific.

Bacteria Strains, Growth Conditions and Cell Culture

The wild-type GAS strain, MGA5005, and its derived mutants (*shp* or *htsA* deletion mutants, revertants of the deletion mutants, and strains carrying *shp*^{M66H}, *shp*^{M153A}, or *htsA*^{H229A}) were grown at 37°C in Todd-Hewitt broth supplemented with 0.5% (w/v) yeast extract (THY).

Proteins

Recombinant Shp was purified as previously described (176). Prepared Shp was a mixture of ferric and ferrous forms. Homogenous ferric Shp was obtained by oxidizing ferrous Shp with ferricyanide and removing excess ferricyanide by gel filtration on a Sephadex G-25 column (1.5 x 30 cm). Homogeneous ferrous Shp was prepared by reducing ferric Shp with sodium dithionite and removing excess sodium dithionite through a Sephadex G-25 column (1.5 x 30 cm). Recombinant wild-type, M79A, and H229A HtsA proteins were purified as described in Chapter II. Purified HtsA proteins were mixtures of holo- and apo-forms. Homogeneous apoHtsA proteins were obtained by loading the mixtures on a DEAE column (2.5 x 6 cm) and eluting the column with a 100-ml linear gradient of 0.05-0.15 M NaCl in Tris-HCl, pH 8.0.

Heme Transfer

Heme transfer from ferric Shp to apo-HtsA was monitored by spectral changes associated with heme transfer. Ferric Shp (2.5 μM) was incubated with wt, H229A, or M79A apoHtsA at indicated concentrations in 20 mM Tris-HCl, pH 8, for 5 min, and the absorption spectrum of each mixture was measured and compared with those of holoShp and corresponding holoHtsA protein.

Heme transfer from ferrous Shp to apoHtsA proteins under aerobic and anaerobic conditions was similarly examined by the spectroscopic method. For reaction under anaerobic conditions, excess sodium dithionite was added into holoShp and apoHtsA before mixing.

Kinetic Analysis of Heme Transfer

A stopped-flow spectrophotometer equipped with a photodiode array detector (SX20; Applied Photophysics) was used to measure time courses of spectral changes associated with heme transfer and/or autooxidation of ferrous Shp. HoloShp at 2.5 μM in one syringe was mixed with apoHtsA at ≥ 5 X [holoShp] in 20 mM Tris-HCl, pH 8.0, in the other syringe. Absorption spectra were measured with time in each reaction after mixing. Changes in absorbance at appropriate wavelengths were analyzed as described in the Results section.

Reactions of HoloHtsA Proteins with H64Y/V68F Apomyoglobin

Whether the HtsA proteins significantly lose heme to H64Y/V68F apomyoglobin, a heme scavenger (220), was determined by comparing the optical absorption spectra of holoHtsA and H64Y/V68F holomyoglobin with those of 2 μM holoHtsA protein/40 μM H64Y/V68F apomyoglobin mixtures. Spectral changes of the reactions were continuously monitored for 24 h and decreased to zero by 6 h after the start of the reactions. Thus, the spectra of the mixtures were taken using a SPECTRAMax 384 Plus spectrophotometer after 6 h incubation in 20 mM Tris-HCl, pH 8.0, for determining relative heme affinity of HtsA proteins.

Other Assays and Measurements

Protein concentrations were measured using a modified Lowry protein assay kit (Pierce) with bovine serum albumin as a standard according to the manufacturer's instructions. Heme content of Shp and HtsA was determined using the pyridine hemochrome assay (241). Briefly, each protein in 750 μl of 20 mM Tris-HCl was combined with 175 μl of pyridine, 75 μl of 1 N NaOH, and ~ 2 mg of sodium dithionite. Absorbance at 418 nm was measured immediately after mixing, and heme concentrations were calculated using ε_{418} = 191.5 mM^{-1} cm^{-1}. A SPECTRAmax 384 Plus spectrophotometer was used for absorption measurements, unless otherwise specified.

Generation of GAS Strains Carrying Ala- or
His-replacement of the Axial Ligand Residue in Shp and HtsA

In-frame Deletion of the Shp and HtsA Gene**.** The 3' and 5' ~1,000-bp flanking fragments of the Shp and HtsA fragments to be deleted were amplified from MGAS5005 chromosomal DNA by PCR using the primers listed in Table 4.1 and were sequentially cloned into pGRV (242) at the BgIII/XhoI and XhoI/BamHI sites, respectively, yielding the suicide plasmid pGRV-Δshp and pGRV-ΔhtsA. The plasmids were each introduced into MGAS5005 by electroporation, as described previously (242). The plasmid was inserted into the MGAS5005 genome through a homologous recombination crossover at one flanking fragment. The strain was selected with spectinomycin (150 μg/ml), and it contained one copy of full-length *shp* or *htsA* and one copy of the shortened *shp* or *hts*A gene with the in-frame deletion (Fig 4.1). This strain was grown in THY without

spectinomycin selection for eight passages (one passage = 0.05 to 0.7 increase in the optical density at 600 nm [OD_{600}]) to allow the second crossover event to occur in the other flanking fragment, generating an in-frame deletion of *shp* (Δ*shp*) or *htsA* (Δ*htsA*), which should be sensitive to spectinomycin (Fig 4.1). The culture was plated on THY agar plates after the last passage, and the colonies were spotted in parallel on THY agar plates with and without spectinomycin to identify strains that were sensitive to spectinomycin. These spectinomycin-sensitive strains were analyzed by PCR to identify Δ*shp* and Δ*htsA* strains that had a shorter *shp* and *htsA* PCR product than the wild-type strain. Δ*shp* and Δ*htsA* lack amino acid residues 30-180 and 152-252, respectively. The region of the mutants' genomic DNA encompassing the shortened *shp* and *htsA* genes of the mutants were sequenced to confirm the in-frame deletion and to rule out spurious mutations.

Table 4.1. Primers used for in-frame deletion of *shp* and *htsA*

Primer	Sequence (5'-3')	E site	Amplicon
1	TCGAGATCTGACAACACTAGATATTGCTATTAG	BgIII	F1 of *htsA* for
2	GTCTCGAGCTGGTATTGCTGGCGCAATTCT	XhoI	*htsA* deletion
3	AGCTCGAGACGGCAGTCAAGGAAGGGAAAG	XhoI	F2 of *htsA* for
4	AGTGTCGACTAAATTCCGATGCTCTCACAG	BamHI	*htsA* deletion
5	TCGAGATCTGTTAGGCTACCTTGGTGAATT	BgIII	F1 of shp for shp
6	GTCTCGAGCTGCATACACAAGATTTGTCATTG	XhoI	deletion
7	AGCTCGAGGAAACAGACAATTCTCAAAATC	XhoI	F2 of shp for shp
8	CTGGATCCTTGTCTGGAATGGCATGAGCTGTT	BamHI	deletion

Construction of Isogenic MGAS5005 Mutant Strains that Carry *shp*^{M153A}, *shp*^{M66H}, and *htsA*^{H229A} Mutations**.** The procedures for generating these mutants contained 3 major steps. First, A DNA fragment containing the *shp* or *htsA* gene with its flanking fragments was PCR cloned into pGRV at the BgIII and BamHI sites using primers 4 and 5 in Table 4.1. Secondly, the *shp* or *htsA* gene in the plasmid were subject to site-directed mutagenesis as described in Chapters II and III to convert the plasmid into ones with mutations of M153A and M66H of *shp* and H229A of *htsA*. Thirdly, introduce the *shp*^{M153A} or *shp*^{M66H} and *htsA*^{H229A} genes into the Δ*shp* and Δ*htsA* mutant strains, respectively, to obtain the desired mutants using the procedure of the construction of the *shp* and *htsA* deletion mutants described above (Fig 4.1).

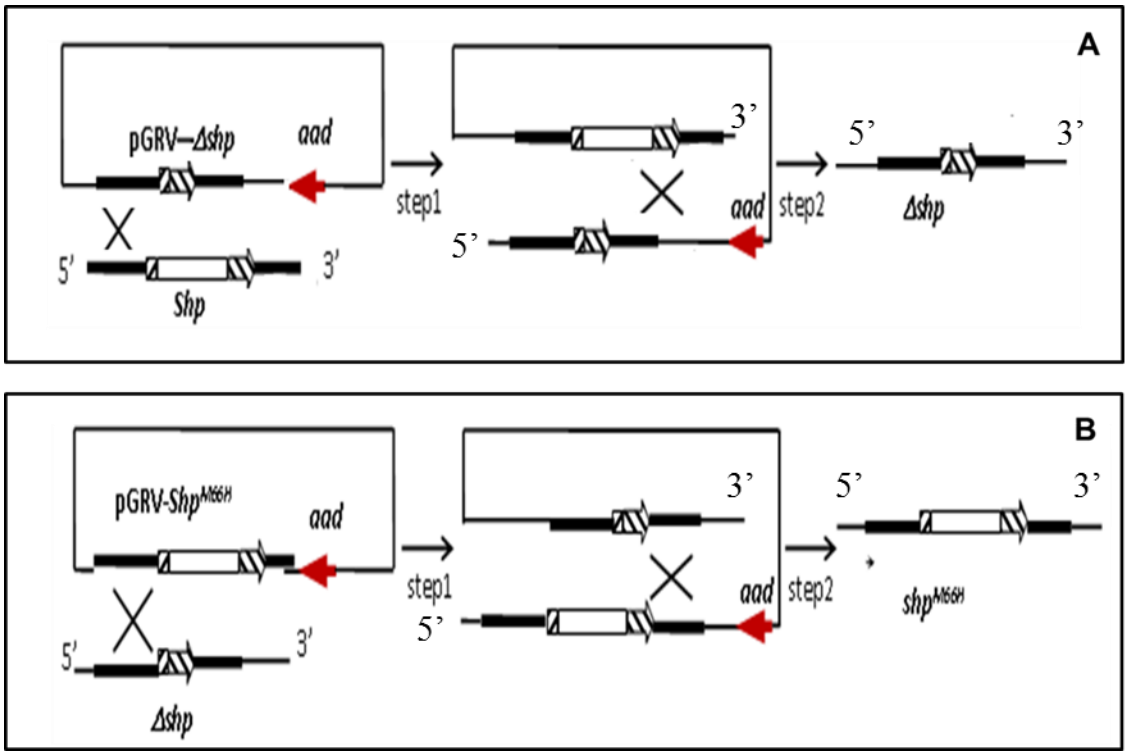

Figure 4.1: Generation of GAS Mutation by Allele Replacement. A, generation of Δshp. B, generation of GAS strain that carries the *shp*^{M66H} mutation.

Mouse Infection

Virulence of the wild-type and mutant strains was compared using a mouse model of subcutaneous GAS infection. Groups of 10 female BALB/c mice (5 weeks old, 20-22 g) were injected subcutaneously with 1.8×10^{8} cfu. The mice were observed daily for 12 days to determine survival rates. The data were statistically evaluated with the Logrank test using GraphPad Prism 5 software. All animal experiments were performed per protocol that was approved by the Montana State University Institutional Animal Care and Use Committee.

Results

Effects of His229Ala and Met79Ala Replacements on Affinity of HtsA for Heme Binding

Affinities of hemoproteins for heme can be estimated by measuring the rates of heme association to apo-proteins and dissociation from holo-proteins. This method cannot be used to determine the affinity of the HtsA proteins because of their incomplete or no heme loss to H64Y/V68F apomyoglobin, the heme scavenger in measurement of heme dissociation. Thus, we could only estimate the relative heme affinity of the HtsA proteins based on their reactions with H64Y/V68F apomyoglobin. According to the spectra of 20:1 apoMb:holoHtsA mixtures (Fig. 4.2), wild-type, M79A, and H229A HtsA proteins lost little, a small fraction, and most of their heme, respectively, to H64Y/V68F apomyoglobin, indicating an order of heme affinity for these proteins of wt > M79A >> H229A. These results indicate that histidine 229 is more important than methionine 79

for the affinity of HtsA for heme, though the methionine 79 ligand also contributes to the affinity.

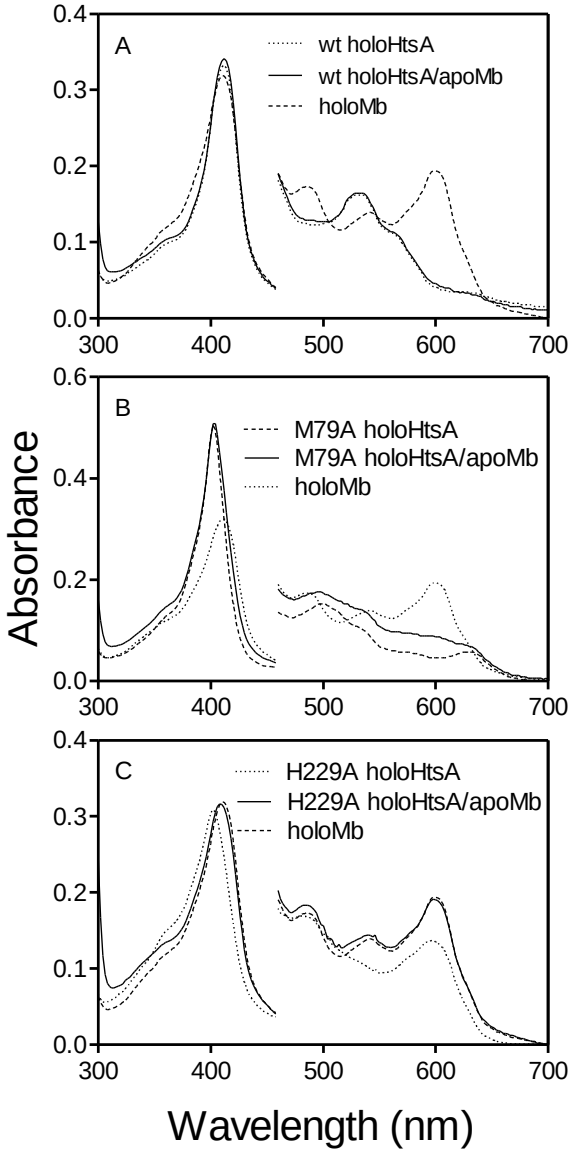

Figure 4.2: Reactions of H64Y/V68F Apomyoglobin with the holoHtsA Proteins Demonstrating the Relative Heme Affinities of HtsA Proteins. Presented are the absorption spectra of the mixtures of 40 μM H64Y/V68F apoMb with 2 μM wt (A), M79A (B), and H229A (C) holoHtsA after 6 h incubation. The spectra of holo-Mb and corresponding holoHtsA protein are included for comparison.

Efficient Heme Transfer from
Ferric Shp to HtsA^{M79A} but not to HtsA^{H229}

To determine whether both axial ligands of the HtsA heme iron are critical for ferric Shp-to-HtsA heme transfer, we examined heme transfer from ferric Shp to apoHtsA^{H229A} and apoHtsA^{M79A} using the spectroscopic method. The optical spectra of the HtsA axial mutants are distinct from Shp. Particularly, HtsA^{H229A} has a high spin, pentacoordinate heme iron, which has a characteristic spectrum with the Soret peak at 402 nm and the charge transfer bands at 482 and 600 nm. Similarly, HtsA^{M79A} has a spectrum with the 402-nm Soret peak and 498- and 630-nm charge transfer bands, which is typical of high spin, hexacoordinate heme iron with histidine and water ligands. In contrast, ferric Shp has a spectrum with the 428-nm Soret peak and 532- and 560-nm charge transfer bands, which is typical of low spin, hexacoordinate heme iron. Thus, these spectral differences can be used to determine whether heme is transferred from Shp to the HtsA mutants.

When ferric Shp was mixed with excess apoHtsA^{H229A}, the spectrum of the mixture was not exactly overlaid with the spectrum of either holoShp or holoHtsA^{H229A} but is very similar to the spectrum of holoShp (Fig 4.3A), indicating most of the heme was still on Shp. Thus, elimination of the His229 axial ligand decreases the efficiency of heme transfer from ferric holoShp to apoHtsA.

In the reaction of ferric Shp and apoHtsA^{M79A}, the Soret peak shifted rapidly from 428 nm to 402 nm with a concurrent decrease of beta and alpha bands at 530 nm and 560 nm, and an additional peak at 630 nm showed up (Fig. 4.3B). The resulting spectrum has peaks at 402, 498, 536, and 630 nm with a greater extinction coefficient of the Soret peak

than that of the holoShp, indicating that ferric Shp transferred its heme to $HtsA^{M79A}$. Therefore, elimination of the Met79 axial ligand does not change the efficiency of Shp-to-HtsA heme transfer.

M79A Replacement Alters Kinetic
Mechanism of Ferric Shp-to-HtsA Heme Transfer

In Chapter III, we found that alanine replacement of the Met66 or Met153 axial ligand of the Shp heme iron alters the kinetic mechanism with observed two kinetic phases and slows down heme transfer by stabilizing the intermediate, suggesting the direct axial displacement mechanism in Shp-to-HtsA heme transfer. In another word, the side chains of the axial ligand residues from apoHtsA are inserted to the axial positions of heme in Shp and displace the axial ligands of Shp. In the direct axial ligand displacement model of the Shp/$apoHtsA^{M79A}$ reaction, one axial bond in Shp is first displaced by His229 of HtsA, and the cleavage of the other axial bond in Shp should be slower because the facilitation of its cleavage by the Met79 residue of HtsA is missing due to the Met79Ala replacement. Thus, the Shp/$apoHtsA^{M79A}$ reaction should follow a kinetic mechanism with two kinetic phases. Indeed, ΔA_{402} in this reaction fits a two-exponential equation, but not a single exponential equation (Fig. 4.3C), indicating that the ferric Shp/$HtsA^{M79A}$ reaction has double kinetic phases, instead of a single kinetic phase. Thus, the Met79Ala replacement changed the kinetic mechanism, supporting the direct axial ligand displacement mechanism. The rate constants of the fast and slow phase were found to be 9.1 s^{-1} and 1.7 s^{-1}, respectively.

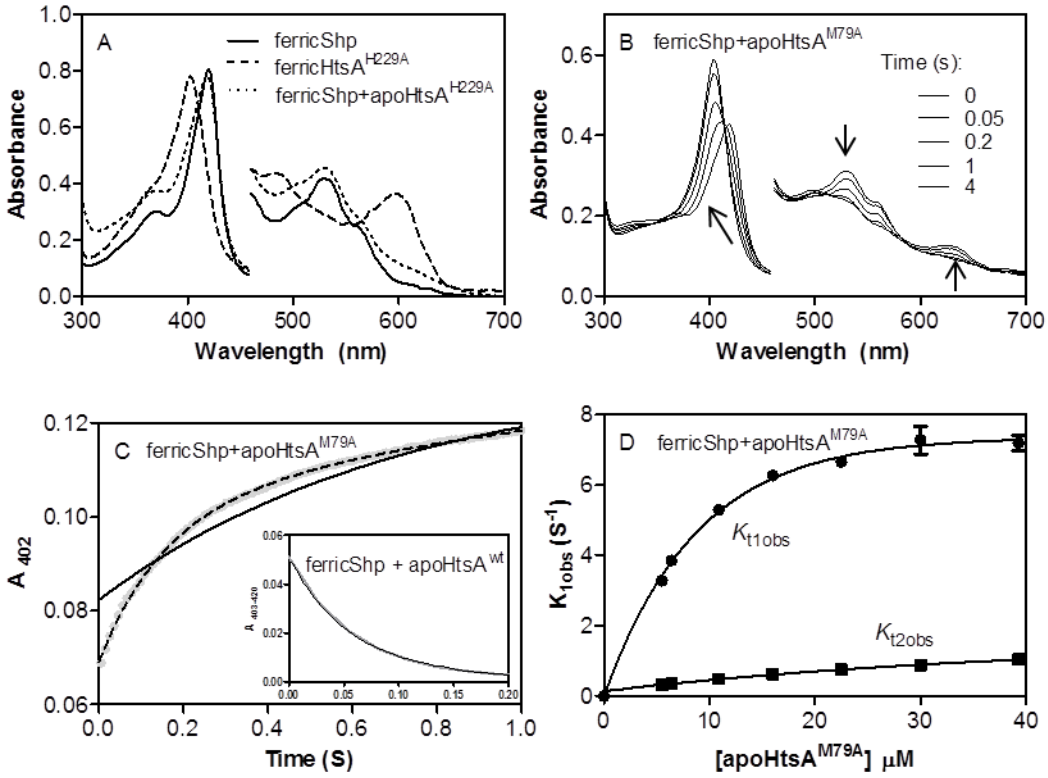

Figure 4.3: Optical Absorption Spectra and Kinetic Analysis of Heme Transfer from Ferric Shp to ApoHtsA^{H229A} and ApoHtsA^{M79A}. A, absorption spectra of 7 μM hemiShp (Solid line), hemiHtsA^{H229A} (dashed line), and the mixture of 7 μM hemiShp with 35 μM apoHtsA^{H229A} (dotted line). B, absorption spectra of the reaction of 7 μM hemiShp with 30 μM apoHtsA^{M79A} is presented as a function of time. C, time courses of spectral change at the indicated wavelengths for the reactions of ferric Shp with apoHtsA^{M79A} or apoHtsA (inset). The grey curves represent the observed data, and the black curves are theoretical lines obtained by fitting the data to two-exponential (dotted curve) and single exponential (solid curve) equations, respectively. D, the observed rate constants k_{t1obs} and k_{t2obs} plotted as a function of [apoHtsA^{M79A}] in the ferric Shp-HtsA^{M79A} reaction. The rate constants at different [apoHtsA^{M79A}] were obtained from double-exponential fitting as in panel C.

Ferrous Shp Cannot Transfer its Heme to HtsA^{M79A} and HtsA^{H229A}

To study whether the HtsA axial mutants can take up heme from ferrous Shp, ferrous Shp was mixed with excess apoHtsA^{M79A} and apoHtsA^{H229A} under anaerobic

condition, and spectra of the mixtures were recorded. The spectra of both mixtures were identical to the spectrum of ferrous Shp (Fig. 4.4), indicating that heme was still associated with Shp. Thus, elimination of either of the axial ligands demolished the ability of HtsA to take up heme from ferrous Shp. These results indicate that the heme axial ligand residues in HtsA are both critical for heme transfer from ferrous Shp to HtsA.

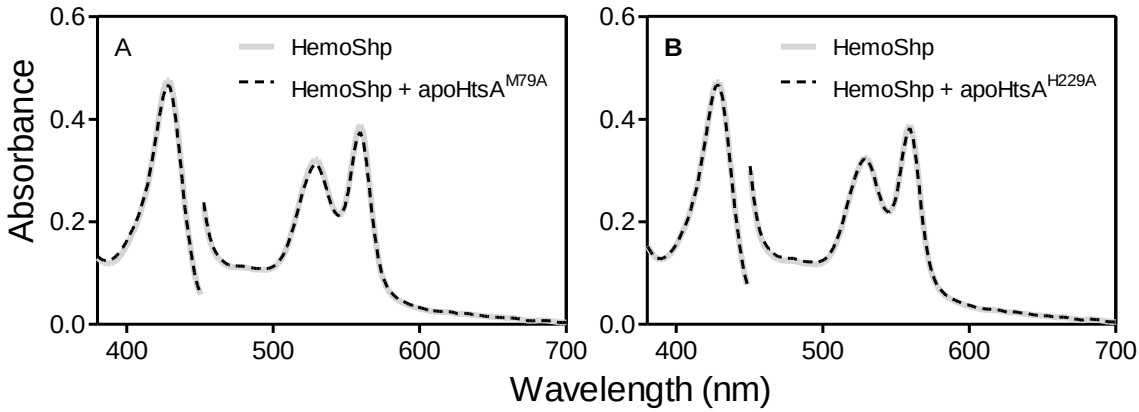

Figure 4.4: Optical Spectra of Ferrous Shp with ApoHtsA^{M79A} or apoHtsA^{H229A} (B). The grey line is the optical spectra of ferrous Shp. The dashed line is the optical spectra of a mixture of 7 μM ferrous Shp and 35 μM apoHtsA^{M79A} (A) or apoHtsA^{H229A} (B) in the presence of dithionite. Measurements were taken 5 minutes after mixing.

ApoHtsA^{H229A} Induces Autoxidation of Ferrous Shp

The reactions of ferrous Shp with apoHtsA^{M79A} add apoHtsA^{H229A} were also examined under the aerobic condition. The spectra of ferrous Shp and excess apoHtsA^{H229A} after mixing in the presence of oxygen were recorded by a stopped-flow spectrophotometer. The Soret peak changed rapidly from 428 nm to 420 nm within 10 seconds with a concurrent decline of the α and β peaks at 560 and 530 nm (Fig. 4.5A) and resulted in a spectrum that is similar to that of ferric Shp, indicating oxidation of the

ferrous heme iron in Shp in the presence of HtsA^{H229A}. In contrast, ferrous Shp by itself is stable in the absence of HtsA under the same conditions. Therefore, apoHtsA^{H229A} induces the autoxidation of the ferrous heme iron of Shp.

We next analyzed the kinetics of the autoxidation of ferrous Shp in the presence of varying concentrations of apoHtsA^{H229A}. The time course of ΔA_{431} fits with a single exponential equation (Fig. 4.5A) and the observed rate constant (k_{obs}) depended hyperbolically on [apoHtsA^{H229A}] indicating that the autoxidation is a pseudo-first-order process (Fig 4.5B). These results can be interpreted by Scheme 4.2 in which ferrous Shp first forms a complex with apoHtsA^{H229A} and Shp in the complex is then oxidized. Based on this model, k_{obs} is given by Equation 4.1

$$K_{obs}=\frac{K_{autoxidation}[apoHtsA^{H229A}]}{(K_2+K_{autoxidation})/K_1+[apoHtsA^{H229A}]} \approx \frac{K_{autoxidation}[apoHtsA^{H229A}]}{K_m+[apoHtsA^{H229A}]} \qquad \text{(Eq. 4.1)}$$

where K_m is the Michaelis constant of the reaction, and k_1, k_2, and $k_{autoxidation}$ are the rate constants of the individual reactions proposed in Scheme 4.1. Fitted values of $k_{autoxidation}$ and K_m equal to 1.3 s^{-1} and 7.9 μM, respectively.

$$Shp(FeII) + HtsA^{H229A} \underset{k_2}{\overset{k_1}{\rightleftharpoons}} Shp(FeII) :: HtsA^{H229A} \xrightarrow[O_2]{k_{autoxidation}} Shp(FeIII) + HtsA^{H229A}$$

SCHEME 4.1

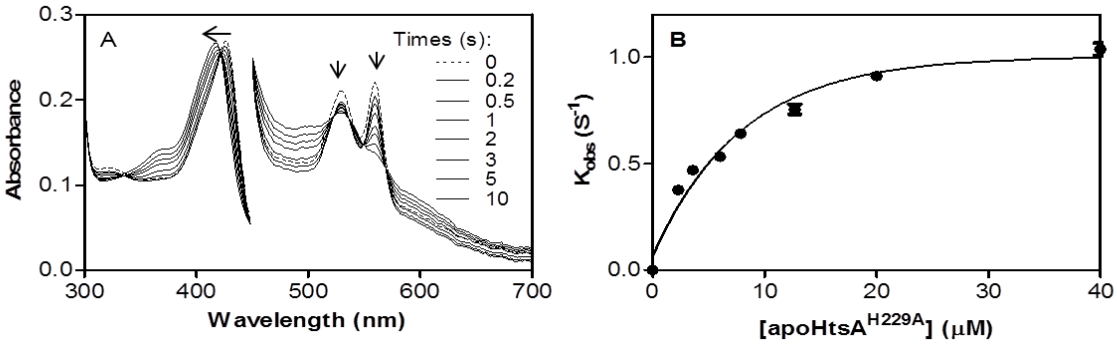

Figure 4.5: Optical Spectra and Kinetic Analysis of Reactions with Ferrous Shp and HtsA^{H229A} under Aerobic Condition. A, optical spectra of a reaction of 3.4 μM ferrous Shp with 60 μM HtsA^{H229A} as a function of time. B, plot of the observed rate constant as function of [apoHtsA^{H229A}]. The rate constants at different apoHtsA^{H229A} concentrations were obtained from single-exponential fitting of the spectral change associated with Shp oxidation.

ApoHtsA^{M79A}-Induced Autoxidation of Ferrous Shp

In the reaction of ferrous Shp with excess apoHtsA^{M79A} under the aerobic condition, the Soret peak of the spectra shifted from 428 nm to 402 nm within 15 seconds after mixing with concurrent decrease of the strong α and β peaks and appearance of the 630-nm peak (Fig. 4.6A), resulting in a spectrum that is similar to that of ferric HtsA^{M79A}. This result indicates that heme ends up in HtsA^{M79A}. Since ferrous Shp cannot transfer its heme to HtsA^{M79A} but ferric Shp can, heme in ferrous Shp must be oxidized before it was transferred to HtsA^{M79A}. The ΔA_{431} time courses fit with a single exponential equation (Fig. 4.6B), and the observed rate constant had a hyperbolic relationship with [apoHtsA^{M79A}]. These features are similar to those of apoHtsA^{H229A}-induced autoxidation of ferrous Shp, indicating that the data of the ferrous Shp/apoHtsA^{M79A} reaction could be analyzed using Equation 4.1, resulting in K_m of 4.2 μM and k of 0.66 s^{-1}. This rate constant apparently represents HtsA^{M79A}-induced autoxidation of ferrous Shp based on

the following reasons: Firstly, 70% of ΔA_{431} was due to autoxidation, and, secondly, this rate constant is less than one tenth of the rate constant (9.1 s^{-1}) of the fast phase of heme transfer from ferric Shp to $HtsA^{M79A}$ that contributed 63% of ΔA431 due to heme transfer from ferric Shp to $apoHtsA^{M79A}$. Furthermore, the rate constant of the ferrous Shp/$apoHtsA^{M79A}$ reaction is close to the rate constant of $HtsA^{H229A}$-induced autoxidation. Thus, the results of the ferrous Shp/$apoHtsA^{M79A}$ reaction can be interpreted by Scheme 4.2 in which ferrous Shp forms a complex with $apoHtsA^{M79A}$ and the Shp heme in the complex is oxidized and subsequently transferred to $HtsA^{M79A}$. The autoxidation is the rate-limiting step.

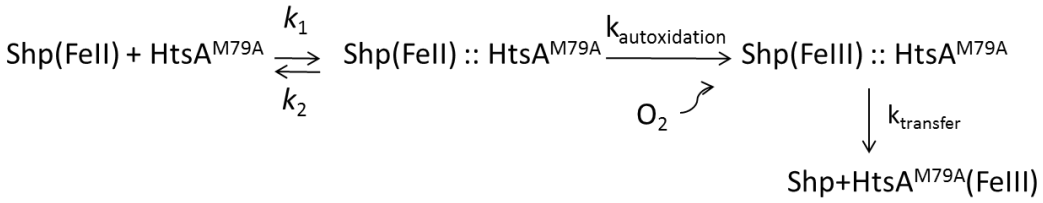

SCHEME 4.2

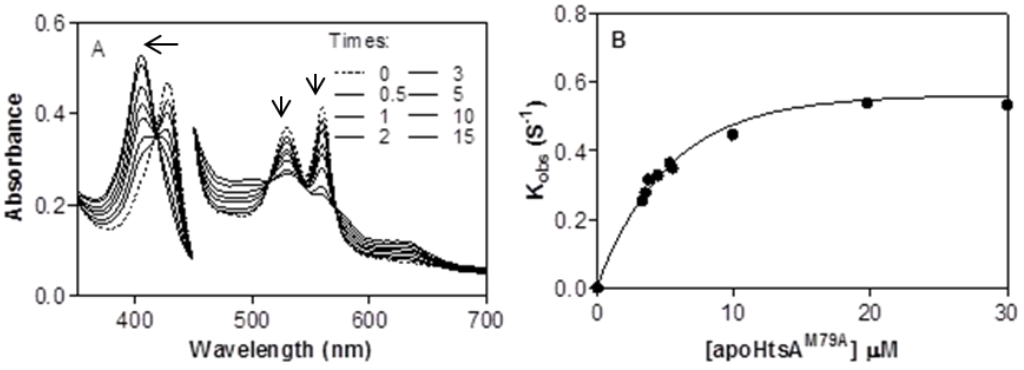

Figure 4.6: Optical Spectra and Kinetic Analysis of Reactions with Ferrous Shp and $HtsA^{M79A}$ under the Aerobic Condition. A, optical spectra of a reaction of 5.2 µM ferrous Shp with 60 µM $HtsA^{M79A}$ presented as a function of time. B, plot of the observed rate constant as a function of [$apoHtsA^{M79A}$]. The rate constants at different $apoHtsA^{M79A}$ concentrations were obtained from single-exponential fitting of the spectral change.

ApoHtsA$^{M79A/H229A}$-does not
Induce Autoxidation of Ferrous Shp

Both apoHtsA^{M79A} and apoHtsA^{H229A} induced the autoxidation of ferrous Shp. It is not known whether the remaining axial ligand residue in each mutant is required for the induction of the Shp autooxidation. To address this issue, the double axial ligand mutant of HtsA, apoHtsA$^{M79A/H229A}$ was prepared and tested. Unlike in the reactions of ferrous Shp with apoHtsA^{M79A} and apoHtsA^{H229A}, the A_{560} peak specific for reduced Shp did not decrease in the reaction of ferrous Shp with apoHtsA$^{M79A/H229A}$ (Fig. 4.7), indicating that apoHtsA$^{M79A/H229A}$ could not induce the autoxidation of Shp. These results suggest that one of the two axial residues is required for induction of the Shp autooxidation.

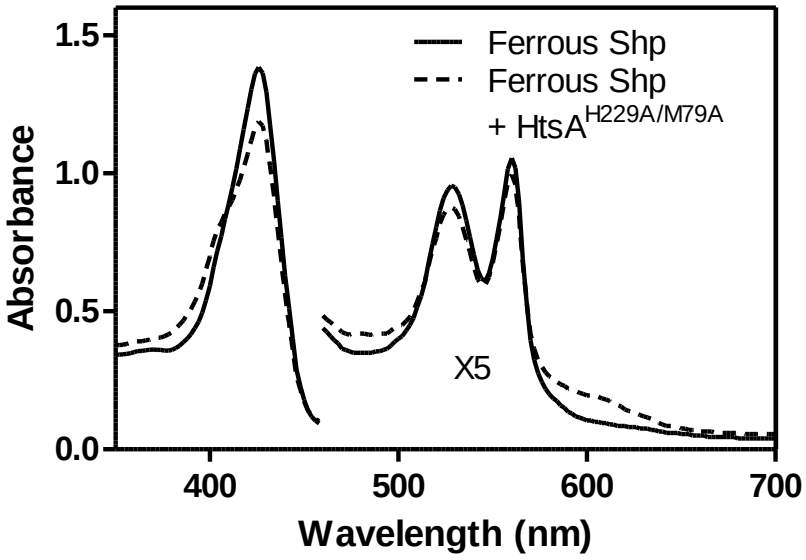

Figure 4.7: ApoHtsA$^{H229A/M79A}$ does not Induce Autoxidation of Ferrous Shp. Optical spectra for the reaction of ferrous Shp with apoHtsA$^{H229A/M79A}$. The solid line is UV-Vis spectrum of 11 μM ferrous Shp. The dashed line is the UV-Vis spectrum of a mixture of 11 μM ferrous Shp and 90 μM HtsA$^{H229A/M79A}$ that was recorded at 30 minutes after mixing.

Effect of the Axial Residue
Mutations of Shp and HtsA on GAS Virulence

The M153A replacement in Shp interrupts heme transfer from Shr to Shp, and the M66H replacement in Shp and H229A replacement in HtsA interrupt in vitro heme transfer from Shp to HtsA. To probe heme acquisition by GAS in vivo, these mutations were introduced into the genome of MGAS5005, yielding isogenic GAS strains carrying *shp*^{M66H} (Δ*shp*-*shp*^{M66H}), *shp*^{M153A} (Δ*shp*-*shp*^{M153A}), and HtsA^{H229A} (Δ*htsA*-*htsA*^{H229A}). Fig. 4.8 shows PCR confirmation of Δ*shp*-*shp*^{M66H} strain as an example to demonstrate how the mutant strains were obtained. PCR and sequencing results show that the strains obtained had the desired mutations.

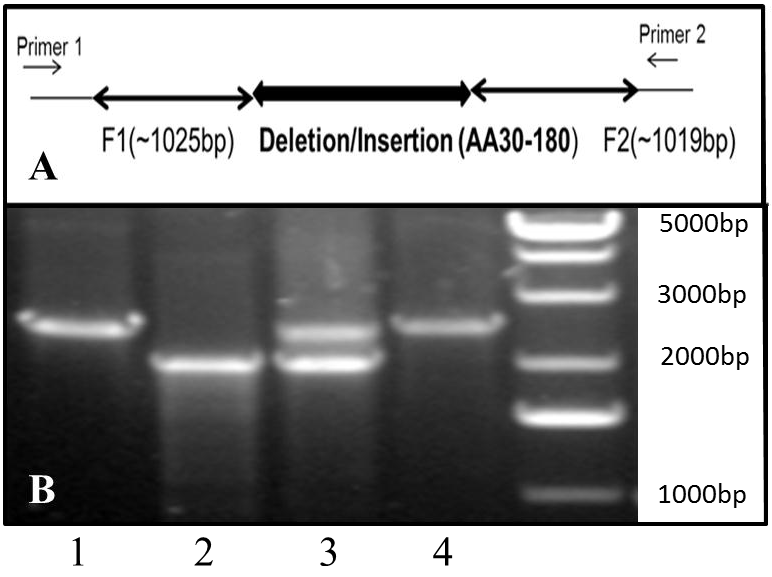

Figure 4.8: PCR Confirmation of a GAS Strain Carrying the M66H^{Shp} Replacement. The strain was obtained by putting the *shp*^{M66H} into the Δ*shp* strain as described in Fig. 4.1. A, the location of PCR Primers on the genome. F1 and F2 are recombination fragments used to generate Δ*shp*. The bolded region between F1 and F2 is the deletion (insertion) fragment. (B) Image of DNA agarose gel electrophoresis of the PCR products of different strains using primers P1 and P2. Lanes: 1, wt strain; 2, Δ*shp*; 3, Δ*shp*-p*Shp*^{M66H} obtained from the first crossover between Δ*shp* and p*Shp*^{M66H}; and 4, Δ*shp*-*shp*^{M66H}.

These strains were compared with the deletion mutants and their revertants in virulence using a mouse model of subcutaneous infection. Under the conditions used, the virulence of Δshp-shp^{M153A} appears to be reduced but the change is not significant compared to Δ*shp-shp* (P value = 0.123) (Fig. 4.9A). Unexpectedly, the virulence of Δ*shp-shp*^{M66H} is significantly increased compared to Δ*shp-shp* (P value = 0.0482) (Fig. 4.9A). Δ*htsA*, Δ*htsA-htsA*, and Δ*htsA-htsA*^{H229A} all had similar virulence. As discussed later, more studies are needed to examine the heme acquisition process *in vivo*.

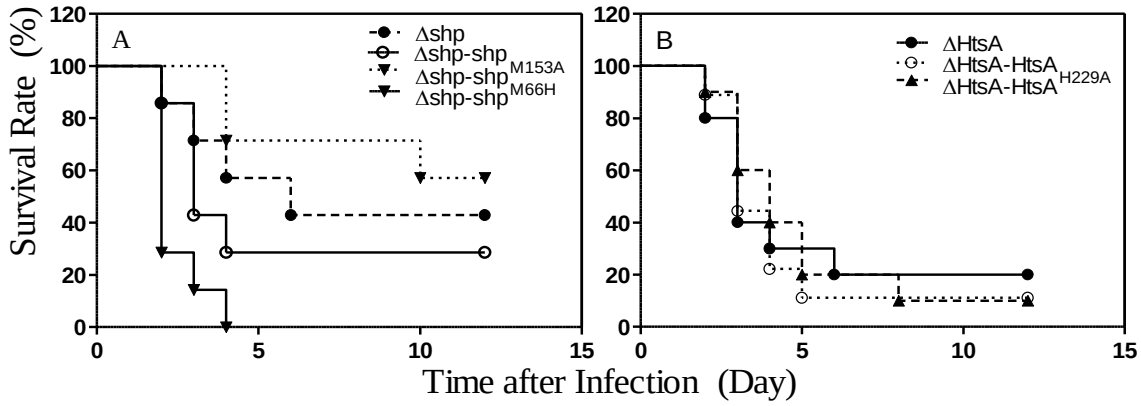

Figure 4.9: Virulence of GAS Mutants Carrying the Axial Ligand Mutations of the Heme Iron in Shp and HtsA . Groups of 7 (A) or 10 (B) Balb/C mice were subcutaneously infected with 1.8 x 10^8 cfu of each of the testing strains. (A) Survival rates for the *shp* strains. (B) Survival rates for the *htsA* strains.

Discussion

In this study, the mechanism of the Shp-to-HtsA heme transfer reaction was probed using HtsA axial mutants. The H229A replacement dramatically decreases the affinity of the HtsA for heme and efficiency of heme transfer from ferric Shp to HtsA. In contrast, the H79A replacement has limited detrimental effect on the heme affinity of

HtsA and the efficiency of heme acquisition from ferric Shp by HtsA. However, the M79A mutation altered the kinetic mechanism of the Shp-to-HtsA heme transfer from a single kinetic phase to double kinetic phases. $HtsA^{H229A}$ and $HtsA^{M79A}$ cannot take up heme from ferrous Shp but induce rapid autoxidation of the heme iron in ferrous Shp. These results indicate or support (a) that the heme axial ligand in heme acceptor can be critical for heme acquisition from heme donor by enhancing the affinity of the acceptor for heme, (b) that Shp and apoHtsA interact to each other to form an activated complex, and (c) that the two heme axial ligands in HtsA directly participate in axial ligand displacement during the transfer reaction.

The Role of the Heme Axial Ligand in Heme Acceptor in Driving the Equilibrium of the Heme Transfer Reaction

It is known that the axial ligands of the heme iron in HasA, HasR, ShuA, and *Porphyromonas gingivalis* heme receptor HmuR are critical for heme transfer and acquisition (182, 185, 243-246). However, it is unclear why these axial ligands are required for heme acquisition. One theory is that the axial ligands contribute to the affinity of hemoproteins for heme. It is usually difficult to measure the heme affinity of hemoproteins with extremely high affinity. We could estimate the affinity of Shp by measuring rates of heme association to apoShp and dissociation from its holo form using H64Y/V68F apoMb as a heme scavenger. We could not measure the affinity of HtsA for heme because HtsA does not lose heme to H64Y/V68F apomyoglobin. However, H64Y/V68F apomyoglobin is still valuable to estimate relative affinities of hemoproteins. The heme association constant for H64Y/V68F apomyoglobin is estimated to be 1×10^{12} M^{-1} at pH 7.0 based on a bimolecular rate constant of 1×10^{8}

M^{-1} s^{-1} for heme association to H64Y/V68F apomyoglobin (247) and a dissociation rate constant of 1.1×10^{-5} s^{-1} for this double mutant (220). Based on the spectra of their reaction mixtures with H64Y/V68F apomyoglobin, wild-type, M79A, and H229A HtsA proteins appear to have association constants for heme binding of $>10^{12}$ M^{-1}, and the order of the affinity is wild-type HtsA > M79A >> H229A. His229 is more important than Met79 for the affinity of HtsA for heme.

The H229A replacement of HtsA reduced the affinity of HtsA for heme. The reduction in the heme affinity of $HtsA^{H229A}$ mutant could be a primary reason of why $HtsA^{H229A}$ could not efficiently acquire heme from ferric Shp. This interpretation is supported by the observations that the M79A replacement did not dramatically affect the heme affinity of HtsA and that $HtsA^{M79A}$ can efficiently take up heme from ferric Shp. Thus, the axial ligand of heme acceptor can drive the equilibrium of the transfer reaction by enhancing the heme affinity of acceptor.

It is interesting that only one axial ligand is critical for the affinity of HtsA for heme. This phenomenon is not limited to HtsA. The axial ligand residue of Shp, Met153, is critical for the high affinity of Shp for heme whereas the other axial ligand residue, Met66, destabilizes heme binding (Chapter III) (248). These observations are consistent with the fact that some bacterial proteins involved in heme acquisition have only one axial ligand. For example, the Isd heme acquisition system in *Staphylococcus aureus* includes surface proteins IsdA, IsdB, IsdC, and IsdH and ABC transporter IsdDEF. IsdA, IsdC, and IsdH have a pentacoordinate heme iron with tyrosine as the only axial ligand (180, 181, 249). The optical absorption spectra suggest that the heme iron in

IsdB is pentacoordinate as well (189). Therefore, it appears that only one axial ligand of heme iron is critical for high affinity of hemoprotein for heme.

Activated Shp and apoHtsA Complex

The formation of the complexes of apoHtsA with ferrous Shp and ferric Shp prior to heme transfer releases 23 kJ/mol and 26 kJ/mol free energy, respectively, which are proposed to be used to facilitate heme transfer to apoHtsA. This mechanism of activated heme transfer is also observed in heme transfer from IsdA to IsdC (188, 250) and may apply in general to all bacterial heme transport systems. Transfer of heme from the high-affinity site in HasA into a lower-affinity site in HasR is coupled with the exergonic complex formation of the two proteins (182). Upon docking of HasA to HasR, one of the two axial bonds in HasA is initially broken, but the position and orientation of the heme is preserved. Subsequent steric displacement of heme by a HasR residue ruptures the other axial coordination, leading to heme transfer into the receptor (243, 251). However, there was no direct evidence for the weakening of the heme binding in the donor by the formation of the donor/acceptor complex of the activated heme transfer in these systems. The finding that apoHtsA^{H229A} and apoHtsA^{M79A} induce rapid autoxidation of ferrous Shp provides direct evidence for the formation of an activated Shp/HtsA complex. The hyperbolic dependence of the autoxidation rate of ferrous Shp on HtsA^{H229A} and HtsA^{M79A} concentrations indicate that ferrous Shp forms a complex with the HtsA mutants prior to its autoxidation, and the induced rapid oxidation of ferrous Shp indicate that the formation of the complex change the environment of the bound heme and that the

axial bond is weakened so that O_2 can access to the iron and displace the axial bond in Shp. Thus, Shp and HtsA can form an activated complex.

Heme Axial Ligand Displacement Mechanism

In chapter III, we characterized the alternation in the kinetic mechanism of Shp-to-HtsA heme transfer caused by the elimination of one ligand in Shp. Both Shp^{M66A}/HtsA and Shp^{M153A}/HtsA reactions have two kinetic phases, whereas Shp/HtsA reaction has only one kinetic phase. We proposed a mechanism called the "plug-in" model to interpret these findings. In this model for the Shp/apoHtsA heme transfer reaction, the empty heme pocket plugs in along the two sides of the bound heme in Shp, and the two side chains of axial ligands in apoHtsA are therefore in close proximity of the axial bonds of the heme iron and then replace the two axial ligands of Shp at about same time and pull it into the heme binding pocket of HtsA. In the Shp^{M66A}/apoHtsA and Shp^{M153A}/apoHtsA heme transfer reactions, the side chain of one axial ligand from HtsA inserts into the empty side of the Shp axial mutant, forming a Shp-heme-HtsA ternary complex with one axial ligand from each protein, and then the side chain of the other axial ligand from HtsA replaces the axial ligand in the Shp mutant and pulls heme to the HtsA side.

This model can also explain the effect of the M79A replacement of HtsA on the kinetic mechanism of the heme transfer reaction. The alanine replacement of Met79 in HtsA also changes the kinetic mechanism of the Shp/HtsA reaction from one with a single kinetic phase to one with two kinetic phases. In this case, the cleavage of one axial bond in Shp is facilitated by the HtsA His229 residue, whereas the cleavage of the other

axial bond in Shp should be slower because Met79 is absent, resulting in the two kinetic phases in the Shp/apoHtsA^{M79A} reaction. Because the final product is the hexacoordinate M79A heme iron with His229 and H_2O as its axial ligands, it is possible that the second kinetic phase represents the reaction of the pentacoordinate holoHtsA^{M79A} with H_2O. If the H_2O coordination is much faster than the formation of pentacoordinate M79A, which is most likely the case, the first mechanism would be more plausible. However, we don't have data to rule out the second mechanism.

Neither HtsA^{M79A} nor HtsA^{H229A} could take heme from ferrous Shp, and, thus, both Met79 and H229A are required for HtsA to acquire heme from ferrous Shp. It is interesting that HtsA^{M79A} takes heme from ferric Shp but does not from ferrous Shp. One possible reason is that ferrous Shp has higher affinity for heme than HtsA^{M79A}. It is also possible that the relative heme affinities of ferrous HtsA^{M79A} and Shp are similar to those of ferric HtsA^{M79A} and Shp, that is, ferrous HtsA^{M79A} still has higher heme affinity than ferrous Shp. This scenario would suggest that the cleavage of the axial bonds of the heme iron in ferrous Shp is directly displaced by the heme axial ligands of HtsA. This would make sense because axial bonds in ferrous hemoproteins are stronger than those in corresponding ferric hemoproteins. Cleavage of the axial bonds in reduced hemoproteins would have high activation energy, which would be reduced if the cleavage of the axial bonds in the heme donor and the formation of the axial bonds in the acceptor occur at the same time. Although we cannot distinguish the two possibility, the observation that the axial ligands of the HtsA heme iron are both required for heme acquisition from ferrous Shp by HtsA is consistent with the proposal that the axial ligand residues in HtsA directly participate in the axial ligand replacement.

Comparison of the reactions of ferrous Shp with wt HtsA, HtsA^{H229A}, and HtsA^{M79A} under the anaerobic conditions strongly suggests that the axial ligands of HtsA were directly involved in the axial ligand displacement. Binding of O_2 to the Shp heme iron prior to the autoxidation in the ferrous Shp/HtsA^{M79A} and ferrous Shp/HtsA^{H229A} reactions, reduced heme is oxidized in Shp, suggesting O_2 replaced one axial ligand in Shp. On the contrary, in the ferrous Shp/HtsA heme transfer reaction, heme is transferred to HtsA with a rate constant at 28 ± 6 s^{-1}, then the reduced heme iron is oxidized in HtsA protein. Results indicate that axial ligands in Shp cannot be replaced by O_2 when they are already placed by axial ligands in HtsA. Furthermore, apoHtsA$^{M79A/H229A}$ did not induce Shp autoxidation, suggesting that the remaining axial residue in apoHtsA^{M79A} and apoHtsA^{H229A} is actively involved in induction of Shp autoxidation. Therefore, axial ligands in HtsA actively participate in the axial ligands replacements.

In Vivo Study of the Heme
Axial Ligand Displacement Mechanism

The M153A replacement in Shp and H229A replacement in HtsA were expected to attenuate GAS virulence based on the in vitro data that Shp^{M153A} could not efficiently acquire heme from Shr and HtsA^{H229A} could not efficiently acquire heme from Shp. However, the M153A replacement in Shp attenuated virulence but not significant and H229A replacement appears not to affect the virulence. There are a couple of possible explanations for this observation. First, the replacement may mainly affect equilibrium of the heme transfer, and this equilibrium can be shifted by the downstream step along the acquisition pathway. Thus, the M153A and H229A replacements may not be able to completely shut off the pathway. Secondly, 6xHis-tagged HtsA^{H229A} could efficiently

acquire heme from ferric Shp *in vitro*, suggesting that the structural features at the N-terminus have a profound effect on the affinity of HtsA for heme. Mature HtsA has a lipid moiety at the N-terminus that could alter the heme affinity of $HtsA^{H229A}$ in vivo, and the replacement thus would not block heme transfer. Thirdly, the M153A mutation of Shp appears to attenuate virulence but the attenuation was not significant. We just tested one dose, which could be too high to demonstrate M153A-caused significant attenuation. More tests with different doses are needed to determine whether the M153A mutation leads to significant attenuation. If not, Shp may also get heme from another source.

M66H mutation, which blocks heme transfer from Shp to HtsA in vitro, surprisingly increased virulence. It is possible that reduced iron levels due to the M66H mutation enhanced expression of virulence factors. This possibility supports the Shp-HtsA heme transfer. It is also possible that Shp has another receptor other than HtsA and this receptor takes heme from Shp either by a higher heme binding affinity or by a mechanism irrelevant on heme binding affinity.

The results of the virulence study using the shp and htsA mutants are contradictory to the previous results of the virulence study using *shp* and *htsA* deletion mutants. Our lab previously observed significant attenuation of GAS virulence due to deletion of *shp* or *htsA* (unpublished data). It is possible that the amino acid replacements of Shp and HtsA cannot completely shut off the heme acquisition process in vivo.

Although we cannot make a definite conclusion from the virulence study, the phenotype of $\Delta shp\text{-}shp^{M66H}$ may provide a tool to examine the GAS heme acquisition process in vivo. In addition, refining the experimental condition is necessary to confirm the result and provide more information to analyze.

SUMMARY AND CONCLUSION

Iron is essential for bacteria to grow, and heme is a major iron source of many bacterial pathogens, including GAS. Although numerous heme acquisition systems have been characterized, the molecular and chemical mechanisms of heme acquisition in bacteria are poorly understood. Particularly, how heme is rapidly transferred from one protein to another remains mysterious. Our laboratory previously reported the kinetic mechanism of the heme transfer from the streptococcal surface protein Shp to HtsA, the lipoprotein component of the heme specific ABC transporter in GAS. This project further studied the Shp-HtsA reaction to understand how one protein rapidly and directly acquires heme from another protein. The model to be tested is that HtsA directly acquire heme from Shp through a direct displacement of the heme iron axial ligands in Shp by the axial residues in HtsA in an activated Shp-apoHtsA complex.

The axial ligands of the Shp and HtsA heme iron were identified to be Met66/Met153 and Met79/His229, respectively. These findings were achieved by replacing each of the Met and His residues, the axial residue candidates, in Shp and HtsA with Ala and examining the effects of replacements on spectral properties of the axial ligands, coordination and spin state of the heme iron. The H229A replacement in HtsA and M66A and M153A replacements in Shp changed the coordination of the heme iron from hexacoordination to pentacoordination in both ferrous and ferric forms. M79A replacement converted the hexacoordinate ferrous HtsA heme iron into a pentacoordinate complex and converted the low-spin, hexacoordinate ferric HtsA into in a high-spin, hexacoordinate heme complex with histidine and water ligation. External axial ligands

are more readily to form a low-spin hexacoordinate adduct with $HtsA^{M79A}$ and Shp^{M66A} than $HtsA^{H229A}$ and Shp^{M153A}, indicating that the M79 side of the HtsA heme and M66 side of the Shp heme are more accessible to the solvent than the other side in each protein. The HtsA H229 and Shp Met153 residues are critical for the affinities of the proteins for heme. The identification of the axial ligands and characterization of the axial mutants did not only generate the mutants and knowledge for testing our hypothesis and interpreting the results but also advanced hemoprotein chemistry.

A number of findings on the effects of the M66A and M153A replacements in Shp on the Shp-to-HtsA heme transfer reaction provide significant insight into the mechanism of the reaction. First, the M66A and M153A replacements alter the kinetic mechanism of the Shp/apoHtsA reaction from one with a single kinetic phase to one with double kinetic phases and unexpectedly slow down heme transfer. The kinetic alternation allows detection of the heme transfer intermediate by both kinetic analysis and absorption spectroscopy. The spectral features of the intermediates imply that they are Shp-heme-HtsA complexes with one axial ligand from each protein. Secondly, Met^{66} destabilizes heme binding to facilitate its rapid transfer. Thirdly, when pH decreases, Shp^{M66A} undergoes a conversion from pentacoordinate heme iron complex into a hexacoordinate heme-H_2O-iron-Met iron complex with an apparent K_a of 7.65, and Shp^{M153A} does not form a similar hexacoordinate complex but the M66-iron axial bond is broken at pH 5. These pH titration results suggest that the heme pocket in Shp can open up at the M66 side of the bound heme and this opening is controlled by a base group. These findings result in a model of the heme transfer mechanism in which the side chains of the axial residues from apoHtsA are inserted into the axial positions of the heme in

Shp to extract it from the surface protein and pull it into the transporter active site. The results also imply a mechanism of how to open up the heme pocket in Shp during the heme transfer.

The characterization of the effects of the M79A and H229A replacements in HtsA on the Shp-to-HtsA heme transfer reaction yielded two major findings: Essential role of the HtsA axial ligands in heme transfer and the conclusive evidence for the formation of an activated Shp-apoHtsA complex prior to heme transfer. Both His229 and Met79 are crucial for heme transfer from ferrous Shp to HtsA. Although apoHtsA^{H229A} and apoHtsA^{M79A} fail to acquire heme from ferrous Shp, they induce rapid autoxidation of ferrous Shp, and the Shp autoxidation involves the Shp-apoHtsA complex, indicating that the axial bonds of the Shp heme iron are weakened in the Shp-apoHtsA complex. Importantly, the HtsA$^{M79A/H229A}$ failed to induce the Shp autooxidation, implying that the weakening of the Shp axial bonds require either of the two axial ligand residues. These findings conclusively establish that the Shp and apoHtsA form an activated Shp-apoHtsA complex with weaker axial bonds and support the direct axial ligand replacement during heme transfer.

The Shp^{M153A} and HtsA^{H229A} replacements reduce the efficiency of the Shr-to-Shp and Shp-to-HtsA heme transfer in vitro, respectively. However, these replacements did not significantly attenuate GAS virulence in mouse model of infection. These results suggest that the replacements may just affect the equilibrium of the transfer reaction but cannot completely shut down the heme acquisition process. Alternatively, the results suggest that the other iron uptake systems also play a role in meeting iron requirement for GAS in vivo.

Overall, this project provides evidence for a direct axial ligand replacement mechanism in which the axial ligand in heme acceptor directly replace the axial ligands in heme donor, which we call the "plug-in" mechanism (Figure 5.1). In addition, we demonstrated the formation of an activated donor-acceptor complex and the model of the opening of the heme pocket in Shp. These findings provide significant insight into the biochemical and chemical events of heme transfer from one protein to another. Thus, our approaches and results have high impact in understanding heme trafficking in prokaryotes and eukaryotes.

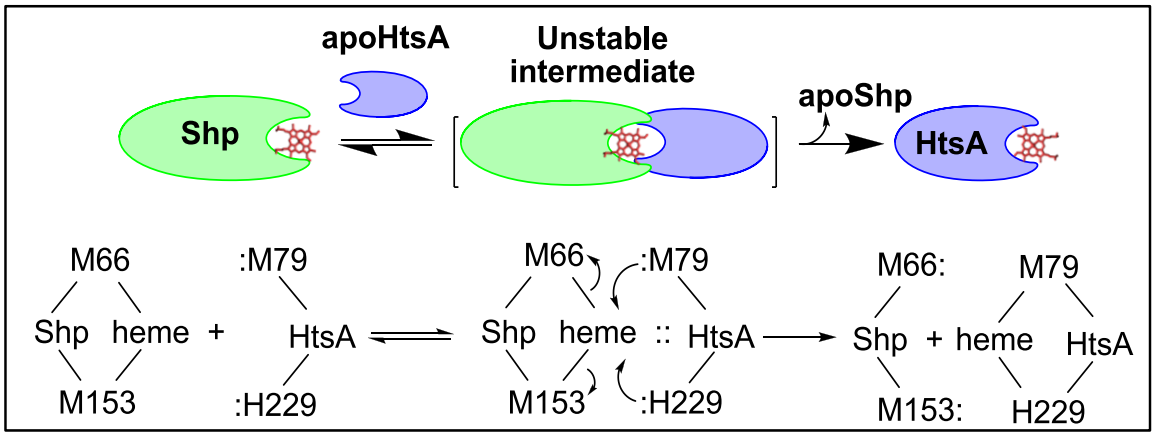

Figure 5.1: A model of the mechanism of the Shp-to-HtsA heme transfer reaction derived from the findings in this project. Holo-Shp and apo-HtsA first form an activated donor:acceptor complex, and the axial ligands in apo-HtsA directly replace the axial ligands in holo-Shp and pull heme over to HtsA.

REFERENCES

1. Rosenbach, F. J. (1884) in *Mikro-Organismen bei den Wund-infections-krankheiten des Menschen*, ed. J.F. Bergman (Wiesbaden).
2. Shottmuller, H. (1903) *Munch. Med.* **50,** 849-853.
3. Lancefield, R. C. (1933) *J Exp Med* **57,** 571-595.
4. Sherman, J. M. (1937) *Bacteriol Rev* **1,** 3-97.
5. Karl H. Schleifer, R. K. (1984) *Int J Sys Evol Microbiol* **34,** 31-34.
6. Schleifer, K., Kilipper-Balz, R (1987) *Sys Appl Microbiol* **10,** 1-19.
7. Facklam, R. (2002) *Clin Microbiol Rev* **15,** 613-630.
8. LANCEFIELD, R. C. (1962) *J Immunol* **89,** 307-313.
9. Johnson, D. R., Kaplan, E. L., VanGheem, A., Facklam, R. R. & Beall, B. (2006) *J Med Microbiol* **55,** 157-164.
10. Beall, B., Facklam, R. & Thompson, T. (1996) *J Clin Microbiol* **34,** 953-958.
11. http://www.cdc.gov/ncidod/biotech/strep/M-ProteinGene_typing.htm.
12. Wannamaker, L. W. (1970) *N Engl J Med* **282,** 78-85.
13. Bidet, P., Plainvert, C., Doit, C., Mariani-Kurkdjian, P., Bonacorsi, S., Lepoutre, A., Bouvet, A., Poyart, C. & Bingen, E. (2010) *Arch Pediatr* **17,** 201-208.
14. Brown, C. N., Pollard, T. C., Iyer, S. & Andrade, A. J. (2010) *J Bone Joint Surg Br* **92,** 763-769.
15. Siljander, T., Lyytikainen, O., Vahakuopus, S., Snellman, M., Jalava, J. & Vuopio, J. (2010) *Eur J Clin Microbiol Infect Dis* **29,** 1229-1235.
16. Vikerfors, A., Haggar, A., Darenberg, J., Low, A., Melhus, A., Hedlund, J., Sylvan, S., Norrby-Teglund, A. & Eriksson, B. M. (2009) *Scand J Infect Dis* **41,** 823-830.
17. O'Loughlin, R. E., Roberson, A., Cieslak, P. R., Lynfield, R., Gershman, K., Craig, A., Albanese, B. A., Farley, M. M., Barrett, N. L., Spina, N. L., Beall, B., Harrison, L. H., Reingold, A., Van Beneden, C. & CN , -. . A. B. C. S. (2007) *Clin Infect Dis* **45,** 853-862.

18. Carapetis, J. R., Steer, A. C., Mulholland, E. K. & Weber, M. (2005) *Lancet Infect Dis* **5,** 685-694.

19. O'Brien, K. L., Beall, B., Barrett, N. L., Cieslak, P. R., Reingold, A., Farley, M. M., Danila, R., Zell, E. R., Facklam, R., Schwartz, B. & Schuchat, A. (2002) *Clin Infect Dis* **35,** 268-276.

20. Luca-Harari, B., Darenberg, J., Neal, S., Siljander, T., Strakova, L., Tanna, A., Creti, R., Ekelund, K., Koliou, M., Tassios, P. T., van der, L. i. M., Straut, M., Vuopio-Varkila, J., Bouvet, A., Efstratiou, A., Schalen, C. & Henriques-Normark, B. (2009) *J Clin Microbiol* **47,** 1155-1165.

21. Ferretti, J. J., McShan, W. M., Ajdic, D., Savic, D. J., Savic, G., Lyon, K., Primeaux, C., Sezate, S., Suvorov, A. N., Kenton, S., Lai, H. S., Lin, S. P., Qian, Y., Jia, H. G., Najar, F. Z., Ren, Q., Zhu, H., Song, L., White, J., Yuan, X. & Clifton (2001) *Proc Natl Acad Sci U S A* **98,** 4658-4663.

22. Cunningham, M. w. (2000) *clinical microbiology reviews* **13,** 470-511.

23. Caparon, M. G., Stephens, D. S., Olsen, A. & Scott, J. R. (1991) *Infect Immun* **59,** 1811-1817.

24. Wessels, M. R. & Bronze, M. S. (1994) *Proc Natl Acad Sci U S A* **91,** 12238-12242.

25. Courtney, H. S., Bronze, M. S., Dale, J. B. & Hasty, D. L. (1994) *Infect Immun* **62,** 4868-4873.

26. Hanski, E. & Caparon, M. (1992) *Proc Natl Acad Sci U S A* **89,** 6172-6176.

27. Pancholi, V. & Fischetti, V. A. (1992) *J Exp Med* **176,** 415-426.

28. D. Gerlach, C. S., Z. Tigyi, B. Nilsson, A. Forsgren and A. S. Naidu (1994) *Current Microbiology* **28,** 331-338.

29. Valentin-Weigand, P., Grulich-Henn, J., Chhatwal, G. S., Muller-Berghaus, G., Blobel, H. & Preissner, K. T. (1988) *Infect Immun* **56,** 2851-2855.

30. Visai, L., Bozzini, S., Raucci, G., Toniolo, A. & Speziale, P. (1995) *J Biol Chem* **270,** 347-353.

31. Kreikemeyer, B., Talay, S. R. & Chhatwal, G. S. (1995) *Mol Microbiol* **17,** 137-145.

32. Courtney, H. S., Li, Y., Dale, J. B. & Hasty, D. L. (1994) *Infect Immun* **62,** 3937-3946.

33. Wexler, D. E., Chenoweth, D. E. & Cleary, P. P. (1985) *Proc Natl Acad Sci U S A* **82,** 8144-8148.

34. Jacks-Weis, J., Kim, Y. & Cleary, P. P. (1982) *J Immunol* **128,** 1897-1902.

35. Zinkernagel, A. S., Timmer, A. M., Pence, M. A., Locke, J. B., Buchanan, J. T., Turner, C. E., Mishalian, I., Sriskandan, S., Hanski, E. & Nizet, V. (2008) *Cell Host Microbe* **4,** 170-178.

36. Whitnack, E. & Beachey, E. H. (1982) *J Clin Invest* **69,** 1042-1045.

37. Whitnack, E. & Beachey, E. H. (1985) *J Exp Med* **162,** 1983-1997.

38. Whitnack, E. & Beachey, E. H. (1985) *J Bacteriol* **164,** 350-358.

39. Collin, M. & Olsen, A. (2001) *EMBO J* **20,** 3046-3055.

40. Vincents, B., von Pawel-Rammingen, U., Bjorck, L. & Abrahamson, M. (2004) *Biochemistry* **43,** 15540-15549.

41. von Pawel-Rammingen, U., Johansson, B. P. & Bjorck, L. (2002) *EMBO J* **21,** 1607-1615.

42. Ferretti, J. J., McShan, W. M., Ajdic, D., Savic, D. J., Savic, G., Lyon, K., Primeaux, C., Sezate, S., Suvorov, A. N., Kenton, S., Lai, H. S., Lin, S. P., Qian, Y., Jia, H. G., Najar, F. Z., Ren, Q., Zhu, H., Song, L., White, J., Yuan, X. & Clifton (2001) *Proc Natl Acad Sci U S A* **98,** 4658-4663.

43. Frick, I. M., Akesson, P., Rasmussen, M., Schmidtchen, A. & Bjorck, L. (2003) *J Biol Chem* **278,** 16561-16566.

44. Dale, J. B. & Beachey, E. H. (1986) *J Exp Med* **163,** 1191-1202.

45. Berge, A. & Bjorck, L. (1995) *J Biol Chem* **270,** 9862-9867.

46. Oehmcke, S., Shannon, O., Morgelin, M. & Herwald, H. (2010) *Clin Chim Acta* **411,** 1172-1180.

47. Hynes, W. (2004) *Front Biosci* **9,** 3399-3433.

48. Cue, D., Dombek, P. E., Lam, H. & Cleary, P. P. (1998) *Infect Immun* **66,** 4593-4601.

49. Schrager, H. M., Alberti, S., Cywes, C., Dougherty, G. J. & Wessels, M. R. (1998) *J Clin Invest* **101,** 1708-1716.

50. Cywes, C. & Wessels, M. R. (2001) *Nature* **414,** 648-652.

51. Wessels, M. R. & Bronze, M. S. (1994) *Proc Natl Acad Sci U S A* **91,** 12238-12242.

52. Cywes Bentley, C., Hakansson, A., Christianson, J. & Wessels, M. R. (2005) *Cell Microbiol* **7,** 945-955.

53. Bisno, A. L., Brito, M. O. & Collins, C. M. (2003) *Lancet Infect Dis* **3,** 191-200.

54. Veasy, L. G., Tani, L. Y., Daly, J. A., Korgenski, K., Miner, L., Bale, J., Kaplan, E. L., Musser, J. M. & Hill, H. R. (2004) *Pediatrics* **113,** e168-72.

55. Kansal, R. G., Nizet, V., Jeng, A., Chuang, W. J. & Kotb, M. (2003) *J Infect Dis* **187,** 398-407.

56. Collin, M. & Olsen, A. (2003) *Infect Immun* **71,** 2983-2992.

57. Rasmussen, M. & Bjorck, L. (2002) *Mol Microbiol* **43,** 537-544.

58. von Pawel-Rammingen, U. & Bjorck, L. (2003) *Curr Opin Microbiol* **6,** 50-55.

59. Tillett, W. S., Edwards, L. B. & Garner, R. L. (1934) *J Clin Invest* **13,** 47-78.

60. Cederholm-Williams, S. A., De Cock, F., Lijnen, H. R. & Collen, D. (1979) *Eur J Biochem* **100,** 125-132.

61. Sriskandan, S., Unnikrishnan, M., Krausz, T. & Cohen, J. (2000) *Microbiology* **146,** 2785-2792.

62. Eriksson, A., Eriksson, B., Holm, S. E. & Norgren, M. (1999) *Clin Diagn Lab Immunol* **6,** 133-136.

63. Fernie-King, B. A., Seilly, D. J., Davies, A. & Lachmann, P. J. (2002) *Infect Immun* **70,** 4908-4916.

64. Fernie-King, B. A., Seilly, D. J., Willers, C., Wurzner, R., Davies, A. & Lachmann, P. J. (2001) *Immunology* **103,** 390-398.

65. Hoe, N. P., Ireland, R. M., DeLeo, F. R., Gowen, B. B., Dorward, D. W., Voyich, J. M., Liu, M., Burns, E. H., Jr., Culnan, D. M., Bretscher, A. & Musser, J. M. (2002) *Proc Natl Acad Sci U S A* **99,** 7646-7651.

66. Lukomski, S., Hoe, N. P., Abdi, I., Rurangirwa, J., Kordari, P., Liu, M., Dou, S. J., Adams, G. G. & Musser, J. M. (2000) *Infect Immun* **68,** 535-542.

67. Datta, V., Myskowski, S. M., Kwinn, L. A., Chiem, D. N., Varki, N., Kansal, R. G., Kotb, M. & Nizet, V. (2005) *Mol Microbiol* **56,** 681-695.

68. Madden, J. C., Ruiz, N. & Caparon, M. (2001) *Cell* **104,** 143-152.

69. Meehl, M. A. & Caparon, M. G. (2004) *Mol Microbiol* **52,** 1665-1676.

70. Ghosh, J. & Caparon, M. G. (2006) *Mol Microbiol* **62,** 1203-1214.

71. N'Goundo Magassa1, S. C. &. M. G. C. (2010) *EMBO* **,** 400-405.

72. Kreikemeyer, B., McIver, K. S. & Podbielski, A. (2003) *Trends Microbiol* **11,** 224-232.

73. Sumby, P., Whitney, A. R., Graviss, E. A., DeLeo, F. R. & Musser, J. M. (2006) *PLoS Pathog* **2**.

74. Garcia, A. F., Abe, L. M., Erdem, G., Cortez, C. L., Kurahara, D. K. & Yamaga, K. M. (2010) *Microbiology* .

75. Lancefield, R. C. (1928) *J. Exp. Med.* **47**.

76. LANCEFIELD, R. C. (1962) *J Immunol* **89,** 307-313.

77. Jones, K. F. & Fischetti, V. A. (1988) *J Exp Med* **167,** 1114-1123.

78. Hu, M. C., Walls, M. A., Stroop, S. D., Reddish, M. A., Beall, B. & Dale, J. B. (2002) *Infect Immun* **70,** 2171-2177.

79. Hayman, W. A., Brandt, E. R., Relf, W. A., Cooper, J., Saul, A. & Good, M. F. (1997) *Int Immunol* **9,** 1723-1733.

80. Hruby, D. E., Hodges, W. M., Wilson, E. M., Franke, C. A. & Fischetti, V. A. (1988) *Proc Natl Acad Sci U S A* **85,** 5714-5717.

81. Salvadori, L. G., Blake, M. S., McCarty, M., Tai, J. Y. & Zabriskie, J. B. (1995) *J Infect Dis* **171,** 593-600.

82. Ji, Y., Carlson, B., Kondagunta, A. & Cleary, P. P. (1997) *Infect Immun* **65,** 2080-2087.

83. Kapur, V., Maffei, J. T., Greer, R. S., Li, L. L., Adams, G. J. & Musser, J. M. (1994) *Microb Pathog* **16,** 443-450.

84. Valentin-Weigand, P., Talay, S. R., Kaufhold, A., Timmis, K. N. & Chhatwal, G. S. (1994) *Microb Pathog* **17,** 111-120.

85. Andreini, C., Bertini, I., Cavallaro, G., Holliday, G. L. & Thornton, J. M. (2008) *J Biol Inorg Chem* **13,** 1205-1218.

86. Guengerich, F. P. (2010) *J Biol Chem* **285,** 26727.

87. Waldron, K. J., Rutherford, J. C., Ford, D. & Robinson, N. J. (2009) *Nature* **460,** 823-830.

88. Price, C. A. & Carell, E. F. (1964) *Plant Physiol* **39,** 862-868.

89. Higuchi, K. (1970) *J Cell Physiol* **75,** 65-72.

90. Weinberg, E. D. (1978) *Microbiol Rev* **42,** 45-66.

91. Archibald, F. (1983) *FEMS Microbiology Letters* **19,** 29-32.

92. Archibald, F. (1983) *FEMS Microbiology Letters* **19,** 29-32.

93. Weinberg, E. D. (1997) *Perspect Biol Med* **40,** 578-583.

94. Posey, J. E. & Gherardini, F. C. (2000) *Science* **288,** 1651-1653.

95. Andrews, S. C., Robinson, A. K. & Rodriguez-Quinones, F. (2003) *FEMS Microbiol Rev* **27,** 215-237.

96. Braun, V. & Killmann, H. (1999) *Trends Biochem Sci* **24,** 104-109.

97. Wandersman, C. & Delepelaire, P. (2004) *Annu Rev Microbiol* **58,** 611-647.

98. Wooldridge, K. G. & Williams, P. H. (1993) *FEMS Microbiol Rev* **12,** 325-348.

99. Weinberg, E. D. (1984) *Physiol Rev* **64,** 65-102.

100. Kochan, I. (1973) *Curr Top Microbiol Immunol* **60,** 1-30.

101. Weinberg, E. D. (1992) *Life Sci* **50,** 1289-1297.

102. Flesch, I. E. & Kaufmann, S. H. (1991) *Infect Immun* **59,** 3213-3218.

103. Green, S. J., Nacy, C. A. & Meltzer, M. S. (1991) *J Leukoc Biol* **50,** 93-103.

104. Kammler, M., Schon, C. & Hantke, K. (1993) *J Bacteriol* **175,** 6212-6219.

105. Cornelissen, C. N. (2003) *Front Biosci* **8,** d836-47.

106. Taylor, J. M. & Heinrichs, D. E. (2002) *Mol Microbiol* **43,** 1603-1614.

107. Carrondo, M. A. (2003) *EMBO J* **22,** 1959-1968.

108. Deneer, H. G., Healey, V. & Boychuk, I. (1995) *Microbiology* **141 (Pt 8),** 1985-1992.

109. Paustian, M. L., May, B. J., Cao, D., Boley, D. & Kapur, V. (2002) *J Bacteriol* **184,** 6714-6720.

110. Whitby, P. W., Vanwagoner, T. M., Springer, J. M., Morton, D. J., Seale, T. W. & Stull, T. L. (2006) *J Med Microbiol* **55,** 661-668.

111. Gomez, J. A., Criado, M. T. & Ferreiros, C. M. (1998) *Res Microbiol* **149,** 381-387.

112. Wandersman, C. & Stojiljkovic, I. (2000) *Curr Opin Microbiol* **3,** 215-220.

113. Rohde, K. H., Gillaspy, A. F., Hatfield, M. D., Lewis, L. A. & Dyer, D. W. (2002) *Mol Microbiol* **43,** 335-354.

114. Lewis, L. A., Sung, M. H., Gipson, M., Hartman, K. & Dyer, D. W. (1998) *J Bacteriol* **180,** 6043-6047.

115. Morton, D. J., Whitby, P. W., Jin, H., Ren, Z. & Stull, T. L. (1999) *Infect Immun* **67,** 2729-2739.

116. Paoli, M., Anderson, B. F., Baker, H. M., Morgan, W. T., Smith, A. & Baker, E. N. (1999) *Nat Struct Biol* **6,** 926-931.

117. Wong, J. C., Patel, R., Kendall, D., Whitby, P. W., Smith, A., Holland, J. & Williams, P. (1995) *Infect Immun* **63,** 2327-2333.

118. O-Brien-Simpson, N. M., Veith, P. D., Dashper, S. G. & Reynolds, E. C. (2003) *Curr Protein Pept Sci* **4,** 409-426.

119. Maines, M. D. (1997) *Annu Rev Pharmacol Toxicol* **37,** 517-554.

120. Wilks, A. & Schmitt, M. P. (1998) *J Biol Chem* **273,** 837-841.

121. Skaar, E. P., Gaspar, A. H. & Schneewind, O. (2004) *J Biol Chem* **279,** 436-443.

122. Cope, L. D., Thomas, S. E., Hrkal, Z. & Hansen, E. J. (1998) *Infect Immun* **66,** 4511-4516.

123. Cope, L. D., Yogev, R., Muller-Eberhard, U. & Hansen, E. J. (1995) *J Bacteriol* **177,** 2644-2653.

124. Maresso, A. W., Garufi, G. & Schneewind, O. (2008) *PLoS Pathog* **4**.

125. Gao, J. L., Nguyen, K. A. & Hunter, N. (2010) *J Biol Chem* .

126. Braun, V. (2003) *Front Biosci* **8,** s1409-21.

127. Faraldo-Gomez, J. D. & Sansom, M. S. (2003) *Nat Rev Mol Cell Biol* **4,** 105-116.

128. Ferguson, A. D., Hofmann, E., Coulton, J. W., Diederichs, K. & Welte, W. (1998) *Science* **282,** 2215-2220.

129. Locher, K. P., Rees, B., Koebnik, R., Mitschler, A., Moulinier, L., Rosenbusch, J. P. & Moras, D. (1998) *Cell* **95,** 771-778.

130. Buchanan, S. K., Smith, B. S., Venkatramani, L., Xia, D., Esser, L., Palnitkar, M., Chakraborty, R., van der, H. e. D. & Deisenhofer, J. (1999) *Nat Struct Biol* **6,** 56-63.

131. Ferguson, A. D., Chakraborty, R., Smith, B. S., Esser, L., van der, H. e. D. & Deisenhofer, J. (2002) *Science* **295,** 1715-1719.

132. Chimento, D. P., Mohanty, A. K., Kadner, R. J. & Wiener, M. C. (2003) *Nat Struct Biol* **10,** 394-401.

133. Yue, W. W., Grizot, S. & Buchanan, S. K. (2003) *J Mol Biol* **332,** 353-368.

134. Bracken, C. S., Baer, M. T., Abdur-Rashid, A., Helms, W. & Stojiljkovic, I. (1999) *J Bacteriol* **181,** 6063-6072.

135. Ghigo, J. M., Letoffe, S. & Wandersman, C. (1997) *J Bacteriol* **179,** 3572-3579.

136. Reynolds, P. R., Mottur, G. P. & Bradbeer, C. (1980) *J Biol Chem* **255,** 4313-4319.

137. Wooldridge, K. G., Morrissey, J. A. & Williams, P. H. (1992) *J Gen Microbiol* **138,** 597-603.

138. Letain, T. E. & Postle, K. (1997) *Mol Microbiol* **24,** 271-283.

139. Larsen, R. A., Thomas, M. G. & Postle, K. (1999) *Mol Microbiol* **31,** 1809-1824.

140. Worst, D. J., Gerrits, M. M., Vandenbroucke-Grauls, C. M. & Kusters, J. G. (1998) *J Bacteriol* **180,** 1473-1479.

141. Cowart, R. E. (2002) *Arch Biochem Biophys* **400,** 273-281.

142. Mazmanian, S. K., Liu, G., Ton-That, H. & Schneewind, O. (1999) *Science* **285,** 760-763.

143. Eichenbaum, Z., Muller, E., Morse, S. A. & Scott, J. R. (1996) *Infect Immun* **64,** 5428-5429.

144. Hanks, T. S., Liu, M., McClure, M. J. & Lei, B. (2005) *BMC Microbiol* **5,** 62.

145. Montanez, G. E., Neely, M. N. & Eichenbaum, Z. (2005) *Microbiology* **151,** 3749-3757.

146. Janulczyk, R., Pallon, J. & Bjorck, L. (1999) *Mol Microbiol* **34,** 596-606.

147. Sun, X., Ge, R., Chiu, J. F., Sun, H. & He, Q. Y. (2008) *FEBS Lett* **582,** 1351-1354.

148. Sun, X., Baker, H. M., Ge, R., Sun, H., He, Q. Y. & Baker, E. N. (2009) *Biochemistry* **48,** 6184-6190.

149. Lei, B., Liu, M., Voyich, J. M., Prater, C. I., Kala, S. V., DeLeo, F. R. & Musser, J. M. (2003) *Infect Immun* **71,** 5962-5969.

150. Bates, C. S., Montanez, G. E., Woods, C. R., Vincent, R. M. & Eichenbaum, Z. (2003) *Infect Immun* **71,** 1042-1055.

151. Lei, B., Smoot, L. M., Menning, H. M., Voyich, J. M., Kala, S. V., Deleo, F. R., Reid, S. D. & Musser, J. M. (2002) *Infect Immun* **70,** 4494-4500.

152. Zhu, H., Liu, M. & Lei, B. (2008) *BMC Microbiol* **8,** 15.

153. Mazmanian, S. K., Skaar, E. P., Gaspar, A. H., Humayun, M., Gornicki, P., Jelenska, J., Joachmiak, A., Missiakas, D. M. & Schneewind, O. (2003) *Science* **299,** 906-909.

154. Clarke, S. R., Wiltshire, M. D. & Foster, S. J. (2004) *Mol Microbiol* **51,** 1509-1519.

155. Beasley, F. C. & Heinrichs, D. E. (2010) *J Inorg Biochem* **104,** 282-288.

156. Dale, S. E., Sebulsky, M. T. & Heinrichs, D. E. (2004) *J Bacteriol* **186,** 8356-8362.

157. Morrissey, J. A., Cockayne, A., Hill, P. J. & Williams, P. (2000) *Infect Immun* **68,** 6281-6288.

158. Maresso, A. W., Chapa, T. J. & Schneewind, O. (2006) *J Bacteriol* **188,** 8145-8152.

159. Skaar, E. P., Gaspar, A. H. & Schneewind, O. (2006) *J Bacteriol* **188,** 1071-1080.

160. Gat, O., Zaide, G., Inbar, I., Grosfeld, H., Chitlaru, T., Levy, H. & Shafferman, A. (2008) *Mol Microbiol* **70,** 983-999.

161. Maresso, A. W., Garufi, G. & Schneewind, O. (2008) *PLoS Pathog* **4**.

162. Tarlovsky, Y., Fabian, M., Solomaha, E., Honsa, E., Olson, J. S. & Maresso, A. W. (2010) *J Bacteriol* **192,** 3503-3511.

163. Kunkle, C. A. & Schmitt, M. P. (2007) *J Bacteriol* **189,** 3650-3654.

164. Brown, J. S., Gilliland, S. M. & Holden, D. W. (2001) *Mol Microbiol* **40,** 572-585.

165. Tai, S. S., Lee, C. J. & Winter, R. E. (1993) *Infect Immun* **61,** 5401-5405.

166. Gupta, R., Shah, P. & Swiatlo, E. (2009) *Microb Pathog* **47,** 101-109.

167. Hakansson, A., Roche, H., Mirza, S., McDaniel, L. S., Brooks-Walter, A. & Briles, D. E. (2001) *Infect Immun* **69,** 3372-3381.

168. Jedrzejas, M. J. (2006) *Clin Chim Acta* **367,** 1-10.

169. Tai, S. S., Wang, T. R. & Lee, C. J. (1997) *Infect Immun* **65,** 1083-1087.

170. Tai, S. S., Yu, C. & Lee, J. K. (2003) *FEMS Microbiol Lett* **220,** 303-308.

171. Pramanik, A. & Braun, V. (2006) *J Bacteriol* **188,** 3878-3886.

172. Eaton, W. A. & Hofrichter, J. (1981) *Methods Enzymol* **76,** 175-261.

173. McCabe, M. P., Firth, L. & O'Connor, E. (2009) *J Clin Psychol Med Settings* **16,** 355-362.

174. Sritharan, A., Egan, G. F., Johnston, L., Horne, M., Bradshaw, J. L., Bohanna, I., Asadi, H., Cunnington, R., Churchyard, A. J., Chua, P., Farrow, M. & Georgiou-Karistianis, N. (2010) *J Neurol Neurosurg Psychiatry* **81,** 257-262.

175. Lei, B., Liu, M., Voyich, J. M., Prater, C. I., Kala, S. V., DeLeo, F. R. & Musser, J. M. (2003) *Infect Immun* **71,** 5962-5969.

176. Lei, B., Smoot, L. M., Menning, H. M., Voyich, J. M., Kala, S. V., Deleo, F. R., Reid, S. D. & Musser, J. M. (2002) *Infect Immun* **70,** 4494-4500.

177. Mazmanian, S. K., Skaar, E. P., Gaspar, A. H., Humayun, M., Gornicki, P., Jelenska, J., Joachmiak, A., Missiakas, D. M. & Schneewind, O. (2003) *Science* **299,** 906-909.

178. Liu, M. & Lei, B. (2005) *Infect Immun* **73,** 5086-5092.

179. Grigg, J. C., Vermeiren, C. L., Heinrichs, D. E. & Murphy, M. E. (2007) *J Biol Chem* **282,** 28815-28822.

180. Sharp, K. H., Schneider, S., Cockayne, A. & Paoli, M. (2007) *J Biol Chem* **282,** 10625-10631.

181. Grigg, J. C., Vermeiren, C. L., Heinrichs, D. E. & Murphy, M. E. (2007) *Mol Microbiol* **63,** 139-149.

182. Izadi-Pruneyre, N., Huche, F., Lukat-Rodgers, G. S., Lecroisey, A., Gilli, R., Rodgers, K. R., Wandersman, C. & Delepelaire, P. (2006) *J Biol Chem* **281,** 25541-25550.

183. Letoffe, S., Nato, F., Goldberg, M. E. & Wandersman, C. (1999) *Mol Microbiol* **33,** 546-555.

184. Deniau, C., Gilli, R., Izadi-Pruneyre, N., Letoffe, S., Delepierre, M., Wandersman, C., Briand, C. & Lecroisey, A. (2003) *Biochemistry* **42,** 10627-10633.

185. Burkhard, K. A. & Wilks, A. (2007) *J Biol Chem* **282,** 15126-15136.

186. Zhu, H., Liu, M. & Lei, B. (2008) *BMC Microbiol* **8,** 15.

187. Nygaard, T. K., Liu, M., McClure, M. J. & Lei, B. (2006) *BMC Microbiol* **6,** 82.

188. Liu, M., Tanaka, W. N., Zhu, H., Xie, G., Dooley, D. M. & Lei, B. (2008) *J Biol Chem* **283,** 6668-6676.

189. Zhu, H., Xie, G., Liu, M., Olson, J. S., Fabian, M., Dooley, D. M. & Lei, B. (2008) *J Biol Chem* **283,** 18450-18460.

190. Zhu, H., Xie, G., Liu, M., Olson, J. S., Fabian, M., Dooley, D. M. & Lei, B. (2008) *J Biol Chem* **283,** 18450-18460.

191. Nygaard, T. K., Blouin, G. C., Liu, M., Fukumura, M., Olson, J. S., Fabian, M., Dooley, D. M. & Lei, B. (2006) *J Biol Chem* **281,** 20761-20771.

192. Ran, Y., Zhu, H., Liu, M., Fabian, M., Olson, J. S., Aranda R, 4. t., Phillips, G. N., Jr., Dooley, D. M. & Lei, B. (2007) *J Biol Chem* **282,** 31380-31388.

193. Skaar, E. P., Humayun, M., Bae, T., DeBord, K. L. & Schneewind, O. (2004) *Science* **305,** 1626-1628.

194. Muryoi, N., Tiedemann, M. T., Pluym, M., Cheung, J., Heinrichs, D. E. & Stillman, M. J. (2008) *J Biol Chem* **283,** 28125-28136.

195. Liu, M., Tanaka, W. N., Zhu, H., Xie, G., Dooley, D. M. & Lei, B. (2008) *J Biol Chem* **283,** 6668-6676.

196. Nygaard, T. K., Blouin, G. C., Liu, M., Fukumura, M., Olson, J. S., Fabian, M., Dooley, D. M. & Lei, B. (2006) *J Biol Chem* **281,** 20761-20771.

197. Grigg, J. C., Ukpabi, G., Gaudin, C. F. & Murphy, M. E. (2010) *J Inorg Biochem* **104,** 341-348.

198. Pluym, M., Muryoi, N., Heinrichs, D. E. & Stillman, M. J. (2008) *J Inorg Biochem* **102,** 480-488.

199. Bhakta, M. N. & Wilks, A. (2006) *Biochemistry* **45,** 11642-11649.

200. Aaby, K., Abbey, R. L., Herrmann, J. W., Treadwell, M., Jordan, C. S. & Wood, K. (2006) *J Public Health Manag Pract* **12,** 365-372.

201. Krause, G., Gilsdorf, A., Becker, J., Bradt, K., Dreweck, C., Gartner, B., Lower, J., Marcic, A., Nicoll, A., Pott, E., Schaade, L., Schoeller, A., Stollorz, V., Trader, C. & Razum, O. (2010) *Bundesgesundheitsblatt Gesundheitsforschung Gesundheitsschutz* **53,** 510-519.

202. Garcia Jorda, E. (2010) *Clin Transl Oncol* **12,** 243-245.

203. Excler, J. L. (2005) *Indian J Med Res* **121,** 568-581.

204. Dundar, D., Sayan, M. & Tamer, G. S. (2010) *Microb Drug Resist* .

205. Strus, M., Drzewiecki, A., Chmielarczyk, A., Tomusiak, A., Romanek, P., Kosowski, K., Kochan, P., van der, L. i. M., Lutticken, R. & Heczko, P. B. (2009) *Clin Microbiol Infect* .

206. Callen, J., Georgiou, A., Prgomet, M., Paoloni, R. & Westbrook, J. (2010) *Stud Health Technol Inform* **160,** 1241-1245.

207. Oana, C. & Duca, E. (2010) *Rev Med Chir Soc Med Nat Iasi* **114,** 11-12.

208. Berchialla, P., Scarinzi, C., Snidero, S., Rahim, Y. & Gregori, D. (2010) *J Med Syst* .

209. Alfa, M. J., DeGagne, P., Olson, N. & Fatima, I. (2010) *BMC Infect Dis* **10,** 200.

210. Thomas G. Spiro, J. D. S., Paul Stein (1979) *J. Am. Chem. Soc.* **101,** 2648-2655.

211. Dewey, J., Hana, G., Russell, T., Price, J., McCaffrey, D., Harezlak, J., Sem, E., Anyanwu, J. C., Guttmann, C. R., Navia, B., Cohen, R., Tate, D. F. & CN , -. . H. N. C. (2010) *Neuroimage* **51,** 1334-1344.

212. Lancefield, R. C. (1928) *J Exp Med* **47,** 469-480.

213. Lancefield, R. C. (1928) *J Exp Med* **47,** 91-103.

214. Lancefield, R. C. & Dole, V. P. (1946) *J Exp Med* **84,** 449-471.

215. Kaufhold, A., Podbielski, A., Baumgarten, G., Blokpoel, M., Top, J. & Schouls, L. (1994) *FEMS Microbiol Lett* **119,** 19-25.

216. Penney, T. J., Martin, D. R., Williams, L. C., de Malmanche, S. A. & Bergquist, P. L. (1995) *FEMS Microbiol Lett* **130,** 145-149.

217. Tamayo, E., Montes, M., Garcia-Medina, G., Garcia-Arenzana, J. M. & Perez-Trallero, E. (2010) *BMC Infect Dis* **10,** 233.

218. Sarralde, J. A., Bernal, J. M., Llorca, J., Ponton, A., Diez-Solorzano, L., Gimenez-Rico, J. R. & Revuelta, J. M. (2010) *Ann Thorac Surg* **90,** 503-508.

219. Ransjo, U., Lytsy, B., Melhus, A., Aspevall, O., Artinger, C., Eriksson, B. M., Gunther, G. & Hambraeus, A. (2010) *J Hosp Infect* **76,** 26-31.

220. Mulet, M. E., Perez-Santonja, J. J., Ferrer, C. & Alio, J. L. (2010) *J Refract Surg* **26,** 364-9 LID - 10.3928/1081.

221. Mounsey, K., Ho, M. F., Kelly, A., Willis, C., Pasay, C., Kemp, D. J., McCarthy, J. S. & Fischer, K. (2010) *PLoS Negl Trop Dis* **4**.

222. Stout, J. C., Weaver, M., Solomon, A. C., Queller, S., Hui, S., Johnson, S. A., Gray, J., Beristain, X., Wojcieszek, J. & Foroud, T. (2007) *Cogn Behav Neurol* **20,** 212-218.

223. Allen, A. J., Leonard, H. L. & Swedo, S. E. (1995) *J Am Acad Child Adolesc Psychiatry* **34,** 307-311.

224. Koprowski, H. (2009) *Zoonoses Public Health* .

225. Nara, P. L., Nara, D., Chaudhuri, R., Lin, G. & Tobin, G. (2008) *Vaccine* **26,** 6200-6211.

226. Philipsen, K. R., Christiansen, L. E., Hasman, H. & Madsen, H. (2010) *J Theor Biol* **263,** 134-142.

227. Amachawadi, R. G., Shelton, N. W., Jacob, M. E., Shi, X., Narayanan, S. K., Zurek, L., Dritz, S. S., Nelssen, J. L., Tokach, M. D. & Nagaraja, T. G. (2010) *Foodborne Pathog Dis* **7,** 1089-1097.

228. Bessen, D. E. & Lizano, S. (2010) *Future Microbiol* **5,** 623-638.

229. Hegstad, K., Mikalsen, T., Coque, T. M., Werner, G. & Sundsfjord, A. (2010) *Clin Microbiol Infect* .

230. Hammerum, A. M., Lester, C. H. & Heuer, O. E. (2010) *Foodborne Pathog Dis* .

231. Aranda R, 4. t., Worley, C. E., Liu, M., Bitto, E., Cates, M. S., Olson, J. S., Lei, B. & Phillips, G. N., Jr. (2007) *J Mol Biol* **374,** 374-383.

232. Aslam, M., Diarra, M. S., Service, C. & Rempel, H. (2010) *Foodborne Pathog Dis* **7,** 235-241.

233. Hsieh, Y. C., Lee, W. S., Ou, T. Y. & Hsueh, P. R. (2010) *Eur J Clin Microbiol Infect Dis* **29,** 25-30.

234. Evans, A. C. (1936) *J Bacteriol* **31,** 611-624.

235. Marmo Moreira, L., Lima Poli, A., Costa-Filho, A. J. & Imasato, H. (2006) *Biophys Chem*, **124,** 62-72.

236. Eichenbaum, Z., Muller, E., Morse, S. A. & Scott, J. R. (1996) *Infect Immun* **64,** 5428-5429.

237. Ouattara, M., Cunha, E. B., Li, X., Huang, Y. S., Dixon, D. & Eichenbaum, Z. (2010) *Mol Microbiol* **78,** 739-56 LID - 10.1111/j.1.

238. Fisher, M., Huang, Y. S., Li, X., McIver, K. S., Toukoki, C. & Eichenbaum, Z. (2008) *Infect Immun* **76,** 5006-5015.

239. Liu, M. & Lei, B. (2005) *Infect Immun* **73,** 5086-5092.

240. Ran, Y., Liu, M., Zhu, H., Nygaard, T. K., Brown, D. E., Fabian, M., Dooley, D. M. & Lei, B. (2010) *Biochemistry* **49,** 2834-2842.

241. Fuhrhop, J. H. & Smith, K. M. (1975) *Laboratory methods, in Porphyrins and Metalloporphyrins* (Elsevier Publishing, New York).

242. Hanks, T. S., Liu, M., McClure, M. J. & Lei, B. (2005) *BMC Microbiol* **5,** 62.

243. Krieg, S., Huche, F., Diederichs, K., Izadi-Pruneyre, N., Lecroisey, A., Wandersman, C., Delepelaire, P. & Welte, W. (2009) *Proc Natl Acad Sci U S A* **106,** 1045-1050.

244. Cobessi, D., Meksem, A. & Brillet, K. (2010) *Proteins* **78,** 286-294.

245. Olczak, T. (2006) *Arch Microbiol* **186,** 393-402.

246. Liu, X., Olczak, T., Guo, H. C., Dixon, D. W. & Genco, C. A. (2006) *Infect Immun* **74,** 1222-1232.

247. Ahmed, M. A., Martinez, A., Yee, A., Cahill, D. & Besag, F. M. (2008) *Dev Med Child Neurol* **50,** 300-304.

248. Ran, Y., Zhu, H., Liu, M., Fabian, M., Olson, J. S., Aranda R, 4. t., Phillips, G. N., Jr., Dooley, D. M. & Lei, B. (2007) *J Biol Chem* **282,** 31380-31388.

249. Pilpa, R. M., Fadeev, E. A., Villareal, V. A., Wong, M. L., Phillips, M. & Clubb, R. T. (2006) *J Mol Biol* **360,** 435-447.

250. Muryoi, N., Tiedemann, M. T., Pluym, M., Cheung, J., Heinrichs, D. E. & Stillman, M. J. (2008) *J Biol Chem* **283,** 28125-28136.

251. Caillet-Saguy, C., Piccioli, M., Turano, P., Izadi-Pruneyre, N., Delepierre, M., Bertini, I. & Lecroisey, A. (2009) *J Am Chem Soc* **131,** 1736-1744.

252. Dryla, A., Gelbmann, D., von Gabain, A. & Nagy, E. (2003) *Mol Microbiol* **49**, 37-53.

253. WHO. (2005) in *WHO/FCH/CAH/05.09; WHO/IVB/05.14*.

254. Brown, J. S., Gilliland, S. M. & Holden, D. W. (2001) *Mol Microbiol*, **40,** 572-585.

255. Byrd, T. F. & Horwitz, M. A. (1991) *J Clin Invest*, **88**, 351-357.

256. Wandersman, C. & Delepelaire, P. (2004) *Annu Rev Microbiol*, **58,** 611-647.